NON CO-OPERATIVE DETECTION OF
LPI/LPD SIGNALS VIA
CYCLIC SPECTRAL ANALYSIS

THESIS

Andrew M. Gillman
Flight Lieutenant, Royal Australian Air Force

AFIT/GE/ENG/99M-11

19990413 098

| REPORT DOCUMENTATION PAGE | | | Form Approved OMB No. 0704-0188 |
|---|---|---|---|

| 1. AGENCY USE ONLY *(Leave blank)* | 2. REPORT DATE | 3. REPORT TYPE AND DATES COVERED |
|---|---|---|
| | March 1999 | Masters Thesis |

**4. TITLE AND SUBTITLE**
NON CO-OPERATIVE DETECTION OF LPI/LPD SIGNALS VIA CYCLIC SPECTRAL ANALYSIS

**5. FUNDING NUMBERS**

**6. AUTHOR(S)**
Flight Lieutenant Andrew M. Gillman
Royal Australian Air Force

**7. PERFORMING ORGANIZATION NAME(S) AND ADDRESS(ES)**

Air Force Institute of Technology
2950 P St.
Wright -Patterson AFB OH 45433-6583

**8. PERFORMING ORGANIZATION REPORT NUMBER**

AFIT/GE/ENG/99M-11

**9. SPONSORING/MONITORING AGENCY NAME(S) AND ADDRESS(ES)**
Mr Gerhard Kasischke (AFRL/SNZW)     Deputy Director - Electronic Warfare
(937) 255-5900 Ext 4281                      Australian Defence Headquarters
Air Force Research Laboratory           PO Box E33;  Queen Victoria Tce
2241 Avionics Circle                          Canberra          ACT 2600
Wright Patterson AFB OH 45433-7303   AUSTRALIA

**10. SPONSORING/MONITORING AGENCY REPORT NUMBER**

**11. SUPPLEMENTARY NOTES**
Advisor: Major Michael A. Temple
michael.temple@afit.af.mil
ph: 937-255-3636 x 4703

**12a. DISTRIBUTION AVAILABILITY STATEMENT**

Approved for public release; distribution unlimited

**12b. DISTRIBUTION CODE**

**13. ABSTRACT** *(Maximum 200 words)*

This research proposes and evaluates a novel technique for detecting LPI/LPD communication signals using a digital receiver primarily designed to detect radar signals, such as a Radar Warning Receiver (RWR) or an Electronic Support Measures (ESM) receiver.

The proposed Cyclic Spectrum Analysis (CSA) receiver is a robust detector that takes advantage of the spectral correlation properties of second-order cyclostationary signals. A computationally efficient algorithm is used to estimate the Spectral Correlation Function (SCF). Using state-of-the-art FFT processing, it is expected that the proposed CSA receiver architecture could estimate the entire cyclic spectrum in approximately 0.6 ms. The estimate is then reduced to an energy related test statistic that is valid for all cycle frequencies within the receiver bandwidth. By producing an estimate of the cyclic spectrum, the CSA receiver also benefits post-detection tasks such as signal classification and exploitation.

As modeled, the ideal CSA receiver detection performance is within 1.0 dB of the radiometer in benign signal environments and consistently outperforms the radiometer in adverse signal environments. The effect on detection performance when the CSA receiver is implemented with channelized and quadrature digital receiver architectures is also examined.

**14. SUBJECT TERMS**
Cyclostationarity, Spectral Correlation, LPI, LPD, Signal Detection, Electronic Warfare

**15. NUMBER OF PAGES**
120

**16. PRICE CODE**

| 17. SECURITY CLASSIFICATION OF REPORT | 18. SECURITY CLASSIFICATION OF THIS PAGE | 19. SECURITY CLASSIFICATION OF ABSTRACT | 20. LIMITATION OF ABSTRACT |
|---|---|---|---|
| UNCLASSIFIED | UNCLASSIFIED | UNCLASSIFIED | UL |

AFIT/GE/ENG/99M-11

NON CO-OPERATIVE DETECTION OF

LPI/LPD SIGNALS VIA

CYCLIC SPECTRAL ANALYSIS

THESIS

Presented to the faculty of the Graduate School of Engineering

of the Air Force Institute of Technology

Air University

In Partial Fulfillment of the

Requirements for the Degree of

Master of Science of Electrical Engineering

Andrew M. Gillman, B.Eng.

Flight Lieutenant, Royal Australian Air Force

March, 1999

NON CO-OPERATIVE DETECTION OF

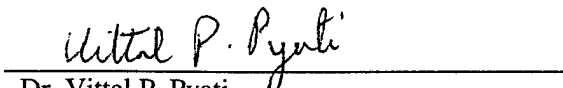LPI/LPD SIGNALS VIA

CYCLIC SPECTRAL ANALYSIS

Andrew M. Gillman, B.Eng.

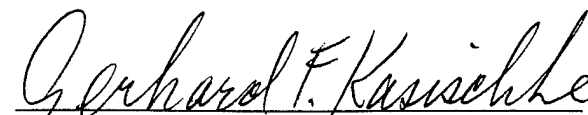Flight Lieutenant, Royal Australian Air Force

Approved:

_____

Michael A. Temple, Ph.D., Major, USAF
Committee Chairman

3 Nov 99
date

_____

Dr. Vittal P. Pyati
Committee Member

3 Mar 99
date

_____

Mr. Gerhard F. Kasischke
Committee Member

3 Mar 99
date

## Acknowledgements

# Table of Contents

v

# List of Figures

**Abstract**

This research proposes and evaluates a novel technique for detecting LPI/LPD communication signals using a digital receiver primarily designed to detect radar signals, such as a Radar Warning Receiver (RWR) or an Electronic Support Measures (ESM) receiver. The inherent flexibility of the digital receiver allows the incorporation of detection and estimation methods that would otherwise require dedicated hardware.

The proposed Cyclic Spectrum Analysis (CSA) receiver is a robust detector that takes advantage of the spectral correlation properties of second-order cyclostationary signals. A computationally efficient algorithm is used to estimate the Spectral Correlation Function (SCF). The estimate is then reduced to an energy related test statistic that is valid for all cycle frequencies within the receiver bandwidth. By producing an estimate of the cyclic spectrum, the CSA receiver also benefits post-detection tasks such as signal classification and exploitation.

Using state-of-the-art FFT processing, it is expected that the proposed CSA receiver architecture could estimate the entire cyclic spectrum in approximately 0.6 ms. As modeled, the ideal CSA receiver detection performance is within 1.0 dB of the radiometer in benign signal environments and consistently outperforms the radiometer in adverse signal environments. For example, in the presence of nonstationary noise, the CSA receiver performance is relatively unaffected whereas the radiometer performance is degraded by as much as 10 dB.

The effect on detection performance when the CSA receiver is implemented with channelized and quadrature digital receiver architectures is also examined. The channelized receiver implementation performs as well as the ideal CSA receiver, and more significantly, detection performance is independent of the channel selected. The quadrature receiver implementation outperforms the ideal CSA receiver in all cases by approximately 1 dB. As the signal bandwidth increases relative to the receiver bandwidth, the quadrature receiver performance approaches that of the ideal receiver.

NON CO-OPERATIVE DETECTION OF

LPI/LPD SIGNALS VIA

CYCLIC SPECTRAL ANALYSIS

## 1. Introduction

### 1.1 Research Motivation

Historically, the Electronic Warfare (EW) community has treated the problems of detecting communication and radar signals as distinct. The design considerations in detecting these signals were so different that non co-operative (or unintended) radar receivers, such as a Radar Warning Receiver (RWR) or Electronic Support Measures (ESM) receiver, bear little or no resemblance to a non co-operative communication receiver. However, despite the fundamental differences between radar and communications, from a non co-operative point of view the two areas are becoming increasingly similar. Communication systems are now using frequencies previously used exclusively by radar; both radar and communication systems are employing similar modulation techniques to reduce the probability of detection or interception. In terms of frequency coverage, it should be possible for an RWR or ESM receiver to detect a communication signal. Indeed, for certain modulation techniques, the linear non co-operative radar receiver can employ the same detection strategy for both radar and communication signals.

However, communication systems are increasingly using modulation techniques designed to reduce the probability of detection or interception by an unintended receiver. Such signals are known as Low Probability of Detection (LPD), or Interception (LPI) signals. Once the principal domain of covert military communication systems, these techniques are becoming commonplace amongst commercial communication systems as they also reduce the probability the signals will

1

be interfered with. One of the most common techniques spreads the spectral components of transmitted signals over a bandwidth much larger than necessary. This is termed Spread Spectrum (SS) and can be achieved through either multiplying the data with a spreading code (direct sequence) or by randomly offsetting the center frequency of the signal (frequency hop). Because the unintended receiver (or non co-operative receiver) has no knowledge of the particular spreading code, it does not have the ability to "de-spread" the signal and therefore, is presented with a significantly reduced Signal-to-Noise Ratio (SNR) compared to the co-operative receiver. So while the communication and radar frequency bands may overlap, the traditional non co-operative radar receiver which is constrained to linear detection due to the microwave hardware, is unable to detect these lower SNR signals. Even receivers employing Digital Signal Processing (DSP) techniques following detection are not be able to detect negative SNR signals.

With advances in Analog-to-Digital Converter (ADC) technology, the logical move in ESM and RWR receivers has been towards the use of digital receivers which sample the received signal at IF prior to detection. By incorporating DSP in the detection stage, greater design flexibility is achieved, allowing detection and estimation that would have previously required dedicated hardware components.

Techniques designed exclusively for detecting LPI/LPD communication signals can be broken down into two basic categories, energy detection and cyclic feature detection techniques. These two techniques are derived by modeling the signal as a random process with detection accomplished via application of the Likelihood Ratio Test (LRT).

The traditional method for addressing the problem of detecting weak signals in noise is through modeling the signal as a stationary stochastic process. This technique yields the *radiometer* which produces an approximation to the exact optimal detector solution. However, because the radiometer simply compares total energy levels, it does not perform well in

environments with varying energy levels, i.e. environments with varying noise power levels or narrowband interference.

It is now well established that, in fact, most communication and radar signals are more appropriately modeled as *cyclostationary* stochastic processes. Cyclostationary processes differ from stationary processes in that they have periodic statistics; processes with periodic second order statistics also exhibit spectral correlation. When the problem of detecting weak signals in noise is applied to the second order cyclostationary model, it has been shown that the optimal detectors are cyclic feature detectors centered around what is known as the *Spectral Correlation Function* (SCF), the cyclic equivalent to the Power Spectral Density (PSD) [12]. Those LPI schemes that do not have second order features, such as transfer domain modulations, are not considered in this research.

There are essentially two important advantages of cyclic spectral analysis over conventional power spectrum analysis. The first is an enhanced discriminatory capability, i.e. signals with overlapping power spectrum features can have non-overlapping cyclic spectrum features. The second advantage is that the cyclic spectrum contains more information about signal characteristics than the power spectrum. Not only are chip rate, bandwidth and timing information more easily determined by cyclic spectral analysis, but specific modulation types exhibit distinct cyclic features. These advantages mean that cyclic feature detectors perform better than traditional techniques, such as radiometry, in adverse signal environments.

The optimal single-cycle Maximum Likelihood (ML) cyclic feature detector has been derived and its performance evaluated [15]. However, it has proven impractical for non co-operative detection. The detector is known as *single-cycle* because analysis is restricted to one particular cycle frequency where a strong cyclic feature is expected. This entails having knowledge of the signal parameters, such as chip rate, or searching across all possible cyclic

frequencies. In a truly non co-operative receiver single-cycle analysis would need to be combined with a searching strategy across all spectral frequencies of interest.

## 1.2 Research Goal

The goal of this research is to:

1. Propose a method of detecting LPD/LPI communication signals using a non co-operative digital receiver;

2. Evaluate the performance of this detection technique through simulation in benign and adverse signal environments, comparing results to the radiometer; and

3. Determine the technique's effectiveness when combined with typical digital receiver architectures.

## 1.3 Thesis Organization

Chapter 2 introduces background theory and presents a review of current literature. A brief introduction to the theory of cyclostationarity is presented, along with both the probabilistic definition and a deterministic interpretation of the Spectral Correlation Function (SCF). Spectral estimation theory as it relates to both Power Spectral Density (PSD) estimation and SCF estimation is discussed. The basics of detection theory are covered, including the detection of weak signals in noise from both a stationary and a cyclostationary viewpoint. Various optimal and sub-optimal detectors are derived, their performance analyzed and compared .

Chapter 3 explains the Cyclic Spectrum Analyzer (CSA) receiver design. The concept of the single-cycle detector derived in Chapter 2 is extended and its relationship to the CSA receiver is explained. An overview of the CSA receiver is presented with each component discussed in detail. Three different digital receiver architectures are covered, the *ideal, channelized* and *quadrature digital* receiver. Each is introduced and the algorithm used to estimate the SCF is presented. Possible methods for reducing the SCF to a test statistic that can be easily calculated,

stored and compared to a threshold are discussed. Additionally, the limitations and assumptions necessary are covered.

Chapter 4 presents the results of simulating the CSA receiver under various conditions. Initially, a number of simulations are carried out to determine optimal operating parameters for the algorithm and to determine the best method of data reduction. The performance of the Ideal CSA Receiver is then determined through simulation and compared to the radiometer in the presence of stationary noise, nonstationary noise and narrowband interference. The detection performance of the Channelized and Quadrature CSA Receivers is considered. The effect of the differing frequency response on the detection performance of different channels is quantified. Expressions are derived for the received SCF for a complex or a real quadrature receiver. Based on these expressions, the optimum input method is selected and the detection performance under benign and adverse conditions is simulated. The effects of non-ideal bandpass filters on detection performance is quantified.

Finally, Chapter 5 provides a summary of the results, a conclusion and recommendations for further research in this area. The Appendix contains a list of symbols and terminology used throughout this thesis.

# 2. Background

## 2.1 Introduction

This chapter introduces the background theory used throughout the remainder of the thesis and presents a survey of current literature. The concept of cyclostationarity is introduced in Section 2.2, including both the probabilistic definition and a deterministic interpretation of the Spectral Correlation Function (SCF). In Section 2.2.3, spectral estimation theory is discussed. Concepts of the periodogram and cyclic periodogram, and their relationships to Power Spectral Density and the SCF, respectively, are explained. Different algorithms for estimating the SCF are also briefly discussed.

The basics of statistical detection theory are covered in Section 2.4. The derivation of optimal and sub-optimal detector structures for the detection of stationary weak signals in noise is presented. Detectors derived from the Generalized Likelihood Ratio Test (GLRT) are covered, including approximations that lead to the radiometer, or energy detector. Radiometric performance in relation to GLRT derived detectors is also examined and the drawbacks of radiometric detection are examined. The GLRT is then applied to the cyclostationary signal model to produce both optimal and sub-optimal cyclic feature detectors.

The notation and terminology used throughout this thesis, particularly Sections 2.2-2.4, is quite complex. The notation involves the use of time series representations and a generalized theory to allow both analog and digital implementations. A cross-referenced list of notation and terminology is provided in the Appendix.

## 2.2 Cyclostationary Fundamentals

A cyclostationary signal, or process, is characterized by the fact that it exhibits spectral correlation. The spectral correlation is not immediately obvious through conventional spectral

analysis using the PSD. Therefore, cyclic spectral analysis is employed via the Spectral Correlation Function (SCF). The SCF can be explained from both a probabilistic [14,18] and a deterministic viewpoint [10,13]. The probabilistic model is a more traditional approach and gives strong insight into the relationship between stationary and cyclostationary processes. However, it is argued that the difficulty in applying the stochastic-process model to statistical spectral analysis is that the concept of the ensemble, or population, is not always appropriate in these applications [13]. Sometimes only one realization of the ensemble is available and in these cases, the time-series model (non-probabilistic or deterministic model) is more intuitive. Certainly, the deterministic model is useful for visualizing the formation of the SCF.

The assumption of ergodicity allows the transition between the two approaches. Ergodicity requires a very specific set of properties for both the stochastic process and the time-series; specifically, all ensemble averages of the stochastic process and all time-averages of the time-series must exist, and the corresponding time and ensemble averages must be equal as the length of the time-series approaches infinity. However, for the detection schemes discussed here, only second order cyclostationarity is of concern. It is a reasonable assumption for most communication signals that the first- and second-order statistics satisfy the ergodic property, therefore, the probabilistic and deterministic views are equivalent [41].

### 2.2.1 Probabilistic View

This section summarizes the theory found in [14,18] unless otherwise noted. Given a wide-sense stationary (WSS) random or stochastic process, $x(t)$, if the autocorrelation function is periodic the process is known as wide-sense (second order) cyclostationary. This property is quite common in man-made signals, especially communication and radar waveforms. The autocorrelation function for a cyclostationary signal, $x(t)$, can be written in terms of its Fourier components as

$$R_x(t, t+\tau) \equiv E\left[x(t)x^*(t+\tau)\right]$$
$$= \sum_\alpha R_x^\alpha(\tau)e^{j2\pi\alpha t} \tag{2-1}$$

where $E[\cdot]$ is the expected value operator, $T_0$ is the period, and frequency components, $\alpha$, are given by $\alpha = n/T_0$. The Fourier coefficients, $R_x^\alpha(\tau)$, may be calculated from

$$R_x^\alpha(\tau) \equiv \frac{1}{T_0}\int_{-T_0/2}^{T_0/2} R_x(t, t+\tau)e^{-j2\pi\alpha t}\, dt \tag{2-2}$$

this equation is also known as the Cyclic Autocorrelation Function (CAF). Those frequencies $\alpha$ for which the cyclic autocorrelation function is non-zero are termed the set of cycle frequencies. Using the cyclic Wiener-Khinchin theorem  the Spectral Correlation Function (SCF) may be determined by taking the Fourier transform of the CAF in Eqn. (2-2), yielding

$$S_x^\alpha(f) \equiv \int_{-\infty}^{\infty} R_x^\alpha(\tau)e^{-j2\pi f\tau}\, d\tau \tag{2-3}$$

The SCF is generally plotted on the *bi-frequency plane* as a function of spectral frequency, $f$, and cyclic frequency, $\alpha$. The SCF exhibits a great deal of symmetry. For real signals it is an even symmetric function of $f$ and a Hermitian symmetric function of $\alpha$, indicated by

$$S_x^\alpha(-f) = S_x^\alpha(f)$$
$$S_x^{-\alpha}(f) = S_x^\alpha(f)^* \tag{2-4}$$

To determine the functional form for the CAF and SCF for purely stationary[1] processes, the above expressions are simply evaluated at $\alpha = 0$, yielding

---

[1] In order to distinguish between stationary processes that exhibit cyclostationarity and those that do not, a stationary process that does not exhibit cyclostationarity is termed a *purely stationary* process.

8

$$S_x^\alpha(f)\Big|_{\alpha=0} \equiv \int_{-\infty}^{\infty} R_x^\alpha(\tau)e^{-j2\pi f\tau}\,d\tau\Big|_{\alpha=0}$$

$$= \frac{1}{T_0}\int_{-\infty}^{\infty}\int_{-T_0/2}^{T_0/2} R_x(\tau)\,e^{-j2\pi f\tau}\,dt\,d\tau \qquad (2\text{-}5)$$

$$= \int_{-\infty}^{\infty} R_x(\tau)e^{-j2\pi f\tau}\,d\tau$$

$$= S_x(f)$$

Therefore, for a purely stationary random process, $x(t)$, the CAF reduces to the autocorrelation function, $R_x(t)$, and the SCF reduces to the Power Spectral Density (PSD), $S_x(f)$.

### 2.2.2 Deterministic View

The deterministic approach involves using a time-series, interpreted probabilistically as one finite time realization of an ensemble. The problems associated with only having access to a limited portion of the time series are explored further in Section 2.2.3. However, when developing the theory of spectral correlation it is appropriate to take the limiting form of the time-series, i.e. consider an infinitely long sample. A time-series is normally denoted by a $T$ subscript which refers to the length of the time-series, but, as the length of the time-series approaches infinity the subscript is dropped. Additionally, the statistics formed from a finite time-series are also denoted by subscript $T$ and as the length of the time-series approaches infinity, the subscript is dropped. The terminology '*limit*' is introduced to differentiate between deterministic and probabilistic definitions. The *limit cyclic spectrum* (the deterministic counterpart to the SCF) is developed as follows [13]. The *limit cyclic autocorrelation* function of an infinitely long time series $x(t)$ is defined as

$$\hat{R}_x^\alpha(\tau) \equiv \lim_{T\to\infty}\frac{1}{T}\int_{-T/2}^{T/2} x\left(t+\frac{\tau}{2}\right)x^*\left(t-\frac{\tau}{2}\right)e^{-j2\pi\alpha t}\,dt \qquad (2\text{-}1)$$

Defining two frequency shifted versions of $x(t)$ as

9

$$u(t) \equiv x(t)e^{-j\pi\alpha t}$$
$$v(t) \equiv x(t)e^{j\pi\alpha t}$$

(2-2)

then the *limit cyclic cross correlation* becomes

$$\hat{R}_x^\alpha(\tau) \equiv \lim_{T \to \infty} \frac{1}{T} \int_{-T/2}^{T/2} u\left(t + \frac{\tau}{2}\right) v^*\left(t - \frac{\tau}{2}\right) dt$$

(2-3)

The Fourier transform of this can be written as

$$\Im\left[\hat{R}_x^\alpha(\tau)\right] \equiv \hat{S}_{uv}(f)$$

(2-4)

which is known as the *limit cross spectral correlation* between $u(t)$ and $v(t)$, i.e. two frequency shifted versions of $x(t)$. The *limit cross spectral correlation* is written as the *limit cyclic spectrum* when the total frequency shift, $\alpha$, is introduced as an index

$$\hat{S}_{uv}(f) \equiv \hat{S}_x^\alpha(f)$$

(2-5)

As mentioned previously for a cycloergodic stochastic process, the ensemble averages are equal to the time-averages as the length of the time-series approaches infinity. The relationship between the cyclic spectrum formed with a non-infinite time series and the SCF is discussed in Section 2.2.3. However, for a stochastic process which is cycloergodic in the CAF, then the SCF and the *limit cyclic spectrum* are equal

$$S_x^\alpha(f) = \hat{S}_x^\alpha(f)$$

(2-6)

Therefore the SCF can be interpreted as the measure, or degree, of correlation for two frequency components separated by $\alpha$. The equation for calculating the SCF of a low-pass signal can be represented by Figure 2-1. The notation $\langle \cdot \rangle_T$ simply refers to a time averaging process.
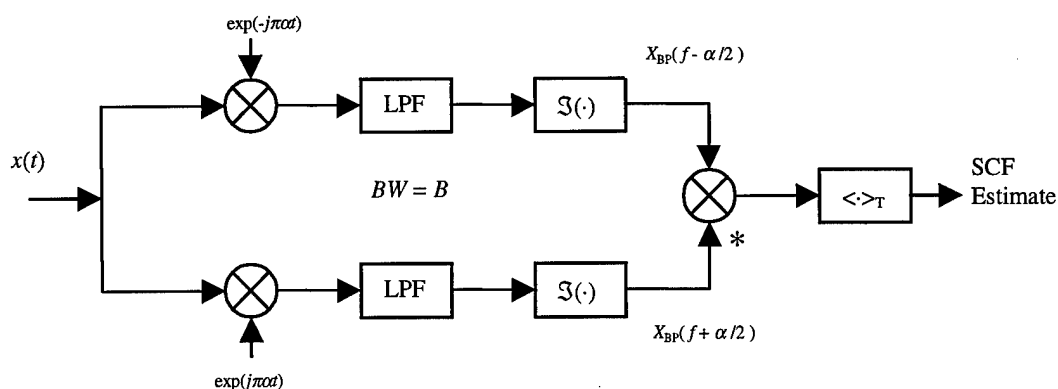
Figure 2-1. Frequency Domain Representation of the Spectral Correlation Function

Figure 2-2 illustrates the steps involved in computing the spectral correlation of an arbitrarily modulated carrier. The figure shows the magnitude of the original low pass spectra $X(f)$, the low pass shifted spectra, $V(f)$ and $U(f)$, and the resultant SCF magnitude for $\alpha = 2f_0$. The BPF has a bandwidth of 25 MHz, and the carrier frequency, $f_0$, is 12.5 MHz.
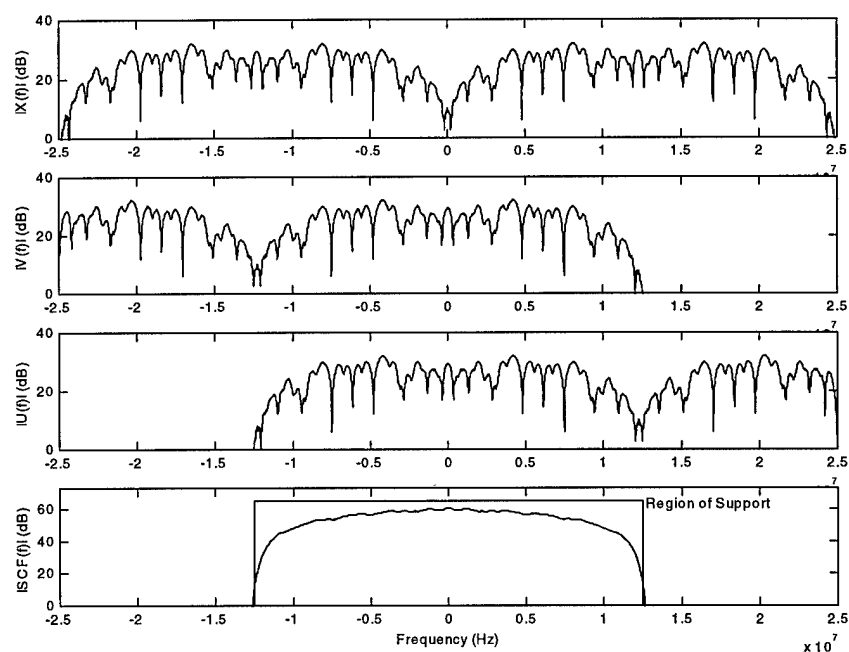


Figure 2-2. Example of Spectral Correlation Evaluated at $\alpha = 2f_0$

11

It is important to note that for a lowpass signal of bandwidth of $B$, the SCF has a limited *region of support* (area of non-zero correlation) in the bi-frequency plane. This can be visualized using Figure 2-2 by moving the two shifted spectra further apart. As $\alpha$ approaches $2B$, the region of support for the SCF (indicated on the lower plot) approaches zero. This leads to a diamond shaped region of support in the bi-frequency plane as illustrated in Figure 2-3.
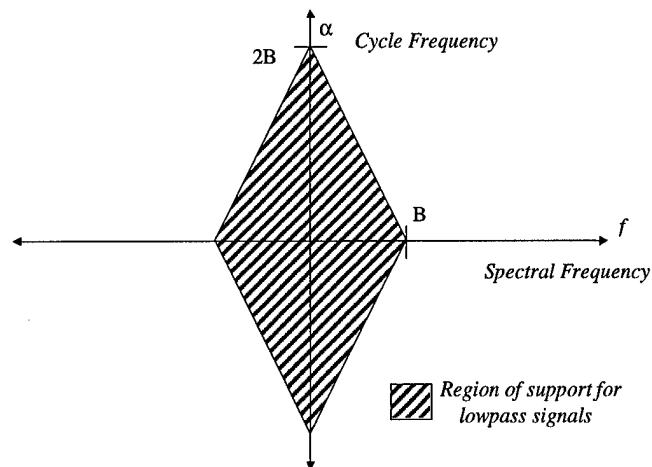


Figure 2-3. Region of Support in the Bi-Frequency Plane for Lowpass Signals

### 2.2.3 Advantages of Cyclic Spectral Analysis

Cyclic spectral analysis is used in many applications, including weak signal detection, waveform classification, parameter estimation and spatial filtering. There are essentially two important advantages of cyclic spectral analysis over conventional power spectrum analysis. The first is the discriminatory capability of cyclic spectral analysis. Signals with overlapping features in the power spectrum can have non-overlapping features in the cyclic spectrum. For example, Eqn. (2-5) shows that the SCF for a purely stationary process only exists at $\alpha = 0$, therefore non-zero cyclic frequency analysis of a signal will reveal the cyclic features of that signal without any component due to the stationary process. The second main advantage is that the cyclic spectrum gives more information about the signal characteristics than the power spectrum. Not only are the

chip rate, bandwidth and timing information more easily determined, but specific modulation types will have distinct cyclic features. [2,11]

## 2.3 Spectral Estimation Theory

Given the usefulness of the SCF, there is naturally a requirement to try and determine the cyclic features for received signals, or to estimate the SCF. The process and theory behind SCF estimation is closely related to PSD estimation. Therefore, this section covers both SCF and PSD estimation.

There are two distinct problems to overcome when estimating the PSD or SCF probabilistic functions of Section 2.2.1. First, the estimator only has access to a finite length time series, $x_T(t)$. Second, the estimator can only formulate time-averages and cannot actually calculate any ensemble averages. As discussed previously, the ergodic property only relates to the limiting form of the time-averages. Therefore spectral estimation theory can be thought of as the study of techniques used to counteract the loss of information caused by processing a non-infinite time series or sampled signal and approximating the expected value operation. The following section summarizes basic spectral estimation theory covered in [13,24,23] unless otherwise referenced.

Spectral estimation methods can be broken into two categories: the so-called traditional methods which are based on direct use of the Fourier transform and are variants of the periodogram, and the more modern methods which are based on parametric modeling and include Auto-Regressive (AR) and Auto-Regressive Moving Average (ARMA) models.

Traditional methods are derived from an alternative definition of the PSD. According to the Wiener-Khinchin theorem, the PSD, $S_x(f)$, for a stationary stochastic process $x(t)$ is the Fourier transform of its autocorrelation function $R_x(\tau)$ and is given by

$$S_x(f) \equiv \int_{-\infty}^{\infty} R_x(\tau) e^{-j2\pi f \tau} d\tau \qquad (2\text{-}1)$$

13

However, it can also be expressed as

$$S_x(f) = \lim_{T \to \infty} E\left\{ \frac{1}{T} \left| \int_{-T/2}^{T/2} x(t) e^{-j2\pi f t} dt \right|^2 \right\} \tag{2-13}$$

which is equivalent to (2-12) assuming the autocorrelation function decays sufficiently rapidly. This form of the PSD tends to be easier to implement and is the basis of the periodogram.

### 2.3.1 The Periodogram

The *periodogram*, $S_{x_T}(f)$, is defined as the squared magnitude of the Fourier transform of a time series, $x_T(t)$, normalized by the length of the segment, $T$

$$S_{x_T}(f) \equiv \frac{1}{T} \left| \int_{-T/2}^{T/2} x(t) e^{-j2\pi f t} dt \right|^2 \tag{2-14}$$

The main advantage of the periodogram is its relation with the Discrete Fourier Transform (DFT) when implemented with sampled data. If the time series $x_T(t)$ is sampled at $f_s = 1/T_s$ to form $N = \lfloor T f_s \rfloor$ samples where $\lfloor \cdot \rfloor$ represents the integer part, then Eqn. (2-14) becomes

$$S_{x_T}(f) \equiv \frac{1}{N} \left| \sum_{k=0}^{N-1} x_T(kT_s) e^{-j2\pi f(kT_s)} \right|^2 \tag{2-15}$$

which can also be written in the form of a DFT as

$$S_{x_T}[k] \equiv \frac{1}{N} \left| \sum_{n=0}^{N-1} x[n] e^{\frac{-j2\pi kn}{N}} \right|^2 \tag{2-16}$$

The periodogram can therefore be efficiently computed using a Fast Fourier Transform (FFT). This form of the periodogram in Eqn. (2-16) is more commonly seen in general spectral estimation literature than its continuous time counterpart of Eqn. (2-14).

It is clear by comparing the periodogram and the PSD definitions, Eqns. (2-14) and (2-13) respectively, that the periodogram will suffer due to the lack of the expected value

14

This can be quantified by analyzing the quality of the periodogram as an estimator. The quality of any estimator can be determined by calculating its mean and variance. Ideally, an estimator should be unbiased (mean of the estimate approaches the mean of the true function) and the variance of the estimator should approach the Cramer-Rao lower bound. The average value of the periodogram approaches the true PSD as the length of the data segment approaches infinity such that

$$\lim_{T \to \infty} E\{S_{x_T}(f)\} = S_x(f) \tag{2-4}$$

so the periodogram is asymptotically unbiased. However, the variance is given by

$$\text{var}[S_{x_T}(f)] = S_x^2(f) \tag{2-5}$$

which is independent of segment length, $T$. In other words, the periodogram is an unreliable estimator because increasing the segment length improves the spectral resolution while variance remains constant. Methods for reducing the variance and compensating for the lack of expected value operation are discussed in the next section.

Other forms of the periodogram include the *time variant periodogram* and the *cross-periodogram*. The *time variant periodogram* can be used as an estimate for Time-Frequency Distributions (TFD's) such as the Wigner-Ville distribution [31,29]. TFD's are useful since they describe how the spectral content of a signal changes with time. The *time variant periodogram* is simply an extension of Eqn. (2-1) and is given by

$$S_{x_T}(t,f) \equiv \frac{1}{T} |X_T(t,f)|^2 \tag{2-6}$$

where $X_T(t,f)$ represents the sliding time-finite Fourier transform of $x(t)$

$$X_T(t,f) \equiv \int_{t-T/2}^{t+T/2} x(w) e^{-j2\pi f w} dw \tag{2-7}$$

15

The *cross-periodogram* is a measure of spectral correlation and is used in such fields as propagation path identification and time- and frequency-difference-of-arrival estimation. The *cross-periodogram* is

$$S_{uv_T}(t,f) \equiv \frac{1}{T} U_T(t,f) V_T^*(t,f) \tag{2-8}$$

where $U_T(t,f)$ and $V_T(t,f)$ are the sliding time-finite Fourier transforms as defined in Eqn. (2-7). The cross periodogram is used as a basis for estimating the SCF as discussed in Section 2.3.3.

### 2.3.2  Resolution, Spectral Leakage and Windowing

A number of steps are usually taken to improve the quality of the periodogram as a PSD estimate, including the application of data-tapering windows to reduce spectral leakage and the application of smoothing windows to reduce the variance. Spectral leakage refers to the periodogram responses at frequencies not near the signal frequency. The application of these windowing techniques is examined in terms of the temporal and spectral resolution of the resulting estimate.

To understand the time and frequency resolution of the time variant periodogram, Eqn. (2-6) can be re-written as

$$\begin{aligned}
S_{x_T}(t,f) &= \frac{1}{T} \left| \left[ x_T(t) e^{-j2\pi f t} \right] \otimes a_T(t) \right|^2 \\
&= \frac{1}{T} \left| \left[ X_T(t,f) e^{j2\pi f t} \right] \otimes A_{1/T}(f) \right|^2
\end{aligned} \tag{2-1}$$

where $a_T(t)$ is a rectangle function of width $T$, and $A_{1/T}(f)$ is a sinc function, the Fourier transform of $a_T(t)$. The convolution operation, denoted by $\otimes$, dictates that the width of the rectangle function and the sinc function determine the temporal and spectral resolution of the time-variant periodogram. The temporal resolution $\Delta t$ and spectral resolution $\Delta f$ satisfy the uncertainty relation

16

$$\Delta t \cong T \cong \frac{1}{\Delta f} \qquad (2\text{-}2)$$

The Fourier pair $a_T(t)$ and $A_{1/T}(f)$ are also known as a data tapering or lag windows. There are a number of different windows that can be used instead of the rectangle function (also known as the Dirchlet window) including, the Bartlett window (a triangle), the Hanning and the Hamming windows (variants of raised cosine functions). The spectral resolution and leakage resulting from the application of these windows can be determined from their main-lobe and side-lobe properties. An important property of data windowing is that $\Delta t \Delta f = 1$. In other words, even with a data-tapering window the resultant estimate still has a time-frequency resolution product of unity and the variance of the periodogram remains unaffected.

Windowing of the spectral estimator can also be used to provide a better PSD estimate. As discussed in the previous section, the periodogram is an unreliable estimator because the variance is independent of the record length. There are ways of using windows to reduce the variance by smoothing or averaging the estimate in time or frequency, however, this usually means an increase in bias [38].

Temporal smoothing can be thought of as the convolution of the periodogram with a window $u_{\Delta t}(t)$ of width $\Delta t$,

$$S_{x_{1/\Delta f}}(t, f)_{\Delta t} \equiv S_{x_T}(t, f) \otimes u_{\Delta t}(t) \qquad (2\text{-}3)$$

resulting in a temporal resolution $\Delta t$ determined by the width of $u_{\Delta t}(t)$ with the spectral resolution $\Delta f$ still related to the data segment length, $T$ per Eqn. (2-2). The time-frequency resolution product is greater than unity because $\Delta t \gg T$. The Bartlett-Welch method is a computationally efficient digital implementation of a time-smoothed time-variant periodogram. It essentially involves averaging over a number of periodograms that overlap in time and the use of data tapering windows to reduce spectral leakage. The temporal-spectral resolution product is $\Delta t \Delta f \cong$

17

*M*, where *M* is half the number of periodograms averaged and the variance of the estimator is inversely proportional to *M*.

Spectral smoothing is achieved by convoluting the periodogram with the Fourier transform of $u_{\Delta t}(t)$, a sinc squared window, $z_{\Delta f}(f)$

$$S_{x_{\Delta t}}(t,f)_{\Delta f} \equiv S_{x_T}(t,f) \otimes z_{\Delta f}(f) \tag{2-4}$$

where the spectral resolution is determined by the null to null width of $z_{\Delta f}(f)$, and the temporal resolution is given by the data segment length per Eqn. (2-2). The Wiener-Daniell method is a popular digital implementation of a spectrally-smoothed time-variant periodogram. As with the Bartlett-Welch method, the reduction in the variance of the estimator is proportional to the temporal-spectral resolution product.

It can be shown[13] that spectral and temporal smoothing operations are approximately equivalent

$$S_{x_{1/\Delta f}}(t,f)_{\Delta t} \cong S_{x_{\Delta t}}(t,f)_{\Delta f}, \qquad \Delta t \Delta f >> 1 \tag{2-5}$$

and that for typical data tapering windows where $\int_{-\infty}^{\infty} |a_T(t)|^2 dt = 1$, they are related to the statistical definition[2] of the PSD, Eqn. (2-5), as

$$\begin{aligned} S_x(f) &= \lim_{\Delta f \to 0} \lim_{\Delta t \to \infty} S_{x_{1/\Delta f}}(t,f)_{\Delta t} \\ &= \lim_{\Delta f \to 0} \lim_{\Delta t \to \infty} S_{x_{\Delta t}}(t,f)_{\Delta f} \end{aligned} \tag{2-6}$$

To summarize, based on careful evaluation of required temporal and spectral resolution, spectral leakage, and estimator bias and variance, both a data tapering window, *a(t)*, and either

---

[2] Strictly speaking the limiting form of the periodogram is equal to the limit spectrum, which for the case of a stationary and ergodic random process is equivalent to the statistical definition of the PSD.

spectral or temporal smoothing may be used to form a much better PSD estimate than the periodogram of Eqn. (2-1).

### 2.3.3 The Cyclic Periodogram

To obtain an estimate of $S_x^\alpha(t,f)$ (2-3) the time-variant cross periodogram is modified slightly and the *time variant cyclic periodogram* is formed

$$S_{x_T}^\alpha(t,f) \equiv \frac{1}{T} X_T\left(t, f + \frac{\alpha}{2}\right) X_T^*\left(t, f - \frac{\alpha}{2}\right) \tag{2-1}$$

where $X_T(t, f)$ and $X_T(t, f)$ are the sliding-time finite Fourier transforms as defined in (2-7). As with the time-variant periodogram, spectral and temporal smoothing are required to produce a reliable estimate[3], and the smoothed estimates are approximately equal.

$$
\begin{aligned}
S_{x_{1/\Delta f}}^\alpha(t,f)_{\Delta t} &\equiv S_{x_{1/\Delta f}}^\alpha(t,f) \otimes u_{\Delta t}(t) \\
&\cong S_{x_{\Delta t}}^\alpha(t,f) \otimes z_{1/T}(f) \equiv S_{x_{\Delta t}}^\alpha(t,f)_{\Delta f}
\end{aligned}
\tag{2-2}
$$

The cyclic resolution is only related to the temporal resolution of the spectra

$$\Delta\alpha \cong \frac{1}{\Delta t} \tag{2-3}$$

Therefore, for a reliable estimate, the cyclic resolution must be much finer than the spectral resolution.

$$\Delta\alpha \ll \Delta f \tag{2-4}$$

---

[3] Not only does analysis of the variance show that the periodogram is an unreliable estimator, but *Grenander's uncertainty condition* also states that for a reliable estimate $\Delta t \Delta f \gg 1$ for a time-variant cross periodogram. The only way to get this is to introduce substantial spectral or temporal smoothing such that $\Delta t \gg T$.

As with the time-variant periodogram, with smoothing such that

$$\frac{1}{\Delta\alpha} \cong \Delta t >> T \cong \frac{1}{\Delta f} \tag{2-5}$$

the statistical definition of the SCF is related to the limit of time-variant cyclic periodogram as

$$
\begin{aligned}
S_x^\alpha(f) &= \lim_{\Delta f \to 0} \lim_{\Delta t \to \infty} S_{x_{1/\Delta f}}^\alpha(t,f)_{\Delta t} \\
&= \lim_{\Delta f \to 0} \lim_{\Delta t \to \infty} S_{x_{\Delta t}}^\alpha(t,f)_{\Delta f}
\end{aligned}
\tag{2-6}
$$

Digital implementations of both the time and frequency smoothed time-variant cyclic periodogram are discussed in the following sections.

In addition to the time and frequency smoothed time-variant cyclic periodogram, the Autocorrelated Cyclic Periodogram (ACP) can also be used to estimate the SCF. The main advantage of the ACP is that the cyclic resolution is not given by (2-3), rather is shown to be $\Delta\alpha \cong 1/T$. This means that there are less stringent requirements for cyclic frequency resolution and for a given performance, the ACP is more efficient than the time-smoothed time-variant cyclic periodogram. However, the ACP has not yet been developed to the algorithm level [53].

### 2.3.4 Spectral Correlation Function Estimation Algorithms

Both the time-smoothed and frequency-smoothed time variant cyclic periodograms can be implemented fairly simply (for example Figure 2-1), but both methods are very inefficient. There has been a substantial amount of work done to modify the underlying equations to increase efficiency and accuracy of the estimate [39,3]. Most of this work revolves around using the FFT to perform channelization and smoothing. The end result has been the development of several different algorithms, each suited for a particular purpose. Variants of the time-smoothed cyclic periodogram are well suited for efficient estimation over the entire bi-frequency plane, whereas,

variants derived from the frequency-smoothed cyclic periodogram are more suited for estimating the SCF at particular cyclic frequencies.

## 2.4  Statistical Detection Theory

The basics of statistical detection theory are presented in this section.  Additionally, the problem of detecting weak signals in the presence of noise is examined from both a stationary and a cyclostationary viewpoint.

### 2.4.1  Detection Fundamentals

To detect the presence of a Signal of Interest (SOI), a detector must decide between the null hypothesis ($H_0$), corresponding to the noise only case, and the alternate hypothesis ($H_1$) which is the signal present case.  These hypotheses can be represented as

$$
\begin{aligned}
H_1 &: r(t) = s(t) + n(t) \\
H_0 &: r(t) = n(t)
\end{aligned} \qquad 0 \leq t \leq T \tag{2-1}
$$

where $T$ is the observation time, $s(t)$ is the SOI and $n(t)$ includes everything else in the collection environment, such as noise and interference.

The detector output can be represented by a test statistic, $\lambda$, which is essentially a function of the received signal, and compared to a threshold to determine which hypothesis is chosen.  If $\lambda$ is greater that the threshold value, $\lambda_0$, then the alternate hypothesis ($H_1$) is chosen and the signal is declared present.  Conversely, if $\lambda$ is less than $\lambda_0$, then the null hypothesis ($H_0$) is chosen and the signal is declared not present.  This can be represented mathematically as

$$
G[r(t)] = \lambda \underset{H_0}{\overset{H_1}{\gtrless}} \lambda_0 \tag{2-2}
$$

where $G(\cdot)$ represents the detector structure.

The performance of any detector may be described by the probability of false alarm ($P_{FA}$) and probability of detection ($P_D$). A *false alarm* occurs any time $\lambda$ exceeds the threshold given $H_0$ is true. Obviously, *detection* occurs when $\lambda$ exceeds the threshold given $H_1$ is true. The probability of these two events may be defined by

$$
\begin{aligned}
P_{FA} &\equiv \mathrm{Prob}\left(\lambda > \lambda_0 \mid H_0\right) \\
P_D &\equiv \mathrm{Prob}\left(\lambda > \lambda_0 \mid H_1\right)
\end{aligned}
\tag{2-3}
$$

The relationship between $P_{FA}$ and $P_D$ can be mathematically described using either the deflection, $d_\lambda$, or input Signal to Noise Ratio, $SNR_{IN}$. The *deflection* is defined as

$$
d_\lambda = \frac{\left| E\left(\lambda \mid H_0\right) - E\left(\lambda \mid H_1\right)\right|}{\sqrt{\mathrm{var}\left(\lambda \mid H_0\right)}}
\tag{2-4}
$$

where $E(\cdot)$ is the expected value operator and var$(\cdot)$ is the variance [51]. When the conditional densities are Gaussian, the deflection relates to $P_{FA}$ and $P_D$ as

$$
d_\lambda^{\,2} = Q^{-1}\left(P_{FA}\right) - Q^{-1}\left(P_D\right)
\tag{2-5}
$$

where $Q^{-1}(\cdot)$ is the inverse complementary error function. The Gaussian case is the only case where deflection completely characterizes detector performance, however, it is often used as an approximate measure for other detection problems. Deflection is closely related to output signal to noise ratio of the detector and is therefore often related to $SNR_{IN}$.

For binary hypothesis testing and known conditional probability densities, the Likelihood Ratio Test (LRT) as specified by the Neyman-Pearson (NP) theorem [22], is given by

$$
\lambda = G[r(t)] = \frac{p\left(\lambda \mid H_1\right)}{p\left(\lambda \mid H_0\right)} \underset{H_0}{\overset{H_1}{\gtrless}} \lambda_0
\tag{2-6}
$$

which can be used to easily determine the test statistic, and the detector structure, $G(\cdot)$. The NP theorem, which maximizes $P_D$ for a given $P_{FA}$, is commonly used for these sorts of signal

detection problems. A detector derived using the LRT method is termed an *optimal* detector. However, quite often some parameters of the conditional densities are unknown, and the detector is presented with a composite binary hypothesis. The Generalized Likelihood Ratio Test (GLRT) can be used, replacing the unknown parameters with their Maximum Likelihood Estimates (MLEs). However, any resulting detector structure would generally[4] be *sub-optimal*. Additionally, not every optimal detector can be physically implemented and must therefore be approximated, resulting in a sub-optimal detector [22,19].

There are two ways of graphically representing detector performance. The first is $P_{FA}$ versus $P_D$ and is termed the Receiver Operating Characteristic (ROC) curve. In this case the input signal-to-noise ratio, $SNR_{IN}$, is held constant and the threshold is varied to produce each set of points on the ROC curve. The second method is to plot $P_D$ versus $SNR_{IN}$ for a given $P_{FA}$. This curve is more representative of the detector's true operation where the threshold is set to yield a fixed $P_{FA}$. This is the primary representation format used throughout this thesis.

### 2.4.2  LRT Derived Detectors for Stationary Signals

Clearly, the most important factor in determining detector structure is knowledge of the conditional densities. In turn, knowledge of the conditional densities requires some a-priori knowledge of the SOI.

The simplest approach is to assume $s(t)$ is a stationary gaussian stochastic process and $n(t)$ is additive white gaussian noise (AWGN). In this case the NP detector is simply [22]

---

[4] Although it is possible for a detector to be optimal for certain values of the unknown parameter, a uniformly most powerful detector for all possible values does not usually exist.

$$G[r(t)] = \int_0^T r^2(t) dt \underset{H_0}{\overset{H_1}{\gtrless}} \lambda_0 \qquad (2\text{-}1)$$

which is known as an *energy detector*, or *radiometer*, and is an optimal detector for the stated conditions.

However, the detector usually has some knowledge of the signals structure. As discussed in Section 1.1, this research is concerned with the detection of LPI/LPD signals, a typical LPI signal with second order features is a Direct Sequence Spread Spectrum (DS-SS) Binary Phase Shift Keyed (BPSK) signal. The remaining part of this section looks at the derivation and performance of non co-operative detectors for this particular signal, and examines whether any benefit can be obtained from knowledge of the signal structure. In this case, the waveform under $H_1$ is represented by

$$r(t) = \sqrt{2P}\, c(t) \cos\left[2\pi f_c t + \phi_0\right] + n(t) \qquad 0 < t < NT_c \qquad (2\text{-}2)$$

where $P$ represents the average power, $f_c$ the carrier frequency, and $\phi_0$ the phase offset. Additionally, $n(t)$ is assumed to be AWGN with a Power Spectral Density (PSD) of $S_n(f) = N_0/2$. The *spreading code*, $c(t)$, is represented by

$$c(t) = \sum_{n=-\infty}^{\infty} c_n\, p(t - nT_c - \varepsilon T_c) \qquad (2\text{-}3)$$

where $p(t)$ is a unit amplitude pulse of duration $T_c$ and the signal epoch or chip offset, $\varepsilon$, is a random variable uniformly distributed between 0 and 1. The iid sequence $\{c_n\}$ represents the product of a pseudo-random, periodic binary sequence (spreading code) and a completely random binary sequence (random data) and is equally likely to take on the values +1 or −1.

To determine an upper bound on performance, co-operative detection of the DS-SS BPSK signal in Eqn. (2-2) is considered, i.e. the signal parameters are completely known. The

resultant NP detector is termed a *matched filter*. Naturally, such a structure is not feasible in non co-operative detection. The deflection for the matched filter can be shown to be [34]

$$d_{MF} = \sqrt{2N\gamma_c} \qquad (2\text{-}4)$$

where

$$\gamma_c = \frac{PT_c}{N_0} \qquad (2\text{-}5)$$

The GLRT is applied in [35,34] which consider the coherent synchronous case, the non-coherent synchronous case and the coherent asynchronous case. A *synchronous detector* is where the chip offset, $\varepsilon$, is zero and a *coherent detector* has perfect knowledge of the carrier phase resulting in the phase offset, $\phi_0$, being zero. Naturally, the most likely scenario for a detector is the non-coherent and asynchronous cases; however, analysis of the coherent and synchronous cases provides a useful theoretical upper bound on non co-operative performance, and it may be possible to use these detectors in conjunction with some form of phase-locked loop or chip synchronizer [36,26]. The application of the GLRT to all of these cases produces detectors which cannot be implemented. In all cases, the resultant sub-optimal approximation is a quadratic device. The deflections for these cases are

$$
\begin{aligned}
d_\lambda \big|_{\varepsilon,\phi_0=0} &= \sqrt{2N}\gamma_c \\
d_\lambda \big|_{\varepsilon=0} &= \sqrt{N}\gamma_c \\
d_\lambda \big|_{\phi_0=0} &= \sqrt{\frac{25}{24}N}\gamma_c
\end{aligned}
\qquad (2\text{-}6)
$$

for the synchronous coherent case, synchronous non-coherent case and asynchronous coherent cases respectively.

From the preceding analysis it can be concluded that the radiometer is the optimum realizable detector for any signal modeled as a stationary gaussian random process. Minor

performance gains can be realized by synchronizing with the code timing and phase coherency. However, the added complexity to accomplish these tasks must be taken into account. Even with these modifications, the resultant sub-optimal structures are still essentially energy detectors.

### 2.4.3 Performance of the Radiometer

As stated previously, the radiometer is a sub-optimal LRT procedure when $s(t)$ is a non-gaussian process. Analysis of the radiometer performance under these sub-optimal conditions is now discussed. A common radiometer architecture typically used is shown in Figure 2-1. The bandwidth of the input bandpass filter, $W_{BP}$, is usually set as narrow as possible, effectively minimizing the input signal to noise ratio.
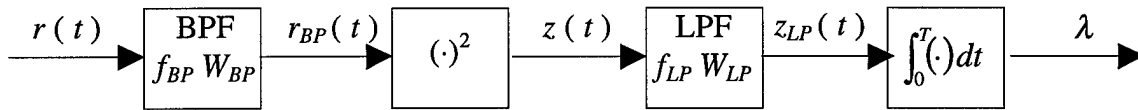


Figure 2-1. Radiometer

Analysis shows that the conditional densities of the test statistic, $\lambda$, have a chi-squared distribution and result in $P_{FA}$ and $P_D$ expressions that cannot be explicitly solved in closed form [48]. There are several different approaches for approximating the distributions so that solutions can be found, including the argument that as the time-bandwidth product ($TW_{BP}$) increases the distributions become asymptotically gaussian as a result of the central-limit theorem. Various radiometer models have been compared to the exact solution in [28]. When the Signal of Interest (SOI) is the BPSK signal given by Eqn. (2-2), the deflection is calculated to be

$$d_\lambda = \sqrt{\frac{N\alpha^4}{W_{BP}T_c}}\gamma_c \tag{2-1}$$

where the attenuation factor $\alpha$ is given by

$$\alpha^2 = \left(\frac{2}{\pi}\right)\int_0^{\pi W_{BP}T_c/2}\left(\frac{\sin x}{x}\right)^2 dx \qquad (2\text{-}2)$$

When the input bandpass filter bandwidth, $W_{BP}$, is chosen such that $W_{BP} \approx 1/T_c$, $\alpha^2$ reduces to

$$\alpha^2 \approx \left(\frac{2}{\pi}\right)\int_0^{\pi/2}\left(\frac{\sin x}{x}\right)^2 dx \approx 0.77 \qquad (2\text{-}3)$$

and the deflection can be rewritten as [34]

$$d_x \approx 0.77\sqrt{N}\gamma_c \qquad (2\text{-}4)$$

The performance of the radiometer and the detectors discussed in the previous section is compared in Figure 2-2. Note that this comparison is for ideal energy detection conditions: stationary additive white Gaussian noise with known $N_0$ and no narrowband interference. The horizontal axis is $E_c/N_0$ which has been previously referred to as $\gamma_c$.
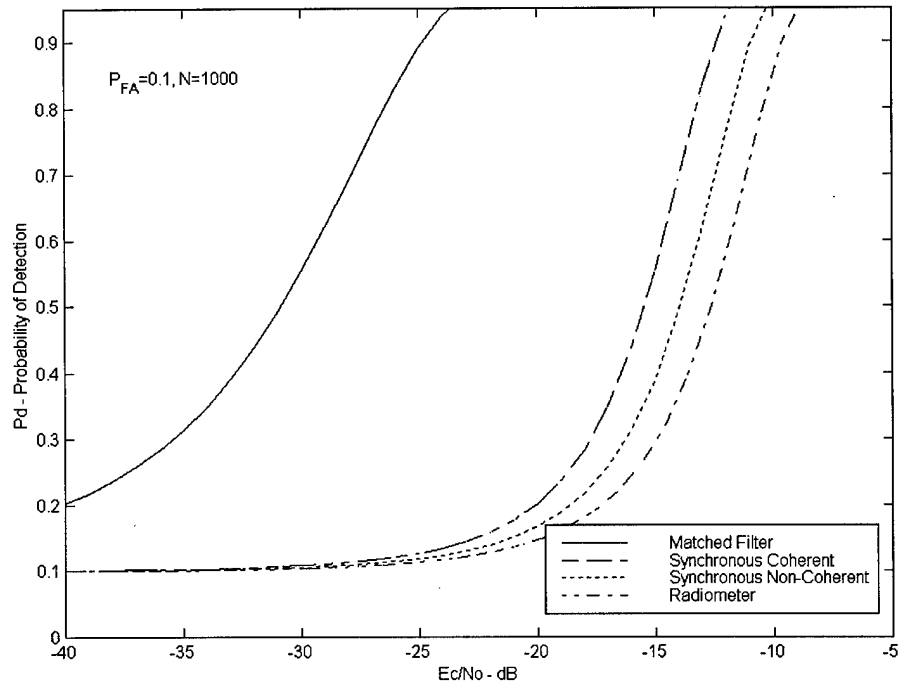


Figure 2-2. Performance Comparison of Energy Detectors

27

### 2.4.4 Disadvantages of Radiometry

Put simply, the task of the radiometer is to distinguish the SOI from background noise and interference purely on the basis of energy measurement. There are two major problems with this method. First, the SOI energy is often easily overwhelmed by the amount of noise and interference in the collection environment. Second, fluctuations within the system itself, such as drifts in gain and phase can result in an increased rate of false alarms or missed detections.

The preceding analysis has shown that the test statistic is dependent on noise power, which in AWGN environments is easily formulated. However, in the real world the noise power fluctuates and there is generally some form of additional non-white noise that the radiometer has to deal with. The first issue that must be addressed is determining and maintaining the threshold value. It has been shown that the limited accuracy with which the threshold can be set, due to uncertainties in noise power, has drastic effect on probability of detection for total power energy detectors [44].

It is desirable to only measure the noise energy level in the absence of the signal to determine the correct threshold value; however, this means that during this threshold calibration process, signal detection is not possible. This is the major problem of Dicke energy detectors which typically experience a 4dB loss in required SNR due to the switching between the antenna signal and the calibrated noise source [40]. One alternative is to employ switched dual channels so that the switching losses are not incurred. In this case, matching the channels becomes a difficult problem for wideband detectors designed for SS signal interception [33,8].

Even if the noise power is measured and maintained, interference from other transmitters (interferers or jammers) still causes major difficulties in distinguishing the SOI purely on the basis of energy measurements. The collection environment in which the radiometer must detect the signal is becoming increasingly populated with both military and commercial communication

systems. When the SOI utilizes Direct Sequence Spread Spectrum (DS-SS) techniques it can be easily buried beneath much stronger groups of interfering signals. In communication systems utilizing code-division or frequency-hop multiple access schemes, multiple SOIs interfere with each other, making it impossible for the energy detector to determine anything more than the signals presence [12].

There are a number of ways for reducing narrowband interference. Transform domain filtering and adaptive filtering techniques used in co-operative systems can be used to minimize the effects of narrowband interference in energy detection systems [48,27]. The Amplitude Distribution Function of a DS-SS waveform is time invariant, thus a detector built around this principle is more robust and significant performance gains have been shown to be theoretically possible, albeit for small time bandwidth products [43]. The dual channel radiometer is discussed in [34,30,33] and can reduce the effects of narrowband interference by implementing correlation in the frequency domain rather than the time domain. All of these suppression techniques will result in added complexity and higher implementation costs when compared to the simple energy detector.

The second major problem with energy detection systems is fluctuations in the phase and gain drift of the high gain amplifiers. These fluctuations place an upper limit on the usable radiometer integration time [30]. Dicke radiometers are capable of calibrating out these fluctuations but remain subject to the disadvantages previously outlined.

### 2.4.5 LRT Derived Detectors for Cyclostationary Signals

The main problem with energy detection schemes is that a detection decision is made solely on the basis of measured energy exceeding a certain threshold. Therefore, these schemes fail to exploit potential temporal or spectral characteristics which may uniquely define the SOI. Some adaptations of energy detection systems overcome this by analyzing successive collected

power spectra and are capable of exploiting basic signal timing characteristics, such as hop rate, or using multi-sensor techniques to exploit spatial distribution of the SOI energy [12].

Given the advantages of cyclic spectral analysis over conventional power spectral analysis as explained in Section 2.2.3, it is not surprising that detectors which exploit the cyclic spectrum typically outperform those based on the power spectrum, especially in the presence of nonstationary noise or narrowband interference [20,47]. These detectors include the common Chip-Rate Detector (CRD), also known as the Pre-Filter Delay and Multiply (PFDM) detector [21,25,32]. It is interesting to note how spectral correlation theory, or cyclostationarity, was not initially used to derive these detectors, rather, it was used after the fact to explain their performance [12]. The PFDM essentially analyzes the cyclic spectrum at a specific chip rate and the presence of a spectral line at that frequency indicates the presence of that particular signal. While the PFDM does exploit the cyclostationarity of the SOI, it is not an optimal detector in that it does not follow exactly from application of the GLRT. The remainder of this section applies the GLRT to the cyclostationary signal model.

In [52,12] it is shown that for a weak signal in white Gaussian noise the GLRT can be approximated by

$$\lambda = \frac{1}{TN_0{}^2} \int_{-T/2}^{T/2} \int_{-T/2}^{T/2} R_s(u,v)r(u)r^*(v)\,du\,dv \tag{2-1}$$

A detector derived from this approximation is also known as the maximum deflection detector because this is the detector structure that maximizes the deflection, $d_\lambda$, given in Eqn (2-4). Although this does not immediately look similar to the form of radiometric detectors discussed in Section 2.4.2, it can be shown that for a purely stationary signal, the detector structure is given by [17]

$$\lambda = \frac{1}{N_0^2} \int_{-\infty}^{\infty} S_s(f)^* S_{r_T}(f) df \qquad (2\text{-}2)$$

where $S_{r_T}(f)$ is the periodogram of $r(t)$. This detector structure is purely theoretical as it relies upon prior knowledge of $S_s(f)$, the PSD of $s(t)$. In fact it is equivalent to the matched filter detector discussed previously. If the only thing known about the SOI is its bandwidth, $B$, then the (sub-optimal) detector becomes approximated by

$$\lambda = \frac{1}{N_0^2} \int_B S_{r_T}(f) df \qquad (2\text{-}3)$$

The output test statistic is identical to that of the total power radiometer described in Section 2.4.3.

If the signal is now modeled as cyclostationary, the CAF in Eqn. (2-1) can be substituted for the autocorrelation in Eqn. (2-1) yielding the following ML detector

$$\begin{aligned}
\lambda_{MC} &= \frac{1}{N_0^2} \sum_\alpha \int_{-T}^{T} R_s^\alpha(\tau)^* R_{r_T}^\alpha(\tau) d\tau \\
&= \frac{1}{N_0^2} \sum_\alpha \int_{-\infty}^{\infty} S_s^\alpha(f)^* S_{r_T}^\alpha(f) df
\end{aligned} \qquad (2\text{-}4)$$

where $S_{r_T}^\alpha(f)$ denotes the cyclic periodogram of $r(t)$ and the summation is for all values of $\alpha$ for which $S_s^\alpha(f)$ is non-zero. The subscript MC denotes *multi-cycle*, due to the $\alpha$ summation . The *single-cycle* version of this detector is simply

$$\lambda_{SC}^\alpha = \frac{1}{N_0^2} \int_{-\infty}^{\infty} S_s^\alpha(f)^* S_{r_T}^\alpha(f) df \qquad (2\text{-}5)$$

Clearly the performance of such a detector depends on the choice of $\alpha$. For example, for a BPSK signal the double carrier cyclic feature, $\alpha = 2f_0$, is much greater than that at the chip rate, $\alpha = 1/T_C$, therefore a single-cycle detector set at the double carrier feature would outperform one

31

set at the chip rate. Additionally pulse shaping reduces the size of the chip rate cyclic features [37]. However, QPSK modulated signals do not contain cyclic features at $\alpha = 2f_0$ therefore a single-cycle QPSK detector would generally be set to the chip rate.

The performance of the optimal single cyclic feature detector described by Eqn. (2-5) has been evaluated and compared to that of the optimal radiometer of Eqn. (2-2) [17,45]. It was confirmed that for either choice of cycle frequency (chip rate or double carrier frequency), the single-cycle detector outperforms the optimal radiometer by a wide margin. Additionally the single-cycle detector performance and simplified versions for source location estimation have been discussed [16]. However, these detectors are all essentially some form of matched filter and unattainable for use in non co-operative detection. By replacing $S_s^\alpha(f)$ of Eqn. (2-4) with by a simple frequency window of length $\Delta f$, the sub-optimal detector becomes,

$$\lambda_{SC}^\alpha(t,f) = \frac{1}{\Delta f} \int_{f-\Delta f/2}^{f+\Delta f/2} S_{r_T}^\alpha(t,v)dv \qquad (2\text{-}6)$$

Additionally, summation over $\alpha$ has been removed because the detector no longer knows which cycle frequencies of $S_s^\alpha(f)$ are non-zero. It can be shown that this is equivalent to a frequency smoothed estimate of the SCF evaluated at a specific cycle frequency and therefore

$$\lim_{\Delta f \to 0} \lim_{T \to \infty} \lambda_{SC}^\alpha(t,f) = \lim_{\Delta f \to 0} \lim_{T \to \infty} S_{r_T}^\alpha(t,f)_{\Delta f} = S_r^\alpha(f) \qquad (2\text{-}7)$$

In other words, the sub-optimal single-cycle detector is equivalent to the SCF in the limiting case.

## 2.5 Summary

This chapter introduced the background theory used throughout the remainder of the thesis and presented a survey of the current literature. The concept of cyclostationarity is introduced in Section 2.2, including both a probabilistic definition and a deterministic

interpretation of the Spectral Correlation Function (SCF). In Section 2.2.3 spectral estimation theory is discussed and the periodogram and cyclic periodogram concepts and their relationships to the Power Spectral Density and SCF, respectively, is explained. Different algorithms used for estimating the SCF are also briefly discussed.

The basics of statistical detection theory is covered in Section 2.4. The derivation of optimal and sub-optimal detector structures for detecting stationary, weak signals in noise is discussed. Detectors derived from the Generalized Likelihood Ratio Test (GLRT) are covered, including approximations leading to the radiometer, or energy detector. Radiometric performance, in relation to the GLRT derived detectors, is also examined and the drawbacks of radiometric detection are covered. The GLRT is then applied to the cyclostationary signal model to produce both optimal and sub-optimal cyclic feature detectors and it is shown that for non co-operative detection the sub-optimal single-cycle detector is equivalent to a frequency smoothed estimate of the SCF evaluated at a particular cycle frequency.

# 3. Receiver Design and Modeling

## 3.1 Introduction

This chapter presents the design of the Cyclic Spectrum Analysis (CSA) receiver and methodology used to analyze its performance. Section 3.2 discusses the overall CSA receiver design, linking to the statistical detection theory presented in Chapter 2 and giving an operational overview of the receiver. Section 3.3 discusses the scope of the research, relating how the research goals are met within time and resource limitations. The theory, design and modeling of each receiver element is then described in turn. Section 3.4 describes the different digital receiver architectures being modeled. Each digital receiver architecture leads to a different CSA receiver implementation: the *Ideal CSA Receiver*, the *Channelized CSA Receiver*, and the *Quadrature CSA Receiver*. The algorithm estimating the cyclic spectrum is then described in Section 3.5, including the development, implementation and modifications made to the algorithm. Section 3.6 describes three different methods for reducing the SCF estimate to an efficient test statistic. Finally, the assumptions made in modeling the receiver performance are summarized in Section 3.7.

## 3.2 Cyclic Spectrum Analysis Receiver Overview

The Cyclic Spectrum Analysis (CSA) receiver model, Figure 3-1, is broken into a number of sections: the Digital Receiver, SCF Estimation, Data Reduction and Hypothesis testing.
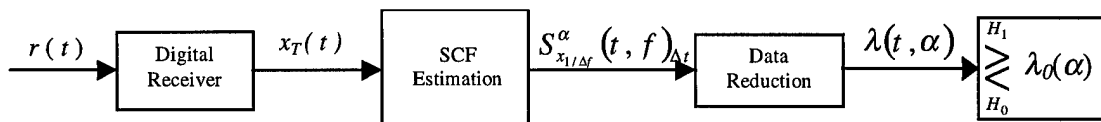


Figure 3-1. Cyclic Spectrum Analysis Receiver Model

34

The first three components are described in detail in following sections, however this section gives an overview of the operation and the design of the receiver.

As discussed in Chapter 2, the CSA receiver must decide between the two hypothesis

$$
\begin{aligned}
H_1 &: r(t) = s(t) + n(t) \\
H_0 &: r(t) = n(t)
\end{aligned} \qquad 0 \le t \le T
\tag{3-1}
$$

where $T$ is the observation time. The digital receiver downconverts the received signal to an Intermediate Frequency (IF) and then samples it. Depending on the digital receiver architecture, the output time series, $x_T(t)$, is either a channelized version of the sampled signal or composed of the sampled in-phase and quadrature components of $r(t)$. In Chapter 2 it was shown that the maximum likelihood single-cycle detector is

$$
\lambda_{SC}^{\alpha} = \frac{1}{N_0^2} \int_{-\infty}^{\infty} S_s^{\alpha}(f)^* S_{x_T}^{\alpha}(f) df
\tag{3-2}
$$

For non co-operative detection, the SCF of $s(t)$, $S_s^{\alpha}(f)$, can be replaced with a frequency window of width $B$. The resultant single-cycle sub-optimal detector given by Eqn. (2-6) is actually a frequency smoothed estimate of the SCF evaluated at a particular cycle frequency. It was shown in Section 2.3.3 that the frequency smoothed estimate and the time smoothed estimate are equivalent per Eqn. (2-2). Therefore, the sub-optimal detector can be written as

$$
\lambda_{SC}^{\alpha}(t, f) = S_{x_{1/\Delta f}}^{\alpha}(t, f)_{\Delta t}
\tag{3-3}
$$

Normally the single-cycle detector is simply evaluated at a cycle frequency that is expected to exhibit a strong cyclic feature when the signal of interest is present. However, in the case of the truly non co-operative detector, the receiver is required to detect all features within the bi-frequency ($\alpha - f$) plane. This requires either: 1) the single-cycle detector to be sequentially evaluated over all possible cycle frequencies ($-f_s \le \alpha \le f_s$), or, 2) estimation of the SCF over the

35

entire bi-frequency plane. Given that computationally efficient algorithms exist which allow efficient SCF estimation the latter is a much more appropriate choice.

The choice of SCF estimation algorithms is relatively straightforward. It is well recognized that time smoothed periodogram based algorithms are much more suitable for estimating the entire SCF than frequency smoothed cyclic periodogram based algorithms (see Section 2.3.4). There are two published time smoothed algorithms, the Strip Spectral Correlation Algorithm (SSCA) and the FFT Accumulation Method (FAM) [39]. Both are quite similar, however, the cyclic and spectral frequency resolution of the SSCA is constant over the entire bi-frequency plane and requires less channelization. This is explained in greater detail in Section 3.5.1. However, all estimation algorithms require a baseband input signal sampled at exactly the Nyquist rate. This requirement leads to some modifications to the digital receiver architectures, these are further explained in Section 3.4.

The output of any SCF estimation algorithm is a function of time, cyclic frequency and spectral frequency. Rather than calculate and store a threshold that is a function of both cyclic and spectral frequency, it is desirable to form a threshold that is simply a function of cyclic frequency. This has the advantage of reducing the amount of required data storage and number of computations. Therefore, the output of the SSCA is converted to a function of time and cyclic frequency only. This stage is data reduction, the process through which the SCF estimate, $S_{x_{1/\Delta f}}^{\alpha}(t,f)_{\Delta t}$, is reduced to the simple test statistic $\lambda(t,\alpha)$. Based on literature, there are three possible data reduction methods which lead to different test statistics, as explored in detail in Section 3.6. The resultant test statistic is then compared to a threshold which is also a function of cycle frequency, $\alpha$,

36

$$\lambda(t,\alpha) \underset{H_0}{\overset{H_1}{\gtrless}} \lambda_0(\alpha) \qquad (3\text{-}4)$$

The SC (single-cycle) subscript has been dropped and the $\alpha$ index converted to functional form since the test statistic is valid for all $\alpha$.

## 3.3 Scope of Research

As stated in Section 1.2, the goals of this research are to:

1. Propose a method of detecting LPD/LPI communication signals using a non cooperative digital receiver;

2. Evaluate the performance of this detection technique through simulation in benign and adverse signal environments, comparing results to the radiometer; and

3. Determine the technique's effectiveness when combined with typical digital receiver architectures.

To meet the research goals, and stay within time and resource constraints, the scope of the research is limited in the following areas. The detection performance of the CSA receiver is evaluated against a typical LPI/LPD waveform with second order features, specifically, a BPSK DS-SS signal. While the proposed detection technique has many post-detection advantages, i.e. in the classification and exploitation of signals, only detection performance is being evaluated. Additionally, to present a meaningful comparison between CSA receiver performance and radiometer performance, only the CSA receiver detection performance at a single cycle frequency is being considered. The test statistic produced by the CSA receiver is actually a sequence of single cycle test statistics; detection is therefore being performed at every cycle frequency. Adverse collection environments considered are limited to two cases: 1) nonstationary noise, and 2) narrowband interference.

## 3.4 Digital Receiver Model

Digital receivers differ from conventional receiver architectures using digital signal processing in that they sample the received signal before the detection step [50]. Current limitations in A/D sampling rates mean that digital receivers still need to convert the received signal down to an Intermediate Frequency (IF) which can then be sampled at or above the Nyquist rate. The two architectures modeled in this thesis, channelized and quadrature, are amongst the most popular digital receiver implementations [49,42]. The ideal digital receiver is included for completeness, as testing will determine the detection performance of the algorithm and data reduction section without any influence from the receiver architecture. This also allows meaningful comparisons to be made between the different digital receiver architectures on the basis of detection performance. As mentioned in Section 3.2, the SCF estimation algorithm requires a baseband signal which is sampled at exactly the Nyquist rate. The channelized and quadrature receivers require some modifications to meet this requirement, these are described in detail in the subsequent paragraphs.

### 3.4.1 Ideal Receiver

The *ideal receiver*, shown in Figure 3-1, is a single channel receiver that simply downconverts and samples the received signal at IF. Both the RF and IF bandpass filters are ideal i.e. they have rectangular spectral responses. Therefore the only effect the ideal receiver has on the signal is the band-limiting and frequency shifting resulting from down-conversion to IF. This ideal receiver is included to enable subsequent detection performance comparisons between channelized and quadrature receivers.

38
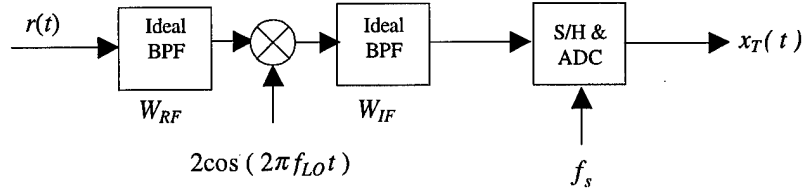
Figure 3-1. Ideal Digital Receiver

To form the *Ideal CSA Receiver*, shown in Figure 3-2, the ideal digital receiver architecture is combined with the SCF Estimation algorithm, data reduction process and hypothesis testing stage.



Figure 3-2. Ideal Cyclic Spectrum Analysis (CSA) Receiver

The bandwidth of the RF and IF bandpass filters are exactly equal and, to meet the SSCA input requirements, the local oscillator frequency, $f_{LO}$, is selected so that the signal is at baseband, i.e. occupies the frequency range $0 < f < W_{IF}$. The bandwidth of the Ideal CSA Receiver is therefore given by

$$W_{CSA} = W_{IF} = W_{RF} \tag{3-1}$$

The input Signal to Noise Ratio, $SNR_{IN}$, is defined at the RF bandpass filter.

### 3.4.2 Channelized Receiver

The *channelized receiver*, shown in Figure 3-1, downconverts the received signal to IF, samples it with an ADC and then uses a digital filter bank to sort signals with differing frequency components. The digital filter, or *channelizer*, can be efficiently implemented using an FFT

39

processor. This method is also used to implement the channelizer in the SSCA and is described in further detail in Section 3.5.1.
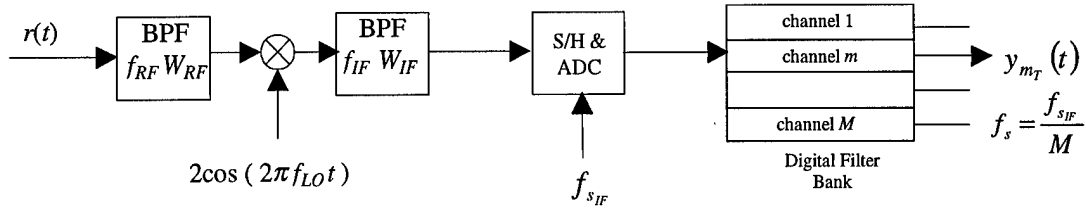


Figure 3-1. Channelized Digital Receiver
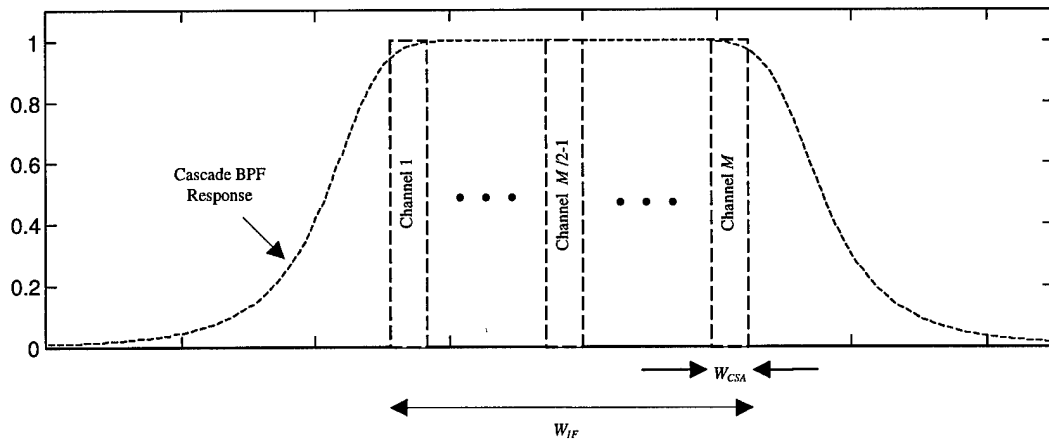


Figure 3-2. Channelized Digital Receiver Filter Response

The digital filter bank divides the IF bandwidth into $M$ channels as shown in Figure 3-2. The output of the $m$th channel is defined as the time series $y_{m_T}(t)$. To meet previously described SSCA requirements, each channel is digitally shifted in frequency to occupy the range $0 < f < W_{IF}/M$. To form the *Channelized CSA Receiver*, shown in Figure 3-3, the channelized digital receiver is combined with the SCF Estimation algorithm, data reduction process and hypothesis testing stage.
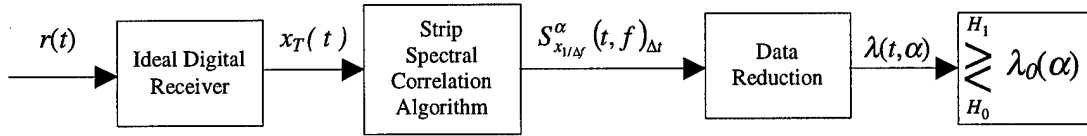
Figure 3-3. Channelized Cyclic Spectrum Analysis (CSA) Receiver

The bandwidth of the channelized CSA receiver is given by

$$W_{CSA} = \frac{f_s}{2} = \frac{f_{s_{IF}}}{2M} = \frac{W_{IF}}{M} = \frac{W_{RF}}{M} \qquad (3\text{-}1)$$

To enable performance comparison with the Ideal CSA Receiver, the input SNR, $SNR_{IN}$, is only defined over the RF bandpass filter portion that is visible to the receiver at the $m$th channel. This ensures that any differences in detection performance will be directly attributable to the effect of the bandpass filtering, and will not include the effects of channelizing the IF passband. Due to differing filter responses within each channel, as shown in Figure 3-2, it is expected that detection performance can differ between a channel with minimal or no attenuation, such as Channel $M/2$-1, and a channel with a large amount of attenuation such as Channel 1 or Channel $M$. For this reason, any simulation and performance evaluation of the Channelized CSA Receiver must include both cases.

### 3.4.3 Quadrature Receiver

An alternative approach to designing a digital receiver is the quadrature receiver shown in Figure 3-1. By sampling both the in-phase and quadrature components of the received signal, the receiver essentially acquires twice as much information. In some applications this permits recovery of phase information from the received signal.

41
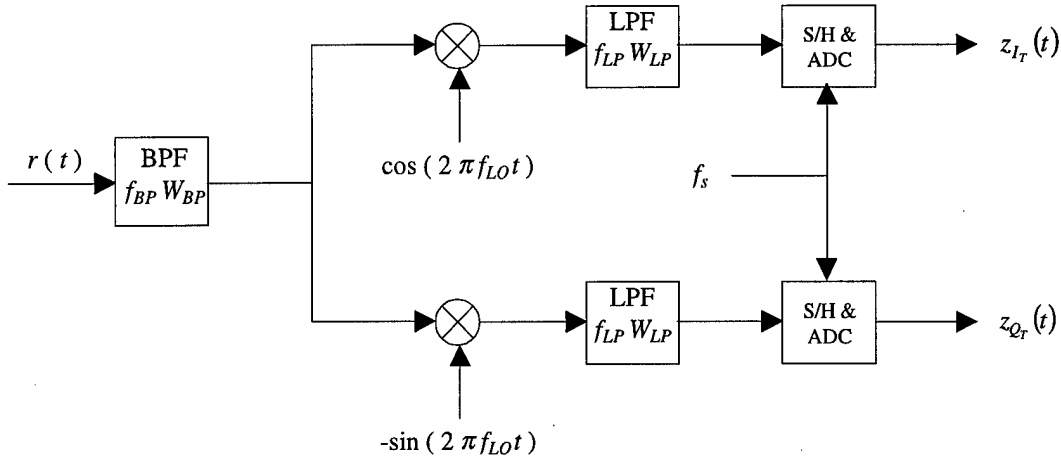
Figure 3-1. Quadrature Digital Receiver

The resultant in-phase and quadrature time series may be combined and input directly into the SSCA either as a complex ordered pair

$$z_T(t) = z_{I_T}(t) + j z_{Q_T}(t) \tag{3-1}$$

or simply summed together

$$z_T(t) = z_{I_T}(t) + z_{Q_T}(t) \tag{3-2}$$

To form the *Quadrature CSA Receiver*, shown in Figure 3-2, the quadrature digital receiver is combined with the SCF Estimation algorithm, data reduction process and hypothesis testing stage.
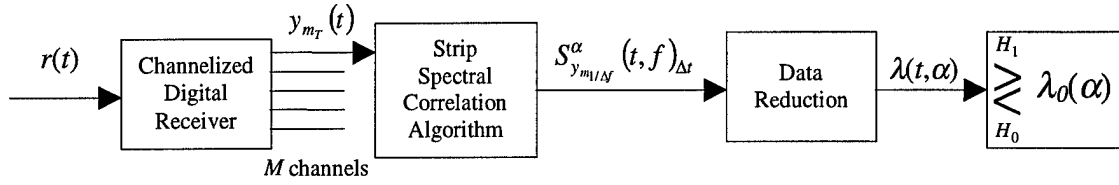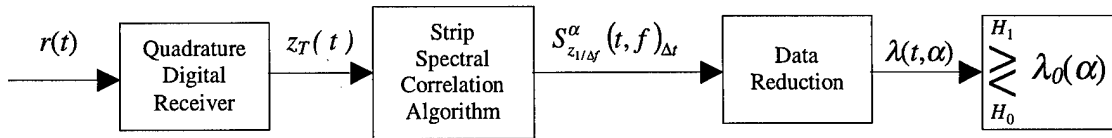


Figure 3-2. Quadrature Cyclic Spectrum Analysis (CSA) Receiver

Note that the quadrature local oscillator reference signal amplitudes are one-half the local oscillator reference signals in the ideal and channelized receivers. This is simply a mathematical

42

convenience to ensure the resultant time series, $x_T(t)$ always has the same power. To cover the same frequency band of interest as the channelized receiver, the quadrature receiver varies the local oscillator frequency so that the IF passband effectively scans over the RF passband. As with the ideal receiver, to meet the SSCA input requirements the local oscillator frequency, $f_{LO}$, is selected so that the signal is at baseband, i.e. occupies the frequency range $0 < f < W_{IF}$. The bandwidth of the Quadrature CSA Receiver is therefore

$$W_{CSA} = W_{IF} = \frac{W_{RF}}{M} \tag{3-3}$$

To ensure that performance comparison does not include the effects of scanning the RF bandpass, the input SNR, $SNR_{IN}$, is defined only over the portion of the RF passband that is visible to the receiver, i.e. $W_{CSA}$.

### 3.4.4  Modeling

The modeling of these digital receivers is a relatively straightforward process. The only modeling decision is the design of the lowpass filter and the IF and RF bandpass filters for the channelized and quadrature receivers. The filters are modeled as fifth order Butterworth filters, and the frequency and phase response is shown in Figure 3-1.
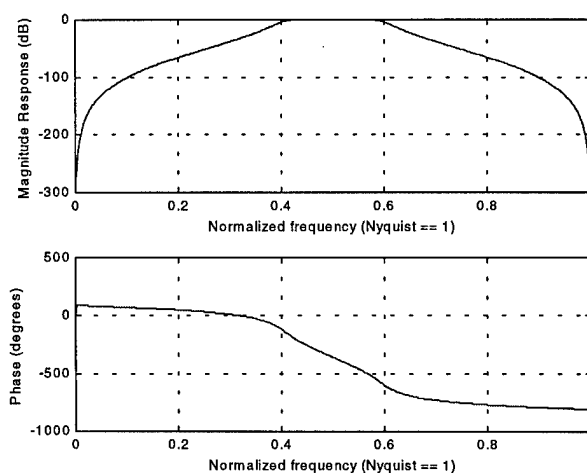


Figure 3-1.  Frequency and Phase Response of Band Pass Filters

43

## 3.5 SCF Estimation

This section describes the algorithm used to estimate the SCF of the received signal. To simplify notation, the ideal digital receiver is considered, i.e. the receiver signal is $x_T(t)$. As described in Section 3.2, the algorithm used in this research is the Strip Spectral Correlation Algorithm (SSCA). The development of the algorithm is covered, then the particular implementation of the algorithm used is discussed. Finally an expression for the processing speed of the algorithm is presented.

### 3.5.1 Algorithm Development

The SSCA [3,39] can be described by Figure 3-1. The input signal is channelized into $P$ bandpass spectra using an $N'$ point FFT. Each spectra is then decimated and translated to baseband by the exponential product. The resultant "complex demodulate" is then interpolated and multiplied by the complex conjugate of the unfiltered received signal and an $N$-point FFT taken to produce a strip of point estimates. This process is repeated for each of the $P$ bandpass spectra and the point estimate strips are combined, covering the entire bi-frequency plane.
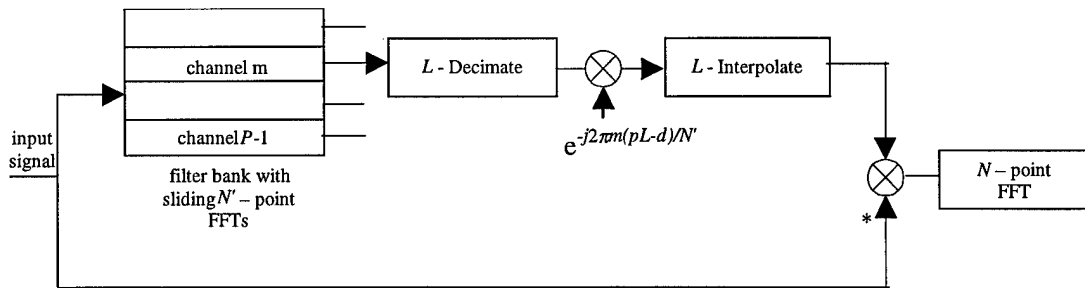


Figure 3-1. Strip Spectral Correlation Algorithm Schematic

The decimated output of the $m$th filter is given by

$$\sum_{k=0}^{N'-1} a(d-k)x(pL-d+k)e^{-j2\pi mk/N'} \tag{3-1}$$

where $d = N'/2 - 1$, $f_m = m/N'$, and $a(d-k)$ is a data-tapering window of length $N'$. The filter output is then frequency shifted to baseband by multiplying by the exponential $e^{-j2\pi mn(pL-d)/N'}$ and the complex demodulate is formed

$$X_T(pL, f_m) = \left[\sum_{k=0}^{N'-1} a(d-k)x(pL-d+k)e^{-j2\pi mk/N'}\right]e^{-j2\pi mn(pL-d)/N'} \tag{3-2}$$

This expression can be shown to be identical to the original complex demodulate equation

$$X_T(pL, f) = \sum_{r=-N'/2}^{N'/2-1} a(r)x(pL-r)e^{-j2\pi f(pL-r)T_s} \tag{3-3}$$

used to describe a time-smoothed version of the cyclic periodogram, Eqn. (2-1) in Section 2.3.3. The only difference is that the SSCA implementation of the complex demodulate of Eqn. (3-2) is more efficient because it uses an $N'$ point FFT.

The next stage in the algorithm computes the time-smoothed cyclic periodogram, $S^\alpha_{x_{1/\Delta f}}(t, f)_{\Delta t}$. The definition given in Section 2.3.3 involves multiplying two complex demodulates together, which can be implemented as

$$S^\alpha_{x_T}(pL, f_{kl})_{\Delta t} = \sum_r X_T(pL, f_k)X_T^*(rL, f_l)g_d(p-r)e^{-j2\pi rq/P} \tag{3-4}$$

where $g_d(p-r)$ is a strip window of length P, and the entire expression can be computed by a $P = N/L$ point FFT. This method is known as the FFT Accumulation Method (FAM) but there are a number of disadvantages to this. First, two channelizing operations are required, effectively doubling the number of FFT operations. Second, the resultant point estimates do not have constant resolution across the bi-frequency plane.

45

The SSCA, as shown in Figure 3-1, replaces the second complex demodulate, $X_T^*(r, f_l)$, with the unfiltered signal $x^*(r)$ in Eqn. (3-4) such that

$$S_{x_T}^\alpha (n,f)_{\Delta t} = \sum_r X_T (r, f_k) x^*(r) g(n-r) e^{-j2\pi rq/N}$$

(3-5)

where $n = pL$, $\alpha = f_k + q\Delta\alpha$ and $f = f_k/2 - q\Delta\alpha/2$. This removes the requirement for two complex demodulates to be calculated and therefore the number of $N'$-point FFTs is halved. However, the unfiltered signal is at a different sampling rate than the complex demodulated produced by Eqn. (3-2). This means that the complex demodulate must be interpolated to match the sampling rate of $x^*(r)$ and an $N$-point FFT is then required to calculate each set of point estimates. The specific interpolation method used is addressed Section 3.5.2.

Each $N$-point FFT produces a strip of point estimates which lie along the line $\alpha = 2f_k - 2f$ in the bi-frequency plane. All strips are $\Delta f$ wide and computed for each $f_k$. The coverage for one strip is shown in Figure 3-2.
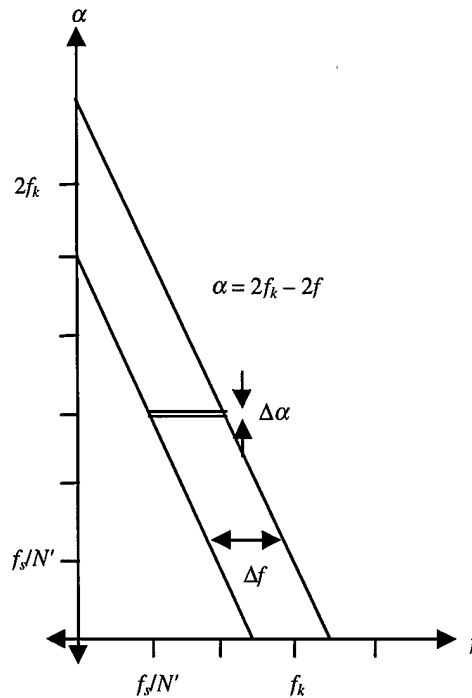


Figure 3-2. Coverage Diagram for the SSCA

46

The width of each strip, and therefore the resolution of the estimate, is given by

$$\Delta f = \frac{f_s}{N'} \quad , \quad \Delta t = \frac{N}{f_s} \cong \frac{1}{\Delta \alpha} \tag{3-6}$$

By producing $P$ strips, the SSCA covers the entire bi-frequency plane for a lowpass signal, as described in Section 2.2.2. The SSCA therefore has an effective lowpass bandwidth of

$$W_{SSCA} = \Delta f \frac{N'}{2} = \frac{f_s}{2} \tag{3-7}$$

In other words, the frequency and cyclic resolution of the estimate are determined by the sampling frequency. Should the receiver bandwidth be less than $f_s/2$, (i.e. the signal has been oversampled) then the algorithm is inefficiently estimating unsupported regions of the bi-frequency plane. Therefore the assumption is made that if the received signal is oversampled, it is decimated so that $W_{CSA} = W_{SSCA} = f_s/2$. Additionally, the fact that the SSCA input bandwidth is lowpass leads to the receiver modifications discussed in the previous section.

### 3.5.2 Algorithm Implementation

The SSCA has been implemented in a variety of forms: assembly [46], C [6] and Matlab [7]. The code used in this research to perform the SSCA is based on that listed in [7]. The verification of the code involved simply comparing the SSCA estimates to those in [7] and to the theoretical functions. A number of modifications are made to improve the accuracy, efficiency and visualization aspects of the algorithm implementation, the most significant modifications are described in the following paragraphs.

The first modification relates to the complex demodulate interpolation method. As mentioned in Section 3.5.1, due to the decimation during the channelization process, the complex demodulate, $X_T(pL, f_l)$, has a sampling rate of $f_s/L$. The SSCA requires the complex demodulate to be multiplied with the complex conjugate of the unfiltered signal, $x^*(r)$, which has

a sampling rate of $f_s$. This requires the demodulate to be interpolated to match the sampling rate of the unfiltered signal. Most descriptions of the SSCA [3, 6, 7, and 39] "hold" the value of the demodulate for $L$ samples, essentially performing a sample and hold operation. This implementation has been found to introduce artificial cyclic features[1]. Therefore a linear interpolation method was substituted to minimize distortion.

The second modification involves implementing the strip window, $g(n)$, in Eqn. (3-5). The strip window was found to reduce the spectra leakage during the smoothing operation that caused artificial cyclic features.

The final significant modification relates to the last stage of most SSCA implementations: mapping the strips of point estimates to the bi-frequency plane. The SSCA produces a total of $N'\times N$ points which require mapping onto the $(2N'+1)\times(2N+1)$ bi-frequency plane, as illustrated in Figure 3-1(a) for $N' = 16$ and $N = 32$. However, the SCF is inherently symmetric and for real signals, only one quadrant of the bi-frequency plane is needed to completely describe the SCF. By mapping only $N'/2+1$ strips as shown in Figure 3-1(b), processing requirements are reduced. Note that this quadrant is the only one where the strips clearly align with the corners of the bi-frequency plane.
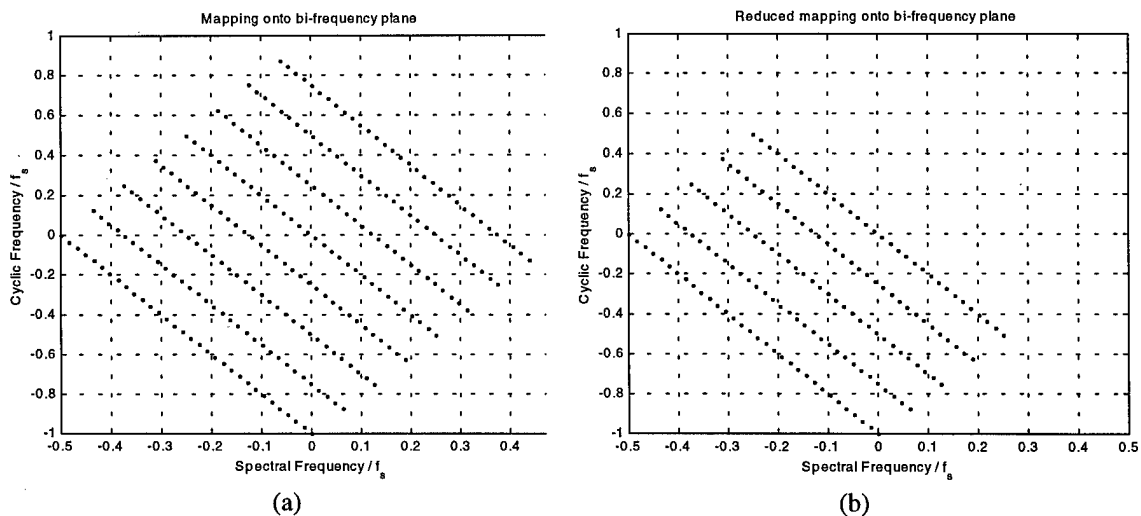


Figure 3-1. SSCA Mapping for $N' = 16, N = 32$

While the mapping operation is definitely necessary for visualizing the SCF, it may not be needed for hardware implementation of a system designed to detect cyclic features [1]. For this reason, mapping is not included in processing speed calculations and comparisons.

### 3.5.3 Processing Time

For any detector, processing time is a critical parameter for characterizing performance. The detector must be able to receive the signal, process the data and decide whether a detection has occurred in sufficient time such that this information is still tactically useful. The method of detection proposed in this thesis involves a particularly large number of computations by comparison to traditional single-cycle detectors such as a Chip Rate Detector (see Section 2.4.5). The number of computations, $C_r$, required to compute a cyclic spectrum estimate for a real valued signal is [39]

$$C_r = NN' \log_2 N + 8N \log_2 N' + 2NN' + 12N \tag{3-1}$$

Using the definitions for the SSCA operating parameters, $N$ and $N'$, in Eqn. (3-6) this can be expressed in terms of $\Delta f$ and $\Delta t$

$$C_r = \frac{(\Delta t \Delta f)}{(\Delta f / f_s)^2} \log_2 \left[ \frac{(\Delta t \Delta f)}{(\Delta f / f_s)} \right] + 8 \frac{(\Delta t \Delta f)}{(\Delta f / f_s)} \log_2 (\Delta f / f_s) + \frac{2\Delta t \Delta f}{(\Delta f / f_s)^2} + \frac{12\Delta t \Delta f}{(\Delta f / f_s)} \tag{3-2}$$

## 3.6 Data Reduction

As discussed in Section 3.2, it is desirable that the SCF estimate, $S^{\alpha}_{x_{1/\Delta f}} (t, f)_{\Delta t}$, be reduced from a function of $\alpha, f$ and $t$, to a test statistic, $\lambda(t, \alpha)$, that is a only a function of $t$ and $\alpha$. This reduces both the amount of data and number of computations required for determining whether a threshold crossing has taken place. In the case of the CSA receiver, the test statistic is

a function both of time, $t$, and cycle frequency, $\alpha$, and is compared to a threshold which is also a function of $\alpha$

$$\lambda(t,\alpha) \underset{H_0}{\overset{H_1}{\gtrless}} \lambda_0(\alpha) \tag{3-1}$$

The SSCA output needs to be reduced to a function of $\alpha$ and $t$. There are four different applicable methods for doing this:

(1)     Magnitude Squared Coherence,

(2)     Maximum Cut,

(3)     Energy, and

(4)     Cycle Frequency Decomposed Degree of Cyclostationarity.

The *Magnitude Squared Coherence* (MSC) function is commonly used in cross-spectral analysis and is a measure of the similarity between two stationary processes [4]. In the cyclostationary case, this can be expressed as

$$\left| C_x^\alpha(f) \right|^2 \equiv \frac{\left| S_x^\alpha(f) \right|^2}{S_x(f+\alpha/2)S_x(f-\alpha/2)} \tag{3-2}$$

When the MSC is used as a test statistic for a gaussian input signal, it produces a Constant False Alarm Rate (CFAR) [5]. However, the difficulty in implementing the MSC in the cyclic spectrum analysis receiver is that the individual power spectrum estimates, $S_x(\cdot)$, must also be estimated. While this process has been implemented, the algorithm employed has not been published [46]. Additionally, the MSC remains a function of spectral frequency. Therefore some other technique (such as those discussed below) is needed to remove the dependence on $f$. For these reasons, the MSC function is not considered herein. The remaining test statistics and their implementation in this research are described in detail in the following paragraphs.

### 3.6.1 Maximum Cut Method

The *maximum cut* function is the simplest to express and is defined as

$$\lambda_{MAX}(t,\alpha) = 10\log_{10}\left\{\max_{f}\left[\left|S^{\alpha}_{x_{1/\Delta f}}(t,f)_{\Delta t}\right|^{2}\right]\right\}$$

(3-1)

This function returns the squared magnitude value of the highest frequency peak for each cyclic frequency.

### 3.6.2 Energy Method

As discussed in Section 2.4, a well established way of detecting weak signals in noise is through the use of *energy* detection. The same principle can be applied to any cyclic cut of the bi-frequency plane. A test statistic that measures energy is

$$\lambda(t,\alpha) = \frac{1}{T}\sum_{f}\left|S^{\alpha}_{x_{1/\Delta f}}(t,f)_{\Delta t}\right|$$

(3-1)

and given $T$ is constant, it can be absorbed into the threshold. The resultant test statistic can then be expressed in dB as

$$\lambda_{E}(t,\alpha) = 10\log_{10}\left[\sum_{f}\left|S^{\alpha}_{x_{1/\Delta f}}(t,f)_{\Delta t}\right|\right]$$

(3-2)

Using an energy related test statistic allows CSA performance at non-zero cyclic frequencies to be easily analyzed with well established radiometer procedures; for $\alpha = 0$, the performance of the CSA approaches that of the radiometer. This can be easily shown using the properties of the SCF shown in Eqn. (2-5). The test statistic can be rewritten as

$$\lambda_{E}(t,0) = 10\log_{10}\left[\sum_{f}\left|S_{x_{1/\Delta f}}(t,f)_{\Delta t}\right|\right]$$

(3-3)

remembering that $S_{x}(f)$ is essentially a band-limited, frequency shifted version of $S_{r}(f)$, then

$$\lim_{\Delta f \to 0} \lim_{\Delta t \to \infty} \lambda_E(t,0) = 10\log_{10}\left[\int_{-\infty}^{\infty} S_x(f,t)df\right]$$

$$= \lim_{T \to \infty} 10\log_{10}\left[\int_B S_{r_T}(f,t)df\right] \qquad (3\text{-}4)$$

which is the radiometer detector in Eqn. (2-3) expressed in dB.

### 3.6.3 Cycle Frequency Decomposed Degree of Cyclostationarity Method

A measure of the Degree of Cyclostationarity (DCS) proposed in [54] is defined as

$$\text{DCS} \equiv \frac{\sum_{\alpha \neq 0} \int_{-\infty}^{\infty}\left|S_x^\alpha(f)\right|^2 df}{\int_{-\infty}^{\infty}\left|S_x^0(f)\right|^2 df} \qquad (3\text{-}1)$$

This is a multi-cycle measure, in that it is a single value formed by summing across all non-zero cycle frequencies. Therefore, it does not take advantage of the discriminatory capabilities of the cyclic spectrum. The *cycle frequency decomposed DCS* is more useful for detection and is defined as

$$\text{DCS}^\alpha \equiv \frac{\int_{-\infty}^{\infty}\left|S_x^\alpha(f)\right|^2 df}{\int_{-\infty}^{\infty}\left|S_x^0(f)\right|^2 df} \qquad (3\text{-}2)$$

It is shown in [54] that optimum detection performance is directly determined by $\text{DCS}^\alpha$. This forms the basis for the cyclic-frequency decomposed DCS test statistic used in this research, now defined as

$$\lambda_{DCS}(t,\alpha) = 10\log_{10}\left[\frac{1}{T}\sum_f \left|S_{x_{1/\Delta f}}^\alpha(t,f)_{\Delta t}\right|^2\right] - 10\log_{10}\left[\frac{1}{T}\sum_f \left|S_{x_{1/\Delta f}}^0(t,f)_{\Delta t}\right|^2\right] \qquad (3\text{-}3)$$

where in the limiting case

$$\lim_{\Delta f \to 0} \lim_{\Delta t \to \infty} \lambda_{DCS}(t, \alpha) = DCS^{\alpha} \qquad (3\text{-}4)$$

## 3.7 Assumptions

To meet research goals and stay within time and resource constraints, some assumptions are necessary. As explained in the scope, this research only considers the detection performance of the CSA receiver against a DS-SS BPSK signal and adverse signal environments only include nonstationary noise, or stationary noise and narrowband interference. Additionally, the following simplifying assumptions have been made throughout:

1) The digital receiver architectures are modified so that the SSCA input signal is a lowpass signal

2) The SSCA input signal is sampled at the Nyquist rate.

3) The received signal is centered about the CSA receiver bandwidth.

## 3.8 Summary

This chapter explains the design of the Cyclic Spectrum Analysis (CSA) receiver and the methodology used to analyze its performance. Section 3.2 presented the overall CSA receiver design, linking to the statistical detection theory presented in Chapter 2 and giving an operational overview of the receiver. Section 3.3 discussed the scope of the research, relating how the research goals are met within time and resource limitations. The theory, design and modeling of each receiver element is then described in turn. Section 3.4 described the different digital receiver architectures being modeled. Each digital receiver architecture leads to a different CSA receiver implementation: the *Ideal CSA Receiver*, the *Channelized CSA Receiver*, and the *Quadrature CSA Receiver*. The algorithm for estimating the cyclic spectrum is then described in Section 3.5, including the development, implementation and modifications made to the algorithm. Section 3.6 described the three different methods for reducing the SCF estimate to an efficient

test statistic. Finally, the assumptions made in modeling the receiver performance are summarized in Section 3.7.

# 4. Analysis and Results

## 4.1 Introduction

This Chapter describes the simulations and results used to determine the performance of the Cyclic Spectrum Analysis (CSA) receiver configurations described in Chapter 3, specifically the: 1) *Ideal CSA Receiver*, 2) *Channelized CSA Receiver*, and the 3) *Quadrature CSA Receiver*. First, optimal SSCA operating parameters are determined based on the accuracy and processing speed of the algorithm. The effect of any bandwidth mismatch between the signal and the receiver is examined briefly. The three data reduction methods described in Section 3.6, *Maximum Cut, Energy* and *Cycle Frequency Decomposed Degree of Cyclostationarity (DCS)*, are implemented and one selected for use throughout the remainder of the simulations based upon analytical traceability, ease of threshold implementation, and the comparative detection performance of the resulting test statistic.

The detection performance of the *Ideal CSA Receiver* is compared to the radiometer in both benign and adverse signal environments. The adverse signal environments consist of nonstationary noise and stationary noise with narrowband interference. The detection performance of the *Channelized CSA Receiver* and the *Quadrature CSA Receiver* is then evaluated. The performance of the channelized receiver is first simulated in the benign and adverse environments. Specifically, the effects of asymmetric spectral attenuation on the 'edge' channels are determined through comparison with a non-attenuated central channel. The detection performance of the quadrature receiver is then simulated. Expressions are derived for the Spectral Correlation Function (SCF) for the complex In-phase and Quadrature (I & Q) input and for the summed I & Q input. The summed I & Q input signal is then simulated in the benign and adverse environments.

55

## 4.2 Estimate Accuracy and Processing Speed

It has been shown in Eqn. (2-3) that for an accurate SCF estimate, the temporal resolution, $\Delta t$, must be much greater than spectral resolution, $\Delta f$. For a time smoothed estimator, such as the SSCA, the cyclic resolution, $\Delta\alpha$, is equal to the inverse of the temporal resolution. Additionally, Eqn. (3-6) shows that the spectral resolution is determined by the length of the first $N'$-point FFT, and the cyclic resolution is determined by the length of the second $N$-point FFT. Clearly, as $N$ and $N'$ increase so does the computation time. Therefore, the need for high resolution and accuracy estimates must be balanced against the need to calculate the estimate quickly.

To determine the SSCA operating parameters that provide sufficient spectral and cyclic resolution, while minimizing processing time, the SSCA is used to estimate the SCF of the DS-SS BPSK signal of interest at IF, given by

$$s(t)=\sqrt{2P}\sum_{n=-\infty}^{\infty}a_n\,q(t-nT_c-t_0)\cos(2\pi f_{IF}t+\phi_0)\tag{4-1}$$

$P$ is the average power, $\phi_0$ and $t_0$ are phase and timing offset, respectively, $a_n$ is a sequence of i.i.d. random variables equally likely to take on the values of $\pm1$, and $q(t)$ is a unit-amplitude rectangular pulse of length $T_c$. The theoretical SCF for the DS-SS BPSK signal is given by [10]

$$\begin{aligned}S_s^\alpha(f)=\frac{P}{2T_c}&[Q(f+\tfrac{\alpha}{2}+f_{IF})Q(f-\tfrac{\alpha}{2}+f_{IF})\\
&+Q(f+\tfrac{\alpha}{2}-f_{IF})Q(f-\tfrac{\alpha}{2}-f_{IF})]\,e^{-j2\pi\alpha t_0}\\
&+\frac{P}{2T_c}[Q(f+\tfrac{\alpha}{2}+f_{IF})Q(f-\tfrac{\alpha}{2}-f_{IF})e^{-j[2\pi(\alpha+2f_{IF})t_0+2\phi_0]}\\
&+Q(f-\tfrac{\alpha}{2}+f_{IF})Q(f+\tfrac{\alpha}{2}-f_{IF})e^{-j[2\pi(\alpha-2f_{IF})t_0+2\phi_0]}]\end{aligned}\tag{4-2}$$

where $Q(f) = T_c\,\mathrm{sinc}(fT_c)$. Given this expression is only supported for a discrete number of cycle frequencies, assuming that the phase and code offset are zero, Eqn. (4-2) can be rewritten as

$$S_s^\alpha(f) = \begin{cases} \frac{P}{2T_c}\left[Q\left(f + \frac{\alpha}{2} + f_{IF}\right)Q\left(f - \frac{\alpha}{2} + f_{IF}\right) + Q\left(f + \frac{\alpha}{2} - f_{IF}\right)Q\left(f - \frac{\alpha}{2} - f_{IF}\right)\right] & \alpha = \frac{k}{T_c} \\ \frac{P}{2T_c}Q\left(f + \frac{\alpha}{2} + f_{IF}\right)Q\left(f - \frac{\alpha}{2} - f_{IF}\right) & \alpha = \frac{k}{T_c} - 2f_{IF} \\ \frac{P}{2T_c}Q\left(f + \frac{\alpha}{2} - f_{IF}\right)Q\left(f - \frac{\alpha}{2} + f_{IF}\right) & \alpha = \frac{k}{T_c} + 2f_{IF} \\ 0 & e.w \end{cases} \tag{4-3}$$

Using this expression as a basis for comparison, the operating parameters of the SSCA were varied and the resultant estimates are shown in Figure 4-1. Table 4-1 presents the corresponding SSCA parameters used including the number of computations required as determined from Eqn. (3-1). Computation time is calculated assuming the Digital Signal Processor can complete a 1024 length complex FFT in 20µs which is representative of the current state-of-the-art [9].

| Figure 4-1 | First FFT Length $N'$ | Second FFT Length $N$ | Resolution Product $\Delta t \Delta f$ | Number of Computations $C_{rm}$ | Computation Time (ms) |
|---|---|---|---|---|---|
| (a) | 8 | 2048 | 500 | 82720 | 0.276 |
| (b) | 8 | 4096 | 1000 | 164704 | 0.549 |
| (c) | 16 | 2048 | 500 | 198208 | 0.661 |
| (d) | 16 | 4096 | 1000 | 394944 | 1.316 |
| (e) | 32 | 2048 | 500 | 461952 | 1.540 |
| (f) | 32 | 4096 | 1000 | 920960 | 3.070 |

Table 4-1. SSCA Parameters and Computation Time
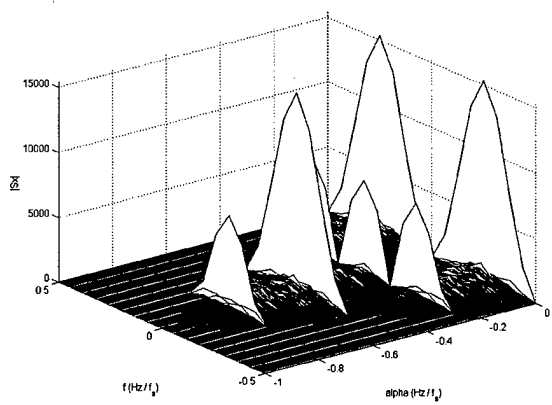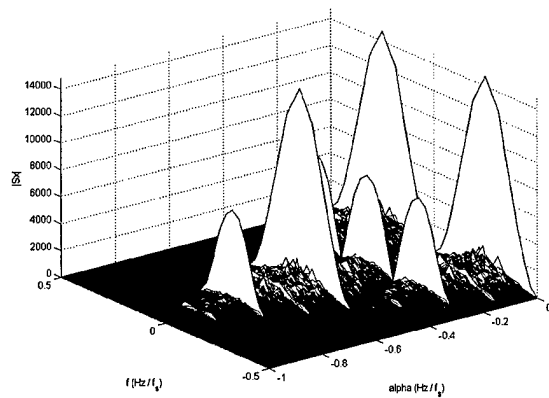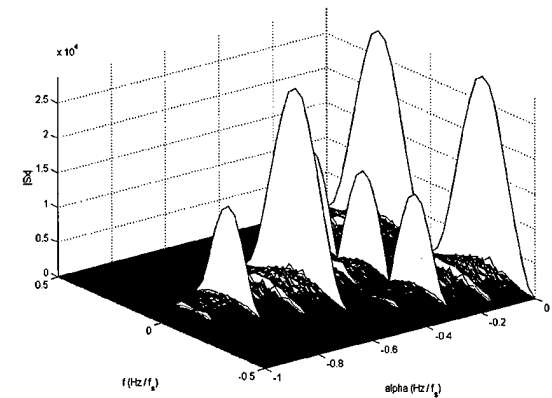
57
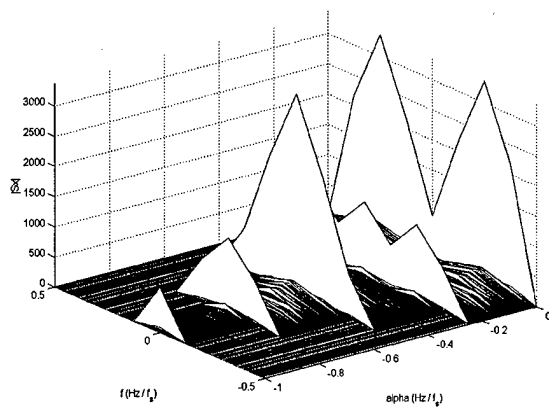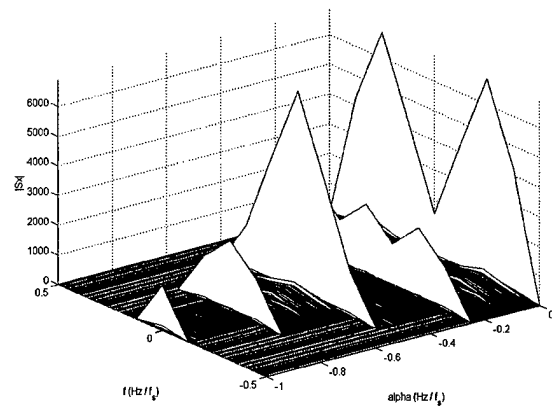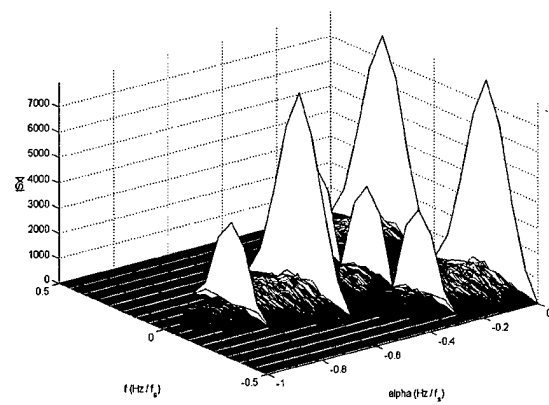
Figure 4-1. SCF Estimates for Various SSCA Operating Parameters

Based on results shown in Figure 4-1, an FFT length of at least 16 is required to provide adequate spectral resolution. In the first two cases, (a) and (b), the spectral resolution is not good enough to properly discern the shapes of the cyclic features. Increasing $N$ from 2048 to 4096 has the effect of reducing the measurement noise, however this reduction is not substantial and either choice provides adequate cyclic resolution. The parameters giving adequate spectral and cyclic resolution while minimizing computation time is $N' = 16$, $N = 2048$, Figure 4-1 (c). Therefore, these operating parameters are used for all proceeding simulations.

## 4.3 Signal Bandwidth Considerations

As stated in Section 3.7, this research assumes the center frequency of the Signal of Interest (SOI) at IF is exactly centered within $W_{CSA}$, the receiver bandwidth. The purpose of this section is to examine the effect of signal bandwidth on detection. Two cases are considered: 1) the SOI null-to-null bandwidth is one-half the receiver bandwidth, i.e. $W_{CSA}$, $= 4/T_c$ ; and 2) the SOI null-to-null bandwidth is twice the receiver bandwidth, i.e. $W_{CSA}$, $= 1/T_c$ . Of primary concern in the second case is whether the relative strength of the cyclic features changes as the SSCA is presented with a limited portion of the signal. The resultant SCF estimations for these two cases are shown in Figure 4-1.
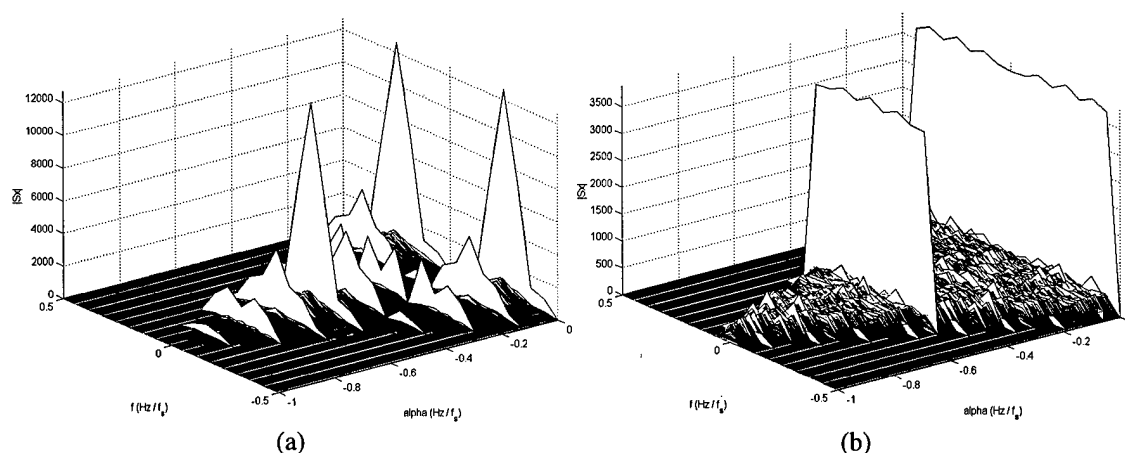


(a)             (b)

Figure 4-1.  SCF Estimates for: (a) $W_{CSA} = 4/T_c$, and (b) $W_{CSA} = 1/T_c$

These correlation surfaces confirm the theory; the expression in Eqn. (4-3) can be used to determine the location and strength of the cyclic features and the receiver bandwidth simply determines the region of support in the bi-frequency plane, as explained in Section 2.2.2. In the unknown bandwidth case, this confirms that the best cyclic frequency for detection is the double carrier feature at $\alpha = 2f_{IF}$. The bandwidth of the signal can then be determined post-detection by relative location of the chip rate features at $\alpha = \{n/T_c, n/T_c\text{-}2f_{IF}, n/T_c\text{+}2f_{IF}\}$, for $n \in Z^+$, $n > 0$. Importantly, this means simulations need only be run with one particular signal bandwidth, with variations in the bandwidth taken into account by changing SNRs.

## 4.4 Data Reduction Methods

Section 3.6 described a number of different methods that may be used to reduce the SSCA output to a test statistic that can be easily and efficiently compared to a threshold. The purpose of this section is to determine which of the three possible methods are most suitable based on a comparison of efficiency, detection performance and analytical traceability. To determine this, the DS-SS BPSK defined in Eqn. (4-1) with a SNR of –3 dB is first applied to the SSCA. The three different data reduction methods are then applied to produce the *Maximum Cut*, $\lambda_{MAX}(\alpha)$, *Energy*, $\lambda_E(\alpha)$, and *Cycle Frequency Decomposed DCS*, $\lambda_{DCS}(\alpha)$, test statistics. These statistics are presented in Figure 4-1 (a), (b) and (c), respectively, with the relative strengths of the main cyclic features provided in Table 4-1. Relative strength is defined as the strength of the cyclic feature when the signal is present (under $H_1$ conditions) subtracted from the strength of that feature when the signal is not present (under $H_0$ conditions).
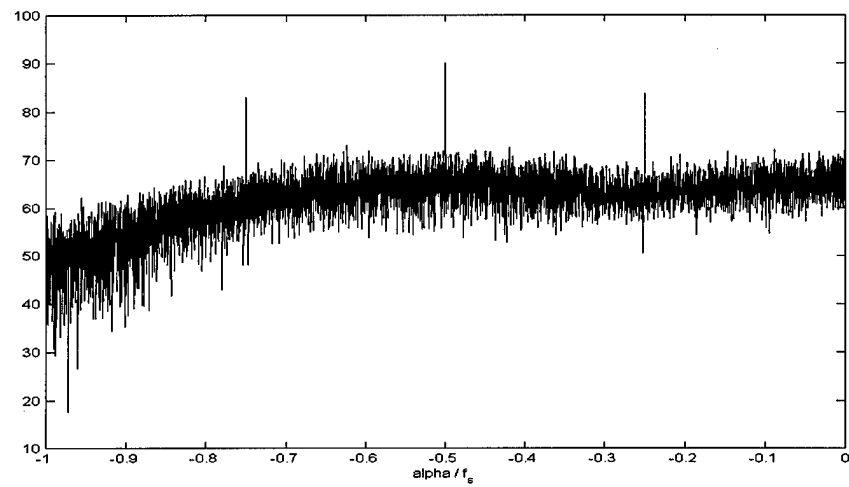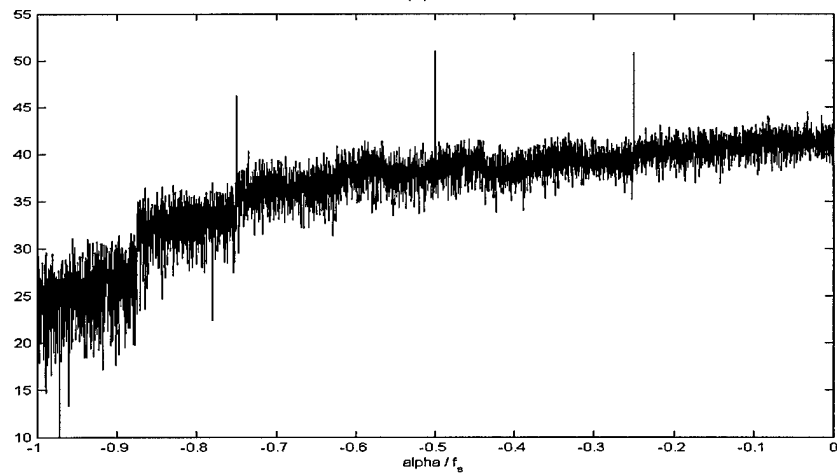
Figure 4-1. Test Statistic Outputs for $SNR_{IN}$ = -3 dB:

(a) $\lambda_{MAX}(\alpha)$, (b) $\lambda_E(\alpha)$, and (c) $\lambda_{DCS}(\alpha)$.

61

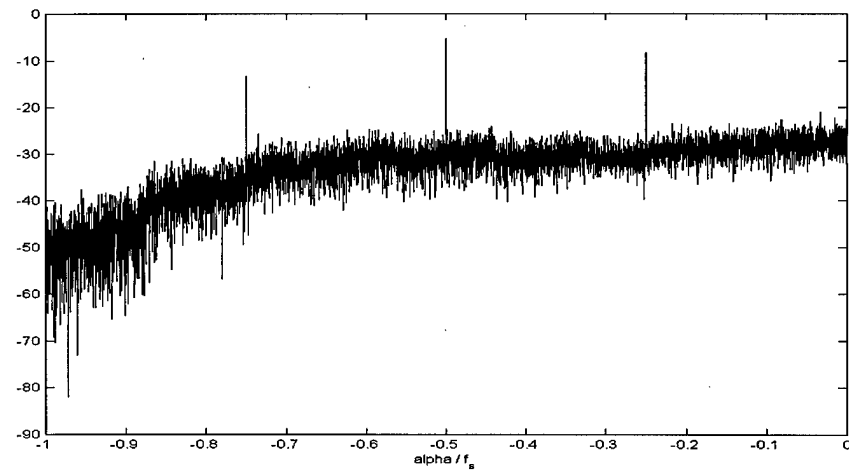| Test Statistic | Relative Strengths (dB) | | |
|---|---|---|---|
| | $\alpha = 1/T_c$ | $\alpha = 2f_{IF}$ | $\Delta\lambda = \lambda(2f_{IF})-\lambda(1/T_c)$ |
| $\lambda_{MAX}(\alpha)$ | 24.85 | 28.73 | 3.88 |
| $\lambda_E(\alpha)$ | 10.65 | 13.14 | 2.49 |
| $\lambda_{DCS}(\alpha)$ | 22.28 | 27.62 | 5.33 |

Table 4-1: Relative Strengths of Test Statistics

Based on the relative strengths in Table 4-1, it appears that the Max Cut data reduction method produces the strongest cyclic features. However, this data is only for one noise realization and one particular SNR.

There are a number of additional observations to be made from each plot in Figure 4-1. The average value of the "noise floor" for the Max Cut test statistic is well behaved, but some form of polynomial curve fitting is required to establish an appropriate threshold that can be applied across the entire statistic. This means added processing complexity in any implementation. Additionally, due of the definition of the Max Cut test statistic, it seems to be much more susceptible to variations in the estimate itself. In other words, if the resolution product, $\Delta t \Delta f$, is not large enough, the Max Cut test statistic is most effected.

The average value of the Energy test statistic "noise floor" is distinctly multi-leveled. This is due to the large frequency resolution of the SSCA, therefore as $\alpha$ approaches $2f_s$ there are only a small number of points. However each region is linear and a properly constructed threshold could easily be applied as determined from the SSCA operating parameters ($N'$ and $N$). The Energy test statistic reflects smaller differences in strength between double carrier and chip rate features. This tends to indicate that the difference in detection performance between the double carrier and chip rate features is less than any other method. The Energy test statistic also provides substantial analytical advantages over the other two test statistics, as described in

Section 3.6.2, and allows radiometric theory to be used for analyzing the receiver performance at non-zero cycle frequencies.

The Cycle Frequency Decomposed DCS test statistic exhibits the same advantages as the Energy statistic because it sums across frequency. However the difference between double carrier and chip rate feature is greater than the Energy test statistic and the threshold is not as easily constructed as the Energy threshold.

Perhaps the most important criteria is the detection performance using these data reduction methods. As mentioned previously, the relative cyclic features strengths in Table 4-1 are for one noise realization and one particular SNR. To determine the relative performance of each test statistic, detection is performed at the double carrier feature, $\alpha = 2f_{IF}$. As described in Section 2.4, Figure 4-2 represents the Probability of Detection $(P_D)$, versus the input SNR $(SNR_{IN})$, for a constant Probability of False Alarm $(P_{FA})$. The input SNR for the CSA receiver is defined in Section 3.4.1. The number of trials, $N_{trials}$, represents the number of noise realizations the receiver model is presented with for each SNR.
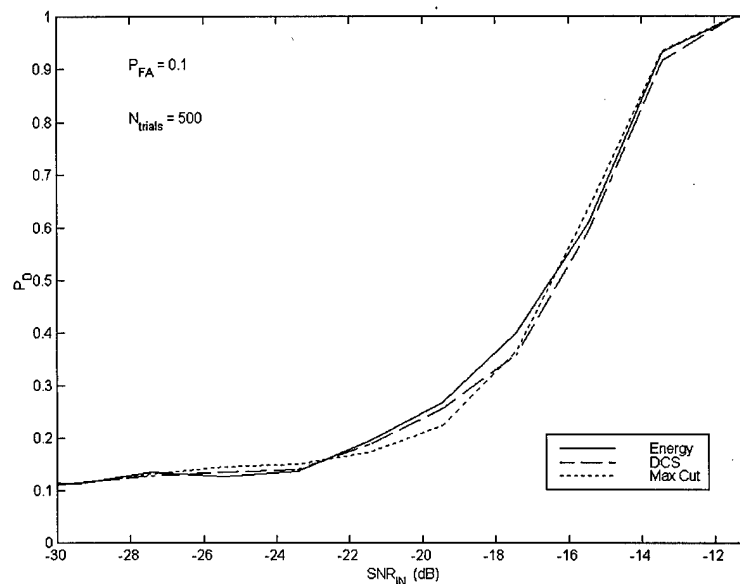


Figure 4-2. Performance Comparison for Test Statistics Evaluated at $\alpha = 2f_{IF}$

These $P_D$ results show that none of the data reduction methods produce test statistics that are clearly superior in detection performance, regardless of SNR. Taking into account the accuracy of the results, the Energy test statistic appears marginally superior for the region $0.1 < P_D < 0.5$, but the detection performance of the test statistics are approximately equal elsewhere.

Given the analytical advantages, the simplicity in constructing a threshold for all cycle frequencies, and the detection performance advantages for the lower $P_D$ region, it appears that the Energy test statistic is the most suitable for the CSA receiver. Therefore the Energy data reduction method and resulting test statistic are used exclusively for the remainder of the simulations described in this chapter.

## 4.5 Ideal CSA Receiver Performance

This section establishes the performance of the Ideal CSA Receiver, shown in Figure 3-2, and compares it to the radiometer described by Eqn. (2-3). Note that the radiometer implementation assumes 1) an ideal BPF of identical width to the bandwidth of the CSA receiver, and 2) the integration time is equal to the length of the data segment. The signal environment varies from stationary noise to nonstationary noise and then stationary noise with narrowband interference is considered.

### 4.5.1 Stationary Noise

In the case of stationary noise, the Ideal CSA Receiver is presented with the following binary hypothesis

$$r(t) = \begin{cases} \sqrt{2P} \sum_{n=-\infty}^{\infty} a_n \, q(t - nT_c) \cos(2\pi f_0 t) + n(t) & (H_1) \\ n(t) & (H_0) \end{cases} \qquad (4\text{-}1)$$

where $a_n$ is a sequence of i.i.d. random variables equally likely to take on the values of $\pm 1$ and $q(t)$ is a unit amplitude rectangular pulse of length $T_c$. The noise component, $n(t)$, is stationary

Additive White Gaussian Noise (AWGN) with a two-sided PSD, $S_n(f)$, of $N_0/2$. The hypothesis may be rewritten in terms of the SCF of ideal digital receiver output signal, $x(t)$, as

$$S_x^\alpha(f) = \begin{cases} S_s^\alpha(f) + S_n^\alpha(f) & (H_1) \\ S_n^\alpha(f) & (H_0) \end{cases} \tag{4-2}$$

where $S_s^\alpha(f)$ is the SCF for the DS-SS BPSK signal as previously shown in Eqn. (4-3). Therefore under $H_1$ conditions, the SCF of $x(t)$ is

$$S_x^\alpha(f) = \begin{cases} \frac{P}{2T_c}\left[Q^2(f + f_{IF}) + Q^2(f - f_{IF})\right] + \frac{N_0}{2} & \alpha = 0 \\ \frac{P}{2T_c}\left[Q\left(f + \frac{\alpha}{2} + f_{IF}\right)Q\left(f - \frac{\alpha}{2} + f_{IF}\right) + Q\left(f + \frac{\alpha}{2} - f_{IF}\right)Q\left(f - \frac{\alpha}{2} - f_{IF}\right)\right] & \alpha = \frac{k}{T_c}, k \neq 0 \\ \frac{P}{2T_c}Q\left(f + \frac{\alpha}{2} + f_{IF}\right)Q\left(f - \frac{\alpha}{2} - f_{IF}\right) & \alpha = \frac{k}{T_c} - 2f_{IF} \\ \frac{P}{2T_c}Q\left(f + \frac{\alpha}{2} - f_{IF}\right)Q\left(f - \frac{\alpha}{2} + f_{IF}\right) & \alpha = \frac{k}{T_c} + 2f_{IF} \\ 0 & e.w \end{cases} \tag{4-3}$$

where $Q(f) = T_c\,\mathrm{sinc}(fT_c)$ and $k \in Z^+$. Under $H_0$ the SCF of $r(t)$ is simply

$$S_x^\alpha(f) = \begin{cases} \dfrac{N_0}{2} & \alpha = 0 \\ 0 & e.w \end{cases} \tag{4-4}$$

Simulation results for the Ideal CSA Receiver and radiometer are presented in Figure 4-1. The results confirm Eqn. (3-4) showing that in the limiting case, Ideal CSA Receiver performance at $\alpha = 0$ approaches that of the radiometer. Additionally, the results indicate that Ideal CSA Receiver performance at $\alpha = 2f_{IF}$ is within 1 dB of the radiometer performance.
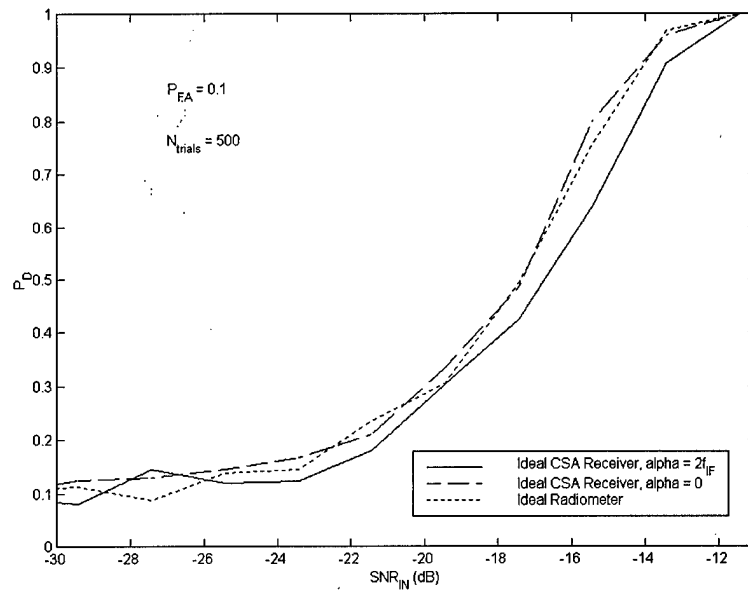
Figure 4-1. Ideal CSA Receiver Performance, Stationary Noise

The analytical advantages of the energy test statistic are used to offer an alternative explanation of the CSA receiver performance. Based on Eqns. (4-3) and (4-4), the detector should be able to determine SOI presence by the existence of cyclic features within the region of support (in this case, at $\alpha = \{1/T_c, 2f_{IF}, 3/T_c\}$), i.e. the threshold could theoretically be set to zero. In reality, the detector is rarely presented with pure AWGN and there will generally be some spectral noise correlation. This is clearly illustrated in Figures 4-6 and 4-7.



Figure 4-2. SCF Estimate under $H_0$

66

Figure 4-3. $\lambda_E(\alpha)$ under $H_0$

While there is some spectral noise correlation at non-zero cyclic frequencies, it is proportionally very little. Consequently, based purely on SNR gains, one would expect a significant performance improvement when using energy detection at $\alpha = \{1/T_c, 2f_{IF}, 3/T_c\}$. However, what is not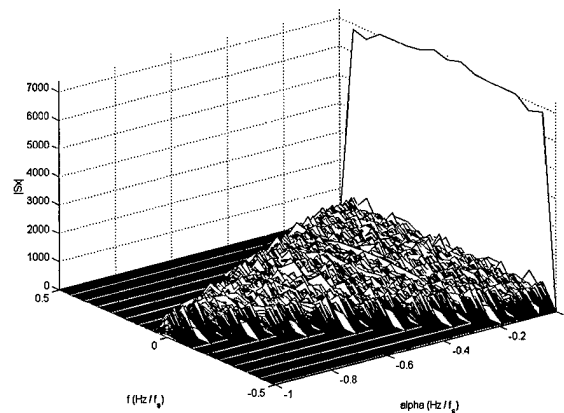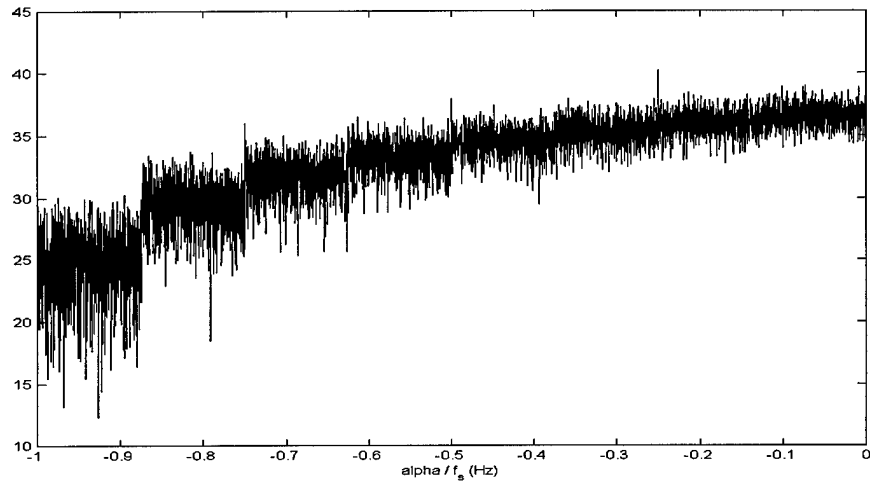 evident from Figure 4-2 is that the amount and distribution of spectral noise correlation is dependant on each noise realization. As expected, the average noise energy at $\alpha = 0$ is approximately constant for stationary noise. However, the proportion of noise energy that is spectrally correlated varies greatly over the bi-frequency plane. This is revealed in Figure 4-4 which examines the mean and variance of the test statistic, $\lambda_E(\alpha)$, evaluated at $\alpha = 0$ and $\alpha = 2f_{IF}$.

The mean of $\lambda_E(2f_{IF})$ is 13.5 dB less than the mean of $\lambda_E(0)$ and the variances are 0.835 dB and 0.005 dB for $\lambda_E(2f_{IF})$ and $\lambda_E(0)$, respectively. This substantial increase in variance explains why the CSA performance $\alpha = 2f_{IF}$ is inferior to its performance at $\alpha = 0$ because it is well established that energy detector performance decreases as the noise power variance increases . Based on these results, it is expected that as the noise quality improves, i.e. the PSD becomes flatter, the amount of spectral correlation will decrease and the performance of the non-zero cycle

67

detector will eventually become superior to that of the radiometer. However, this is not a particularly useful conclusion, as "white" noise is only attainable for large observation times.



(a)                                                    (b)
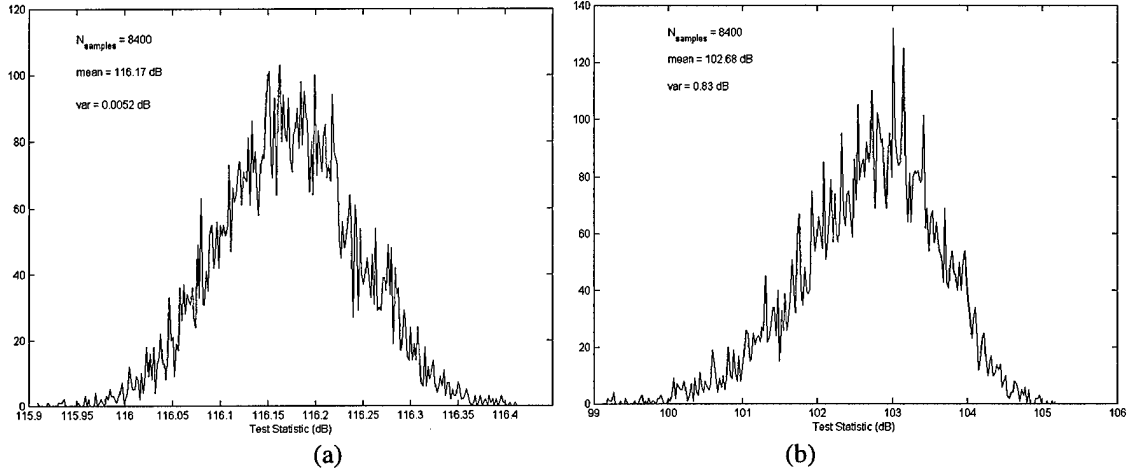
Figure 4-4. Histogram of Test Statistic Distributions under $H_0$ : (a) $\lambda_E(0)$ and (b) $\lambda_E(2f_{IF})$

### 4.5.2 Nonstationary Noise

The second scenario for the Ideal CSA Receiver is for varying noise power, i.e. $n(t)$ is nonstationary. As discussed in Section 2.4.4, this is an environment in which the cyclic detector is expected to outperform the radiometer. Variation in noise power can also be interpreted as uncertainty in noise power, or a limitation in the accuracy of the threshold setting. In this scenario, the detector is presented with a hypothesis formulation identical to Eqn. (4-1) except that $n(t)$ is now modeled as a nonstationary random process. In this simulation the noise power is normally distributed with the following statistics

$$\mu_{N_0} \equiv E\big[R_n(t,0)\big]$$
$$\sigma_{N_0}^2 \equiv E\big[R_n^{\ 2}(t,0)\big] - \mu_{N_0}^2$$

(4-1)

where $R_n(t,0)$ is the autocorrelation of noise, defined in Eqn. (2-1), evaluated at $\tau = 0$. The *co-efficient of variation* maybe defined as [45]

68

$$\rho_N \equiv \frac{\sigma_{N_0}^2}{\mu_{N_0}^2} \tag{4-2}$$

and $\mu_{N_0}$ replaces $N_0$ in the input signal-to-noise ratio definition

$$SNR_{IN} \equiv \frac{PT_c}{2\mu_{N_0}} \tag{4-3}$$

Two distributions of noise power are considered in this section, a small amount of variability with $\rho_N = 0.01$ and a larger amount with $\rho_N = 0.1$. Simulations results are presented in Figure 4-1 and 4-10 for the first and second cases, respectively. Both cases confirm that CSA performance at $\alpha = 2f_{IF}$ is superior to the radiometer and the CSA at $\alpha = 0$ in nonstationary noise conditions. In the first case ($\rho_N = 0.01$), the CSA receiver improves upon the radiometer performance by approximately 8dB. In the second case ($\rho_N = 0.1$), the CSA receiver detection performance exhibits approximately 10 dB performance improvement above the radiometer. In both cases, the noise power variation has caused a degradation in CSA detection performance of less than 1dB compared to the stationary noise case in the previous section.
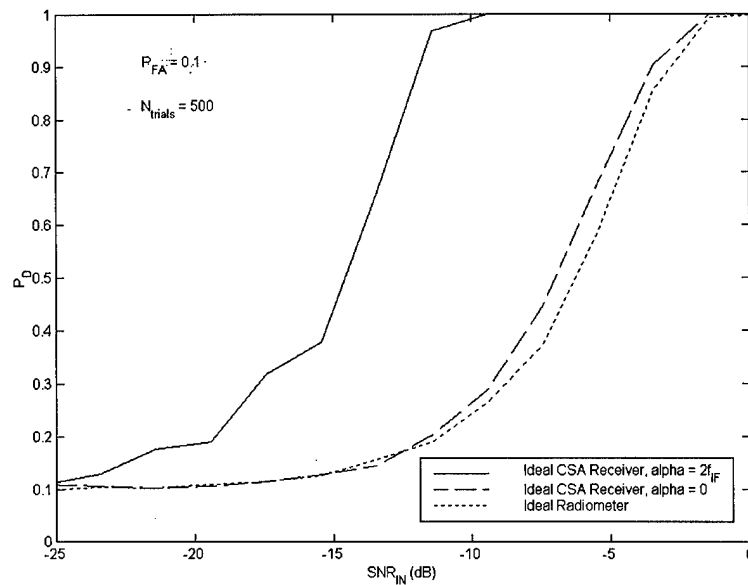


Figure 4-1. Ideal CSA Receiver Performance for Nonstationary Noise, $\rho_N = 0.01$
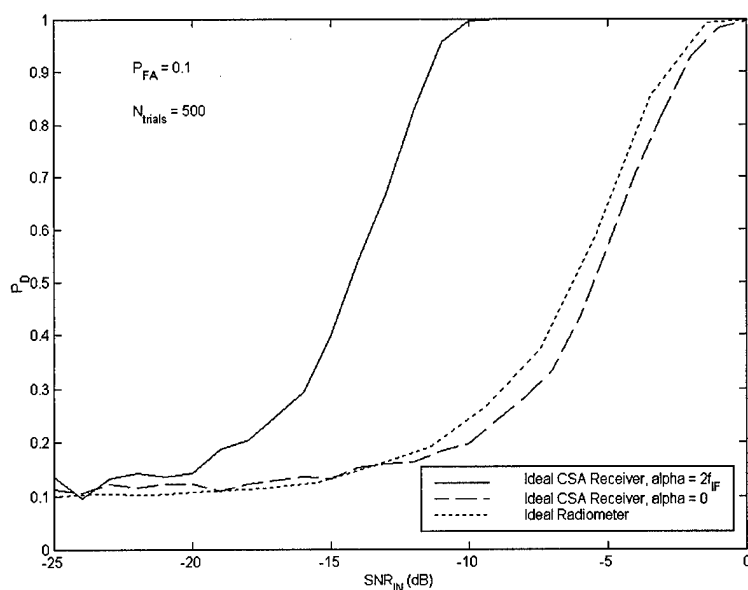
Figure 4-2. Ideal CSA Receiver Performance for Nonstationary Noise, $\rho_N = 0.1$

The test statistic distribution at $\alpha = 0$ and $\alpha = 2f_{IF}$ gives some insight into this performance (see Figure 4-3). As expected, at $\alpha = 0$ the variance of the test statistic has increased from approximately zero to the variance of the noise power. However, the variance at $\alpha = 2f_{IF}$ has only slightly increased. The primary contribution to the variance at $\alpha \neq 0$ appears to be due to the random nature of the spectral correlation for non 'white' noise, as discussed in the previous section, with the variation in noise power having little effect. Therefore, as the variance of the noise power increases, there will be a stronger effect on the test statistic variance at any $\alpha \neq 0$, and a corresponding negative impact on performance. Consequently, the CSA receiver is not completely immune to noise power variations but it is clearly superior to the radiometer. These results also show that the CSA receiver is less sensitive than the radiometer to inaccuracies or uncertainties in the threshold setting.

70
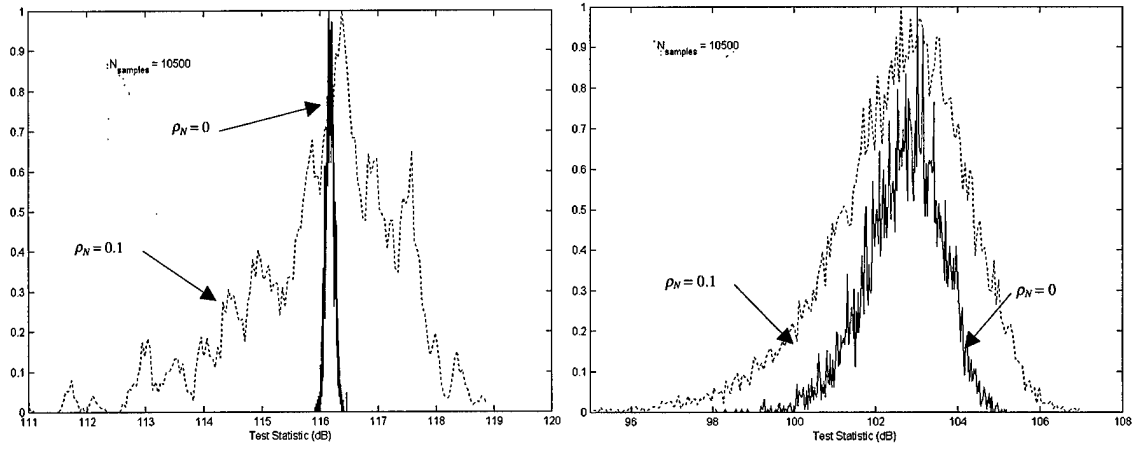
Figure 4-3.  Histogram of Test Statistics under $H_o$ with

Nonstationary Noise for: (a) $\lambda_E(0)$, and (b) $\lambda_E(2f_{IF})$

### 4.5.3  Narrowband Interference

The third scenario evaluates the Ideal CSA Receiver performance in the presence of stationary noise and narrowband interference.  Two narrowband interferers are examined, a simple tone jammer and an amplitude-modulated single sideband (AM-SSB) signal.  First, the tone jammer is introduced into the received signal, so $r(t) = s(t) + j(t) + n(t)$, where $n(t)$ is stationary, and

$$j(t) = \sqrt{2J}\,\cos\!\left(2\pi f_j t\right) \tag{4-1}$$

The SCF of the jammer, $j(t)$, is given by

$$S_j^\alpha(f) = \begin{cases} \frac{J}{2}\delta\!\left(f - f_j\right) + \frac{J}{2}\delta\!\left(f + f_j\right), & \alpha = 0 \\ \frac{J}{2}\delta(f), & \alpha = \pm 2f_j \\ 0, & \text{e.w.} \end{cases} \tag{4-2}$$

Therefore, under $H_1$ for any $f_j \neq k/T_c$ and $f_j \neq f_{IF}$  SCF of the ideal digital receiver output signal, $x(t)$,  is given by

71

$$S_x^\alpha(f) = \begin{cases} \frac{P}{2T_c}\left[Q^2(f+f_{IF}) + Q^2(f-f_{IF})\right] + \frac{J}{2}\left[\delta(f-f_j) + \delta(f+f_j)\right] + \frac{N_0}{2} & \alpha = 0 \\[2mm] \frac{P}{2T_c}\left[Q(f+\frac{\alpha}{2}+f_{IF})Q(f-\frac{\alpha}{2}+f_{IF}) + Q(f+\frac{\alpha}{2}-f_{IF})Q(f-\frac{\alpha}{2}-f_{IF})\right] & \alpha = \frac{k}{T_c}, k \neq 0 \\[2mm] \frac{P}{2T_c}Q(f+\frac{\alpha}{2}+f_{IF})Q(f-\frac{\alpha}{2}-f_{IF}) & \alpha = \frac{k}{T_c} - 2f_{IF} \\[2mm] \frac{P}{2T_c}Q(f+\frac{\alpha}{2}-f_{IF})Q(f-\frac{\alpha}{2}+f_{IF}) & \alpha = \frac{k}{T_c} + 2f_{IF} \\[2mm] \frac{J}{2}\delta(f) & \alpha = \pm 2f_j \\[2mm] 0 & \text{e.w} \end{cases}$$

(4-3)

These simulations consider the case where the signal and jammer have equal power, i.e. SJR = 0 dB and $f_j \neq f_{IF}$. The estimated SCF for SNR = -3 dB is shown in Figure 4-1 and the corresponding test statistic in Figure 4-2. To make the figure clearer, a display threshold has been set for the estimated SCF.
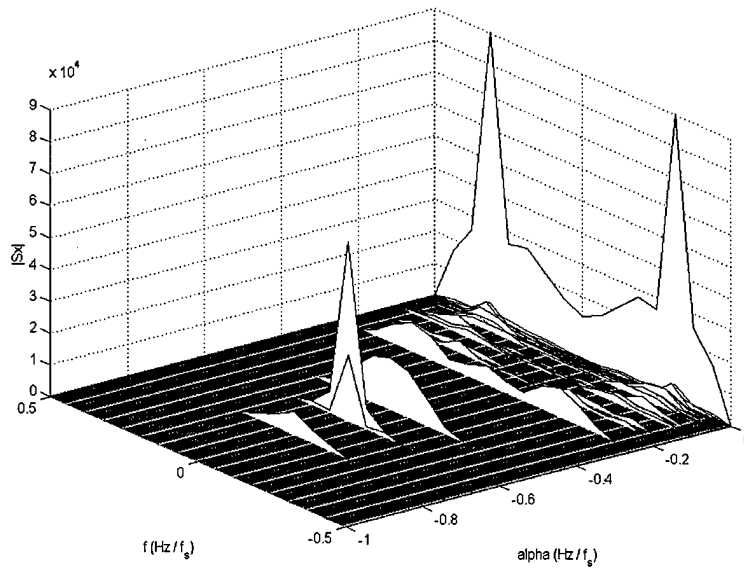


Figure 4-1. SCF Estimate for Tone Jamming Environment

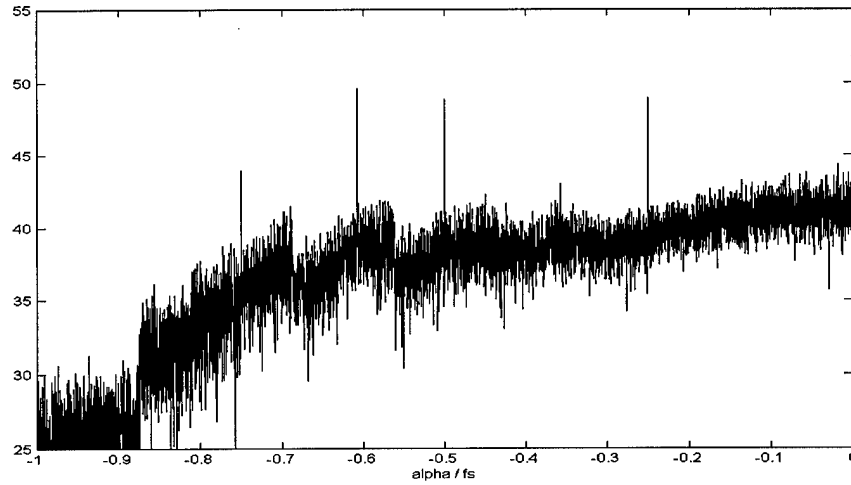$SJR=$ 0 dB, $SNR_{IN} = $ -3 dB, and $\Delta t \Delta f =$ 1000

Figure 4-2. $\lambda_E(\alpha)$ under $H_1$ for Tone Jamming with $SJR = 0$ dB, and $SNR_{IN} = -3$ dB

For this particular scenario, the advantage of estimating the entire bi-frequency plane is clearly demonstrated by comparing Figure 4-2 with Figure 4-1 (b). Not only is SOI detection $\alpha = 2f_{IF}$ unaffected by the introduction of a tone jammer, but the jammer itself is easily detected and the modulation type and parameters easily determined. If the jammer happens to set on the SOI frequency, i.e. $f_j = f_{IF}$, post-processing may be used to compare chip rate features with double carrier features and determine that the increased magnitude is due to the presence of a jammer.

Probability of detection simulation results are presented at Figure 4-3. The radiometer experiences a 7 dB loss in detection performance, and as expected, CSA receiver performance at $\alpha = 2f_{IF}$ is not effected by the tone jammer. However, there is a large discrepancy (approximately 9 dB) between the radiometer and the CSA receiver at $\alpha = 0$. As the case for any signal with an extremely small bandwidth ($W_j < \Delta f$), the CSA receiver tends to overestimate the power due its large frequency resolution. This can be seen by comparing the theoretical jammer SCF in Eqn. (4-2) to the estimated SCF shown in Figure 4-1 where the delta function tends to look more triangular. This has the apparent effect of increasing in jammer power (decreased SJR), by causing decreased detection performance.

73
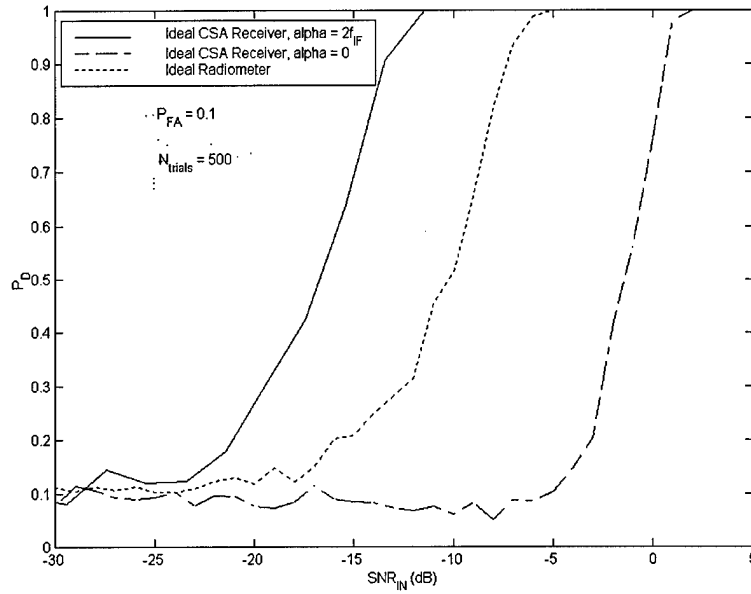
Figure 4-3. Ideal CSA Receiver Performance for Tone Jamming with *SJR* = 0 dB

However, the immunity of the CSA receiver to any narrowband interference depends strongly on the quality of the estimate. In the second case, an AM-SSB signal is introduced into the received signal, so $r(t) = s(t) + i(t) + n(t)$, where $n(t)$ is stationary, and

$$i(t) = \sqrt{2I}\left[m(t)\cos(2\pi f_i t) - \hat{m}(t)\sin(2\pi f_i t)\right] \tag{4-4}$$

where $\hat{m}(t)$ is the Hilbert transform of $m(t)$, given by

$$\hat{m}(t) \equiv \int_{-\infty}^{\infty} \frac{m(t-\zeta)}{\pi\zeta}d\zeta \tag{4-5}$$

In this case the modulating signal, $m(t)$, is a simple tone

$$m(t) = \cos(2\pi f_m t) \tag{4-6}$$

74

reducing $i(t)$ to

$$i(t) = \sqrt{2I} \left\{ \cos(2\pi f_m t)\cos(2\pi f_i t) - \int_{-\infty}^{\infty} \frac{\cos\left[2\pi f_m(t-\zeta)\right]}{\pi\zeta} d\zeta \, \sin(2\pi f_i t) \right\}$$

$$= \sqrt{2I}\left[\cos(2\pi f_m t)\cos(2\pi f_i t) + \sin(2\pi f_m t)\sin(2\pi f_i t)\right] \qquad (4\text{-}7)$$

$$= \sqrt{2I}\cos\left[2\pi\left(f_i - f_m\right)t\right]$$

The SCF of $i(t)$ is given by

$$S_i^\alpha(f) = \begin{cases} \frac{1}{2}\delta(f - f_i + f_m) + \frac{1}{2}\delta(f + f_j - f_m), & \alpha = 0 \\[2mm] \frac{1}{2}\delta(f), & \alpha = \pm 2(f_i - f_m) \\[2mm] 0, & \text{e.w.} \end{cases} \qquad (4\text{-}8)$$

Therefore under $H_1$ for any $(f_i - f_m) \neq k/T_c$ and $(f_i - f_m) \neq f_{IF}$, the SCF of the SSCA input signal, $x(t)$, is given by

$$S_x^\alpha(f) = \begin{cases} \frac{P}{2T_c}\left[Q^2(f + f_{IF}) + Q^2(f - f_{IF})\right] + \\[1mm] \qquad \frac{1}{2}\delta(f - f_i + f_m) + \frac{1}{2}\delta(f + f_j - f_m) + \frac{N_0}{2} & \alpha = 0 \\[2mm] \frac{P}{2T_c}\left[Q(f + \frac{\alpha}{2} + f_{IF})Q(f - \frac{\alpha}{2} + f_{IF}) + Q(f + \frac{\alpha}{2} - f_{IF})Q(f - \frac{\alpha}{2} - f_{IF})\right] & \alpha = \frac{k}{T_c}, k \neq 0 \\[2mm] \frac{P}{2T_c}Q(f + \frac{\alpha}{2} + f_{IF})Q(f - \frac{\alpha}{2} - f_{IF}) & \alpha = \frac{k}{T_c} - 2f_{IF} \\[2mm] \frac{P}{2T_c}Q(f + \frac{\alpha}{2} - f_{IF})Q(f - \frac{\alpha}{2} + f_{IF}) & \alpha = \frac{k}{T_c} + 2f_{IF} \\[2mm] \frac{1}{2}\delta(f) & \alpha = \pm 2(f_i - f_m) \\[2mm] 0 & \text{e.w} \end{cases} \qquad (4\text{-}9)$$

By comparison with Eqn. (4-3), the detection performance at $\alpha = 2f_{IF}$ ($k = 0$) should be identical to the tone jammer case. However, the SCF estimation algorithm (the SSCA) has particular trouble estimating the SCF for an AM-SSB signal and tends to introduce many artificial cyclic features that can interfere during detection. This can be easily observed in the test statistic plotted in Figure 4-4. The expected reduction in detection performance is confirmed by using the simulation results. Figure 4-5 compares the Ideal CSA Receiver detection performance at $\alpha = 2f_{IF}$

in the presence of tone jamming and AM-SSB interference. There is approximately a 1.5 dB decrease in performance due to the AM-SSB interferer.


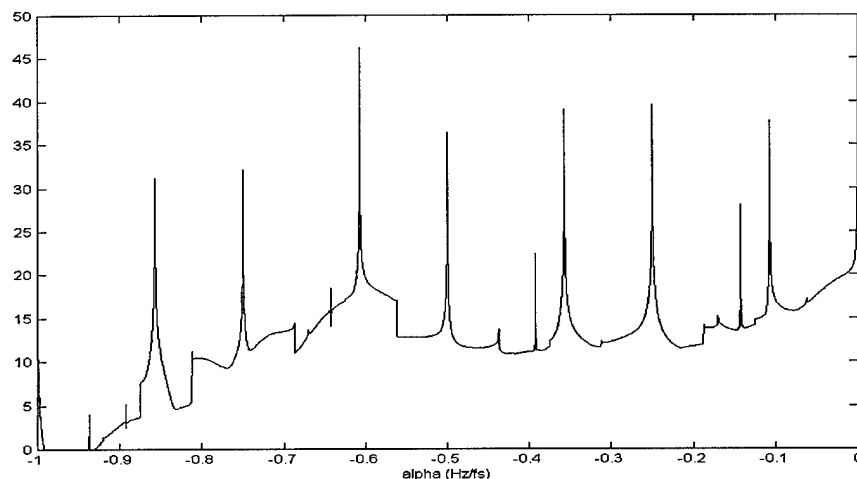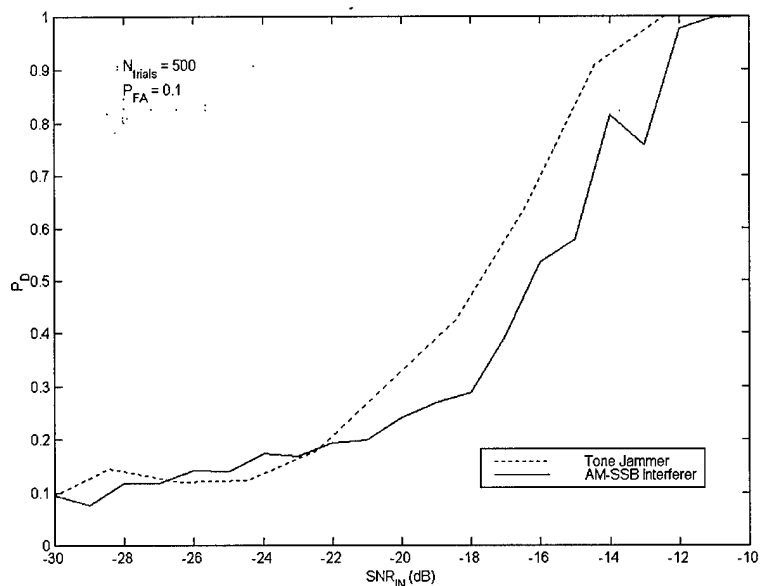
Figure 4-4. $\lambda_E(\alpha)$ for AM-SSB Interferer



Figure 4-5. CSA Receiver Performance for AM-SSB Interference with $SIR = 0$ dB

### 4.5.4 Summary

This section determined the performance of the Ideal CSA Receiver by simulation and compared its performance to the radiometer. As cyclic feature detection theory suggests, the

76

CSA receiver detection performance approaches that of the ideal radiometer in benign (stationary noise) environments. By applying radiometric detection principles to the test statistic, analysis shows that the CSA receiver performance is a function of noise quality. As the noise PSD becomes flatter, it is expected that the CSA receiver will outperform the radiometer. Simulation of a nonstationary noise environment shows that the CSA receiver outperforms the radiometer by approximately 10 dB, exhibiting only a slight decrease (less than 1 dB) in performance when compared to the stationary noise case. Analysis shows that the CSA detector is effected when the variance of the noise power exceeds the variance of the noise spectral correlation. When the signal environment includes tone jamming, CSA receiver performance is not unaffected, whereas the radiometer performs extremely poorly. In the presence of an AM-SSB interferer, the CSA receiver still outperforms the radiometer. However performance is degraded by 1.5 dB due to the artificial cyclic features introduced by the SSCA.

## 4.6  Channelized CSA Receiver Performance

The purpose of this section is to determine Channelized CSA Receiver performance and compare it to the Ideal CSA Receiver examined previously. First, the effect that bandpass filtering has on performance of different channels is determined. The signal environment varies from stationary noise to nonstationary noise and then stationary noise with narrowband interference is considered.

### 4.6.1 Channelized Cyclic Spectrum Characterization

As seen in Figure 3-2, the filter response of the channelized receiver varies drastically between channels at the edge of the passband and channels in the middle of the passband. The asymmetric nature of the filter response for 'edge' channels means that the spectra are no longer

symmetric about $f_{IF}$ after downconversion. Therefore, the detection performance in those channels may be effected. The SCF for the $m$th channel, $S^\alpha_{y_m}(f)$, can be written as

$$S^\alpha_{y_m}(f) \equiv S^\alpha_x(f)H_m\left(f + \tfrac{\alpha}{2}\right)H^*_m\left(f - \tfrac{\alpha}{2}\right) \qquad (4\text{-}1)$$

where $S^\alpha_x(f)$ is the Ideal CSA Receiver SCF and $H_m(\cdot)$ is the cascade filter response for the $m$th channel. Two cases of particular interest are 1) those channels with the most asymmetric attenuation, such as channels 1 and $M$ in Figure 3-2, and 2) those channels with little or no attenuation, such as channel $M/2$-1 in Figure 3-2. For ease of notation, the first case is referred to as Channel 1 and the second case Channel 2. For the filter implementation of this research, the estimated SCF and test statistics for Channels 1 and 2 are shown in Figures 4-17 and 4-18, respectively.
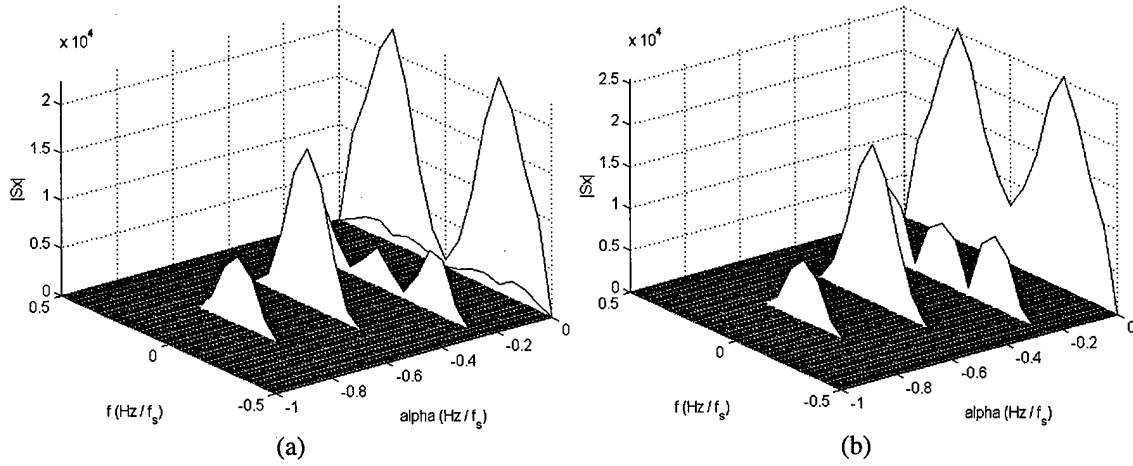


Figure 4-1. SCF Estimate with $SNR_{IN} = 0$ dB for: (a) Channel 1, and (b) Channel 2.
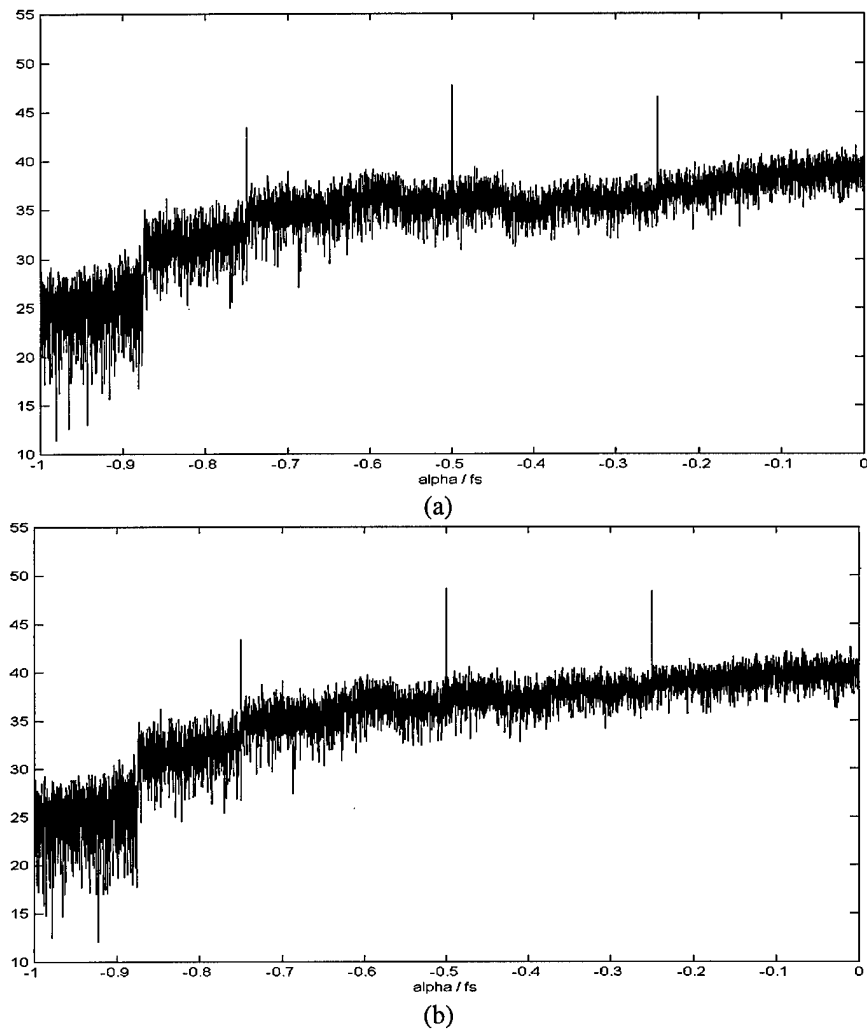
Figure 4-2. $\lambda_E(\alpha)$ under $H_1$ with $SNR_{IN}$ = 0dB for: (a) Channel 1 and (b) Channel 2

While there is a discernable difference in the magnitude of the cyclic features, examining the estimated SCF does not give any indication of expected detection performance. Given that $SNR_{IN}$ is defined at the bandpass filter, any SNR improvement resulting from the additional IF bandpass filtering will translate to a detection performance improvement. The RF and IF filter responses for Channel 2 are both ideal, and the detection performance should be identical to the Ideal CSA Receiver. However, this is not the case for Channel 1. The difference between the PSD of Channel 1 at the RF and IF passbands is evident in Figure 4-3.
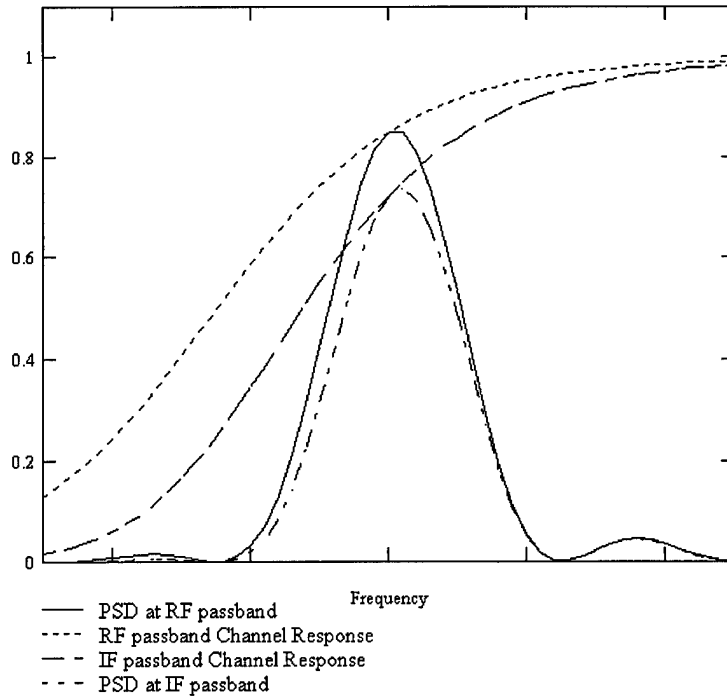
Figure 4-3. Channel 1 Filter Response

As the bandwidth of the signal increases and the signal power becomes more uniformly distributed within the channel bandwidth, the amount of signal power attenuation will increase yet the amount of noise attenuation will stay constant. This will lead to a varying SNR improvement for Channel 1 with respect to the signal bandwidth. The SNR improvement for the $m$th channel is defined as the difference between $SNR_{IN}$ and the SNR of the $m$th channel output, $y_m(t)$. The $m$th channel SNR is defined as

$$\left(\frac{S}{N}\right)_m = \frac{\int_{-\infty}^{\infty} S_s(f)|H_m(f)|^2 df}{\frac{N_0}{2}\int_{-\infty}^{\infty} |H_m(f)|^2 df} \tag{4-2}$$

In Figure 4-4, SNR improvement is plotted against the BW Ratio, which is defined as

$$BW\ Ratio = \frac{2}{T_c W_{CSA}} \tag{4-3}$$
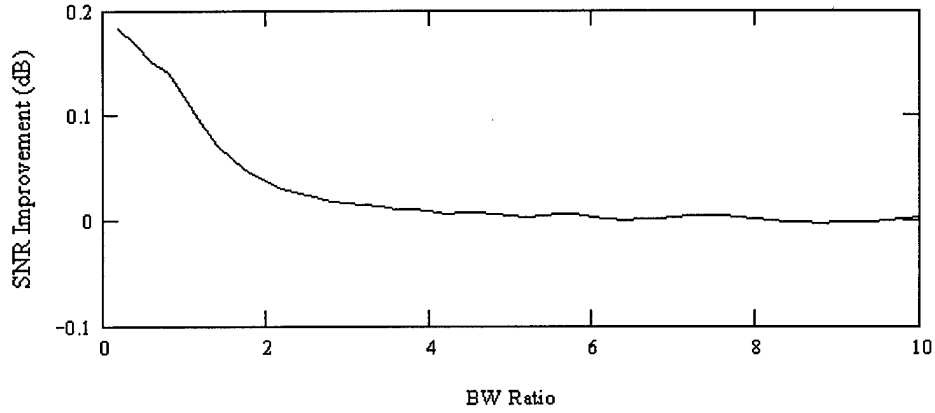
Figure 4-4. Channel 1 SNR Improvement

Based on these results, when the BW Ratio is unity, i.e. the null-to-null bandwidth of the signal is equal to the channel bandwidth, Channel 1 will exhibit a performance improvement of approximately 0.1 dB compared to Channel 2. This is a negligible performance improvement and leads to the conclusion that the Channelized CSA Receiver detection performance is independent of the channel selected. Additionally, it is important to note that Figure 4-4 is specific to the filter realization used in this research. A difference in the type or order of the filter will cause these results to vary.

### 4.6.2 Stationary Noise

In the case of stationary noise, the detector is presented with the following binary hypothesis

$$r(t) = \begin{cases} \sqrt{2P} \sum_{n=-\infty}^{\infty} a_n \, q(t - nT_c) \cos(2\pi f_0 t) + n(t) & (H_1) \\ n(t) & (H_0) \end{cases}$$

(4-1)

The SCF of the $m$th channel output, $y_m(t)$, is given by

$$S_{y_m}^{\alpha}(f) \equiv S_x^{\alpha}(f) H_m\left(f + \tfrac{\alpha}{2}\right) H_m^*\left(f - \tfrac{\alpha}{2}\right)$$

(4-2)

where under $H_1$ conditions

81

$$S_x^\alpha(f) = \begin{cases} \frac{P}{2T_c}\left[Q^2(f+f_{IF})+Q^2(f-f_{IF})\right]+\frac{N_0}{2} & \alpha=0 \\ \frac{P}{2T_c}\left[Q(f+\frac{\alpha}{2}+f_{IF})Q(f-\frac{\alpha}{2}+f_{IF})+Q(f+\frac{\alpha}{2}-f_{IF})Q(f-\frac{\alpha}{2}-f_{IF})\right] & \alpha=\frac{k}{T_c}, k\neq 0 \\ \frac{P}{2T_c}Q(f+\frac{\alpha}{2}+f_{IF})Q(f-\frac{\alpha}{2}-f_{IF}) & \alpha=\frac{k}{T_c}-2f_{IF} \quad (4\text{-}3) \\ \frac{P}{2T_c}Q(f+\frac{\alpha}{2}-f_{IF})Q(f-\frac{\alpha}{2}+f_{IF}) & \alpha=\frac{k}{T_c}+2f_{IF} \\ 0 & \text{e.w} \end{cases}$$

and under $H_0$ conditions

$$S_x^\alpha(f) = \begin{cases} \dfrac{N_0}{2} & \alpha=0 \\ 0 & \text{e.w} \end{cases} \qquad (4\text{-}4)$$

Simulation results for stationary noise are presented in Figure 4-1. As expected, these results show that Channel 1 and Channel 2 detection performance is approximately equal. The small performance improvement predicted by Figure 4-4 is much smaller than the resolution of the results. As discussed previously, the detection performance of Channel 2 is identical to the Ideal CSA Receiver detection performance, therefore the channelized receiver performs identically to the ideal receiver, independent of channel selected.
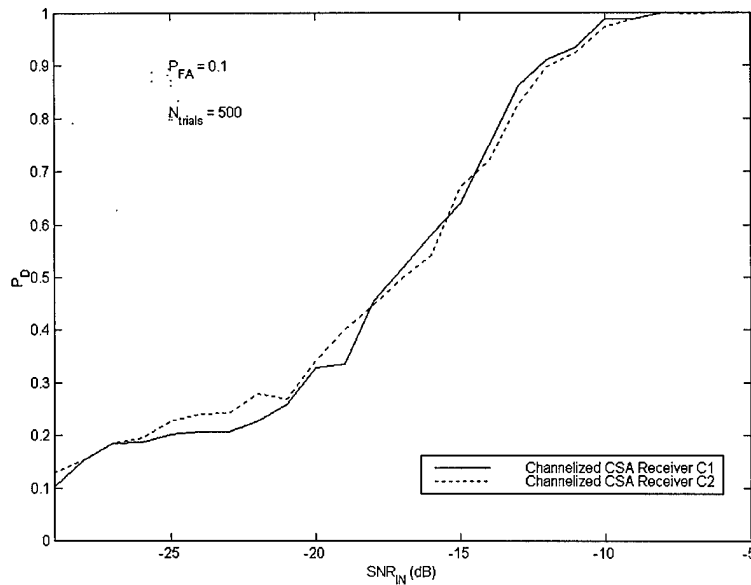


Figure 4-1. Channelized CSA Receiver Performance at $\alpha = 2f_{IF}$ with Stationary Noise

### 4.6.3 Nonstationary Noise

To determine the performance of the Channelized CSA Receiver in the presence of nonstationary noise, $n(t)$ is modeled as being nonstationary with $\rho_N$, the co-efficient of variation defined in Eqn.(4-2), equal to 0.1. Simulation results are presented in Figure 4-1 and as expected, indicate that Channel 1 and 2 detection performances are equal.
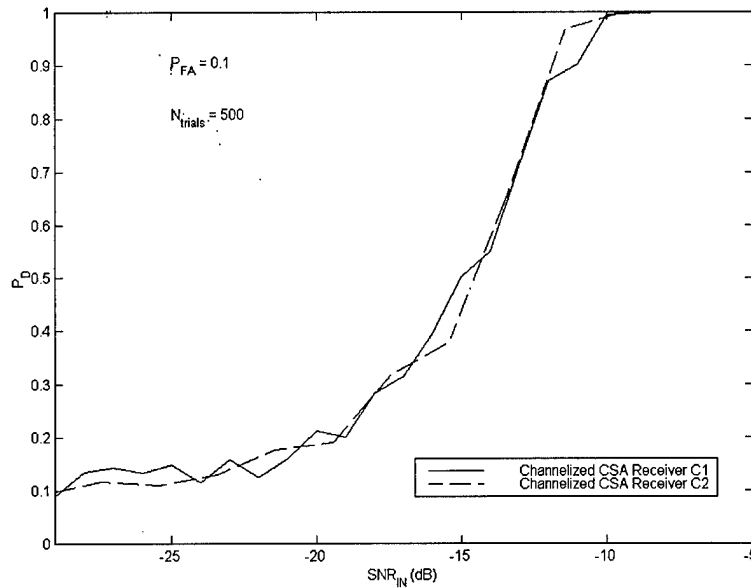


Figure 4-1. Channelized CSA Receiver Performance at $\alpha = 2f_{IF}$
with Nonstationary Noise, $\rho_N = 0.1$

### 4.6.4 Narrowband Interference

The tone jammer and AM-SSB interferer introduced in Section 4.5.3 are now included in the channelized receiver simulation. In general, the SCF of the $m$th channel output is given by Eqn. (4-2). Under $H_1$ conditions, $S_x^\alpha(f)$ for the tone jammer case is given by Eqn. (4-3) and Eqn. (4-9) represents $S_x^\alpha(f)$ for AM-SSB interferer case. Simulation results for the tone jammer and the AM-SSB interferer are presented in Figure 4-1 (a) and (b), respectively. In the tone jammer case the detection performance of both Channelized CSA Receiver channels are unaffected, as

83

predicted by the theory. Figure 4-1 (b) shows that both Channels are slightly affected by the AM-SSB interferer, due to the poor estimate of the cyclic spectrum of $i(t)$ by the SSCA. The theory also suggests that detection performance of Channel 1 should be approximately equal to Channel 2, this is confirmed in both cases.
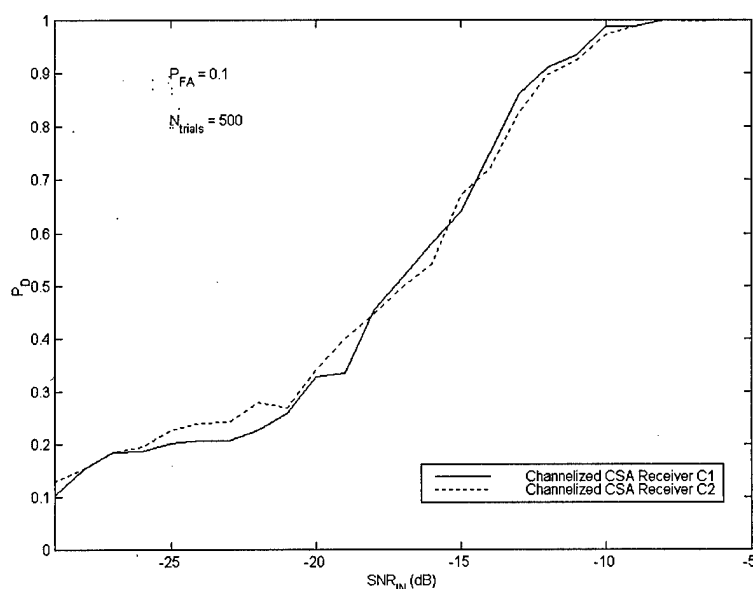


(a)
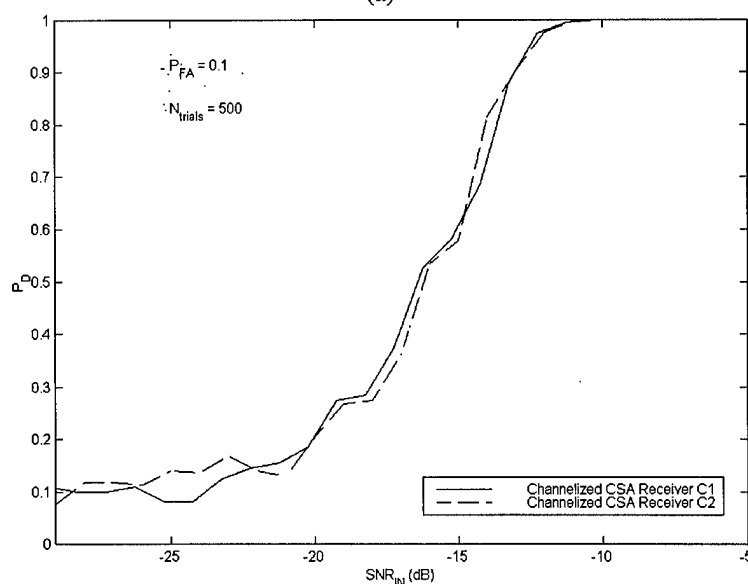


(b)

Figure 4-1. Channelized CSA Receiver Performance at $\alpha = 2f_{IF}$ with:
(a) Tone Jamming, and (b) AM-SSB Interference

### 4.6.5 Summary

The Channelized CSA Receiver performance was determined by simulation and compared to the Ideal CSA Receiver. First, SNR improvements due to filter effects were examined and Channel 1 was found to have a negligible performance gain of 0.1 dB over Channel 2 when the null-to-null bandwidth of the signal equals the bandwidth of each channel. This results from the concentration of the signal power in the middle of the channel bandwidth. As the signal power is distributed more evenly by an increase in signal bandwidth, the attenuation of the signal and noise become identical and the SNR improvement approaches zero. Under all conditions, Channel 1 and Channel 2 performed identically as predicted. Therefore, the Channelized CSA Receiver performance is approximately equal to the Ideal CSA Receiver, independent of the channel selected.

## 4.7 Quadrature CSA Receiver Performance

The purpose of this section is to determine the Quadrature CSA Receiver performance and compare it to the Ideal CSA Receiver simulated in Section 4.5. First, theoretical SCF expressions for real and complex input cases are developed. Based on these expressions, the most suitable input method is selected. The signal environment varies from stationary noise to nonstationary noise and then stationary noise with narrowband interference is considered.

### 4.7.1 Quadrature Input Cyclic Spectrum Characterization

As with the Channelized CSA Receiver, the filter response of the IF and RF bandpass filters will have an effect on the quadrature receiver detection performance. Additionally, how the in-phase and quadrature signals are combined, as real or complex signals, also effects performance. The Quadrature digital receiver, described in Section 3.4.3 produces in-phase and quadrature signals, $z_I(t)$ and $z_Q(t)$ defined as

$$z_I(t) \equiv \tfrac{1}{2}a(t)\cos(2\pi f_{IF}t)$$
$$z_Q(t) \equiv \tfrac{1}{2}a(t)\sin(2\pi f_{IF}t) \tag{4-1}$$

Although these signals are actually time-series, to simplify analysis, stochastic processes are assumed. This assumption allows the calculation of the probabilistic SCF which the CSA Receiver attempts to estimate. The in-phase and quadrature signals can be combined either as a complex ordered pair or summed together as real signals. For the first case, the input signal is defined as $z(t) = z_I(t) + j\,z_Q(t)$. Assuming $z(t)$ is an ergodic random process, the expectation operator, $E\{\cdot\}$, can be interchanged with the time average operator $\langle \cdot \rangle \equiv \lim\limits_{T\to\infty}\int_{-T/2}^{T/2}(\cdot)dt$. Using the CAF definition in Eqn. (2-2)

$$
\begin{aligned}
R_z^\alpha(\tau) &\equiv \left\langle z\!\left(t+\tfrac{\tau}{2}\right)z^*\!\left(t-\tfrac{\tau}{2}\right)e^{-j2\pi\alpha t}\right\rangle \\
&= \left\langle \left[z_I\!\left(t+\tfrac{\tau}{2}\right)+jz_Q\!\left(t+\tfrac{\tau}{2}\right)\right]\!\left[z_I\!\left(t-\tfrac{\tau}{2}\right)-jz_Q\!\left(t-\tfrac{\tau}{2}\right)\right]e^{-j2\pi\alpha t}\right\rangle \\
&= \left\langle \tfrac{1}{2}a\!\left(t+\tfrac{\tau}{2}\right)e^{j2\pi f_{IF}(t+\tau/2)}\tfrac{1}{2}a\!\left(t-\tfrac{\tau}{2}\right)e^{-j2\pi f_{IF}(t-\tau/2)}e^{-j2\pi\alpha t}\right\rangle \\
&= \left\langle \tfrac{1}{4}a\!\left(t+\tfrac{\tau}{2}\right)a\!\left(t-\tfrac{\tau}{2}\right)e^{j2\pi f_{IF}\tau}e^{-j2\pi\alpha t}\right\rangle \\
&= \tfrac{1}{4}\left\langle a\!\left(t+\tfrac{\tau}{2}\right)a\!\left(t-\tfrac{\tau}{2}\right)e^{-j2\pi\alpha t}\right\rangle e^{j2\pi f_{IF}\tau} \\
&= \tfrac{1}{4}R_a^\alpha(\tau)e^{j2\pi f_{IF}\tau}
\end{aligned}
\tag{4-2}
$$

for $a(t)$ a real signal. Using the cyclic Wiener-Khinchin theorem

$$
\begin{aligned}
S_z^\alpha(f) &\equiv \int_{-\infty}^\infty R_z^\alpha(\tau)e^{-j2\pi f\tau}d\tau \\
&= \tfrac{1}{4}\int_{-\infty}^\infty R_a^\alpha(\tau)e^{-j2\pi(f-f_{IF})\tau}d\tau \\
&= \tfrac{1}{4}S_a^\alpha(f-f_{IF})
\end{aligned}
\tag{4-3}
$$

which is a scaled and frequency shifted version of the SCF of $a(t)$. In the case of BPSK modulation, $a(t)$ is given by,

$$a(t) = \sqrt{2P}\sum_{n=-\infty}^{\infty}a_n\,q(t-nT_c)\otimes h(t) \tag{4-4}$$

86

where $h(t)$ is the cascade filter impulse response, $a_n$ is a sequence of i.i.d. random variables equally likely to take on the values of $\pm 1$ and $q(t)$ is a unit amplitude rectangular pulse of length $T_c$. The SCF for $a(t)$ is that of an ASK signal which is [14]

$$S_a^\alpha(f) = \begin{cases} \dfrac{2P}{T_c} Q\left(f + \tfrac{\alpha}{2}\right) Q\left(f - \tfrac{\alpha}{2}\right) H\left(f + \tfrac{\alpha}{2}\right) H^*\left(f - \tfrac{\alpha}{2}\right) & \alpha = \tfrac{k}{T_c} \\ 0 & \text{e.w.} \end{cases}$$

(4-5)

where $Q(f) = T_c \operatorname{sinc}(f T_c)$. To simplify analysis, the filter is assumed to be ideal, so the full expression for the SCF of $z(t)$ can therefore be written as

$$S_z^\alpha(f) = \begin{cases} \dfrac{P}{2T_c} Q\left(f - f_{IF} + \tfrac{\alpha}{2}\right) Q\left(f - f_{IF} - \tfrac{\alpha}{2}\right) & \alpha = \tfrac{k}{T_c} \\ 0 & \text{e.w.} \end{cases}$$

(4-6)

The theoretical and estimated SCF for a lowpass signal are plotted in Figure 4-1 (a) and (b), respectively.
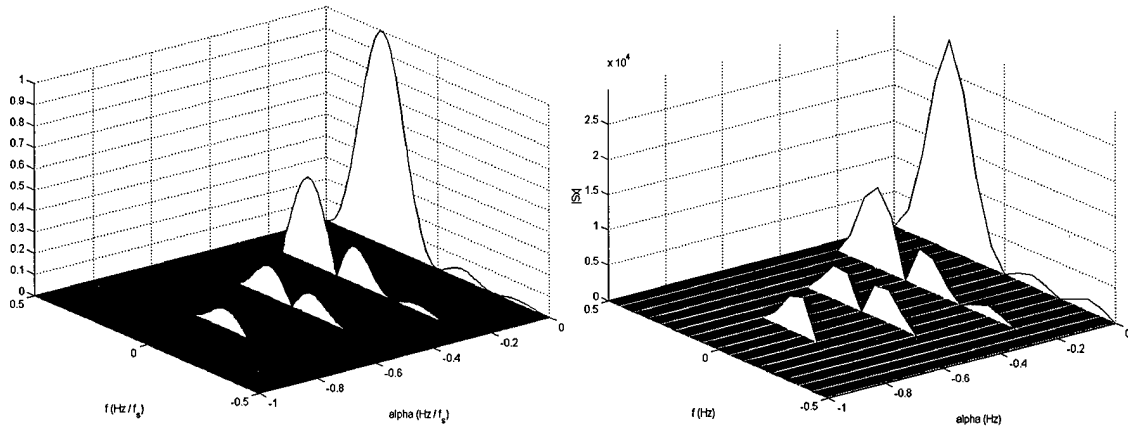


Figure 4-1. Complex Quadrature CSA Receiver SCF: (a) Theoretical, and (b) Estimated

Considering detection of this signal, the most significant thing about Figure 4-1 is the absence of the double-carrier feature at $\alpha = 2f_{IF}$. Therefore, any detection of the signal must be done using one of the chip rate features. Additionally, because the SCF for the complex signal $z(t)$ is no longer symmetric about $f = 0$, the modifications made to the mapping stage of the SSCA, as

87

described in Section 3.5.2, need to be removed. The modified algorithm is not only less efficient because it must perform operations on complex numbers, but also because it must produce all $P$ strips. The SSCA output is shown in Figure 4-1 (b) and the test statistic in Figure 4-2.



Figure 4-2. $\lambda_E(\alpha)$ under $H_1$ for Complex CSA Quadrature Receiver with $SNR_{IN} = 0$dB

For the second case, the in-phase and quadrature signals are simply summed, i.e. the signal is $z(t) = z_I(t) + z_Q(t)$. Following the same procedure and assuming ideal filters, the CAF can be calculated

$$
\begin{aligned}
R_z^\alpha(\tau) &\equiv \left\langle z\left(t+\tfrac{\tau}{2}\right)z^*\left(t-\tfrac{\tau}{2}\right)e^{-j2\pi\alpha t}\right\rangle \\
&= \left\langle \left[z_I\left(t+\tfrac{\tau}{2}\right)+z_Q\left(t+\tfrac{\tau}{2}\right)\right]\left[z_I\left(t-\tfrac{\tau}{2}\right)+z_Q\left(t-\tfrac{\tau}{2}\right)\right]e^{-j2\pi\alpha t}\right\rangle \\
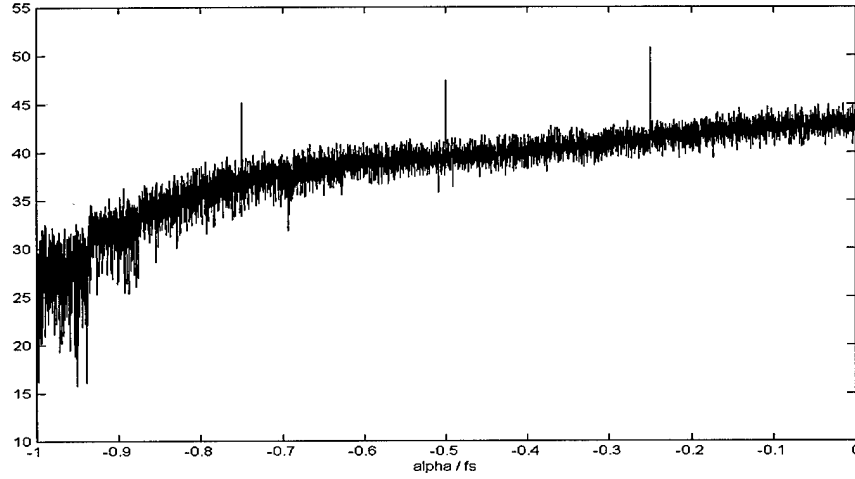&= \left\langle \tfrac{1}{2}a\left(t+\tfrac{\tau}{2}\right)a\left(t-\tfrac{\tau}{2}\right)\left\{\cos\left[2\pi f_{IF}\left(t+\tfrac{\tau}{2}\right)\right]+\sin\left[2\pi f_{IF}\left(t+\tfrac{\tau}{2}\right)\right]\right\}\left\{\cos\left[2\pi f_{IF}\left(t-\tfrac{\tau}{2}\right)\right]\right. \\
&\quad \left. +\sin\left[2\pi f_{IF}\left(t-\tfrac{\tau}{2}\right)\right]\right\}e^{-j2\pi\alpha t}\right\rangle \\
&= \left\langle \tfrac{1}{2}a\left(t+\tfrac{\tau}{2}\right)a\left(t-\tfrac{\tau}{2}\right)\left[\cos\left(2\pi f_{IF}\tau\right)+\sin\left(4\pi f_{IF}t\right)\right]e^{-j2\pi\alpha t}\right\rangle \\
&= R_{z_C}^\alpha(\tau)+R_{z_S}^\alpha(\tau)
\end{aligned}
$$

(4-7)

where for ease of analysis,

$$
\begin{aligned}
R_{z_C}^\alpha(\tau) &\equiv \left\langle \tfrac{1}{2}a\left(t+\tfrac{\tau}{2}\right)a\left(t-\tfrac{\tau}{2}\right)\cos\left(2\pi f_{IF}\tau\right)e^{-j2\pi\alpha t}\right\rangle \\
&= \tfrac{1}{2}R_a^\alpha(\tau)\cos\left(2\pi f_{IF}\tau\right)
\end{aligned}
$$

(4-8)

and

$$R_{z_s}^{\alpha}(\tau) \equiv \left\langle \tfrac{1}{2} a\!\left(t+\tfrac{\tau}{2}\right) a\!\left(t-\tfrac{\tau}{2}\right) \sin(4\pi f_{IF} t) e^{-j2\pi\alpha t} \right\rangle$$
$$= \left\langle \tfrac{1}{4j} a\!\left(t+\tfrac{\tau}{2}\right) a\!\left(t-\tfrac{\tau}{2}\right) \left[e^{-j2\pi(\alpha-2f_{IF})t} - e^{-j2\pi(\alpha+2f_{IF})t}\right] \right\rangle \qquad (4\text{-}9)$$
$$= \tfrac{j}{4}\left[R_a^{\alpha+2f_{IF}}(\tau) - R_a^{\alpha-2f_{IF}}(\tau)\right]$$

the respective Fourier transform pairs can be easily calculated

$$S_{z_c}^{\alpha}(f) \equiv \int_{-\infty}^{\infty} R_{z_c}^{\alpha}(\tau) e^{-j2\pi f\tau}\, d\tau$$
$$= \tfrac{1}{2}\int_{-\infty}^{\infty} R_a^{\alpha}(\tau) \cos(2\pi f_{IF}\tau) e^{-j2\pi f\tau}\, d\tau \qquad (4\text{-}10)$$
$$= \tfrac{1}{4}\left[S_a^{\alpha}(f - f_{IF}) + S_a^{\alpha}(f + f_{IF})\right]$$

These expressions can be used to determine the SCF for any signal represented by the in-phase

and quadrature components in Eqn. (4-1). In other words, the SCF of any signal input to the

quadrature receiver can be determined, so long as $a(t)$ and its corresponding SCF are known. In

the case of the BPSK signal of Eqn. (4-5), the expression can be written as

$$S_{z_c}^{\alpha}(f) = \tfrac{P}{2T_c}\left[Q\!\left(f - f_{IF} + \tfrac{\alpha}{2}\right)Q\!\left(f - f_{IF} - \tfrac{\alpha}{2}\right) + Q\!\left(f + f_{IF} + \tfrac{\alpha}{2}\right)Q\!\left(f + f_{IF} - \tfrac{\alpha}{2}\right)\right] \qquad (4\text{-}11)$$

and similarly

$$S_{z_s}^{\alpha}(f) \equiv \int_{-\infty}^{\infty} R_{z_s}^{\alpha}(\tau) e^{-j2\pi f\tau}\, d\tau$$
$$= \tfrac{j}{4}\int_{-\infty}^{\infty}\left[R_a^{\alpha+2f_{IF}}(\tau) - R_a^{\alpha-2f_{IF}}(\tau)\right] e^{-j2\pi f\tau}\, d\tau \qquad (4\text{-}12)$$
$$= \tfrac{j}{4}\left[S_a^{\alpha+2f_{IF}}(f) - S_a^{\alpha-2f_{IF}}(f)\right]$$

Using Eqn. (4-5), then

$$S_{z_s}^{\alpha}(f) = \tfrac{jP}{2T_c}\left[Q\!\left(f + f_{IF} + \tfrac{\alpha}{2}\right)Q\!\left(f - f_{IF} - \tfrac{\alpha}{2}\right) - Q\!\left(f - f_{IF} + \tfrac{\alpha}{2}\right)Q\!\left(f + f_{IF} - \tfrac{\alpha}{2}\right)\right] \qquad (4\text{-}13)$$

Combining Eqns. (4-11) and (4-13) and utilizing the distributive nature of the Fourier transform,

a full expression for the SCF of $z(t)$ can now be written as

$$S_z^\alpha(f) = S_{z_C}^\alpha(f) + S_{z_S}^\alpha(f)$$

$$= \tfrac{P}{2T_c}\left[Q\!\left(f+\tfrac{\alpha}{2}+f_{IF}\right)Q\!\left(f-\tfrac{\alpha}{2}+f_{IF}\right)+Q\!\left(f+\tfrac{\alpha}{2}-f_{IF}\right)Q\!\left(f-\tfrac{\alpha}{2}-f_{IF}\right)\right] \qquad (4\text{-}14)$$

$$+ \tfrac{jP}{2T_c}\left[Q\!\left(f+\tfrac{\alpha}{2}+f_{IF}\right)Q\!\left(f-\tfrac{\alpha}{2}-f_{IF}\right)-Q\!\left(f-\tfrac{\alpha}{2}+f_{IF}\right)Q\!\left(f+\tfrac{\alpha}{2}-f_{IF}\right)\right]$$

As with Eqn. (4-2), not all components are non-zero for all values of $\alpha$ and this can be rewritten

as

$$S_z^\alpha(f)=\begin{cases} \tfrac{P}{2T_c}\left[Q\!\left(f+\tfrac{\alpha}{2}+f_{IF}\right)Q\!\left(f-\tfrac{\alpha}{2}+f_{IF}\right)+Q\!\left(f+\tfrac{\alpha}{2}-f_{IF}\right)Q\!\left(f-\tfrac{\alpha}{2}-f_{IF}\right)\right] & \alpha=\tfrac{k}{T_c} \\[2mm] \tfrac{jP}{2T_c}Q\!\left(f+\tfrac{\alpha}{2}+f_{IF}\right)Q\!\left(f-\tfrac{\alpha}{2}-f_{IF}\right) & \alpha=\tfrac{k}{T_c}-2f_{IF} \\[2mm] \tfrac{-jP}{2T_c}Q\!\left(f+\tfrac{\alpha}{2}-f_{IF}\right)Q\!\left(f-\tfrac{\alpha}{2}+f_{IF}\right) & \alpha=\tfrac{k}{T_c}+2f_{IF} \\[2mm] 0 & \text{e.w} \end{cases} \qquad (4\text{-}15)$$

The theoretical and estimated SCF for a lowpass signal are shown in Figure 4-3 (a) and (b) respectively. Note that the magnitude of Eqn. (4-15) is identical to the magnitude of SCF for the BPSK, per Eqn. (4-3). Accordingly, assuming ideal input bandpass filters, the detection performance of the Quadrature CSA Receiver utilizing the summed in-phase and quadrature signals should be identical to the Ideal CSA Receiver. However, the bandpass filters of the quadrature receiver are fifth order Butterworth filters, described in Section 3.4.4, so any variation between the performance of the ideal and quadrature receivers can be directly attributed to the filters. This is explored further at the end of the section.
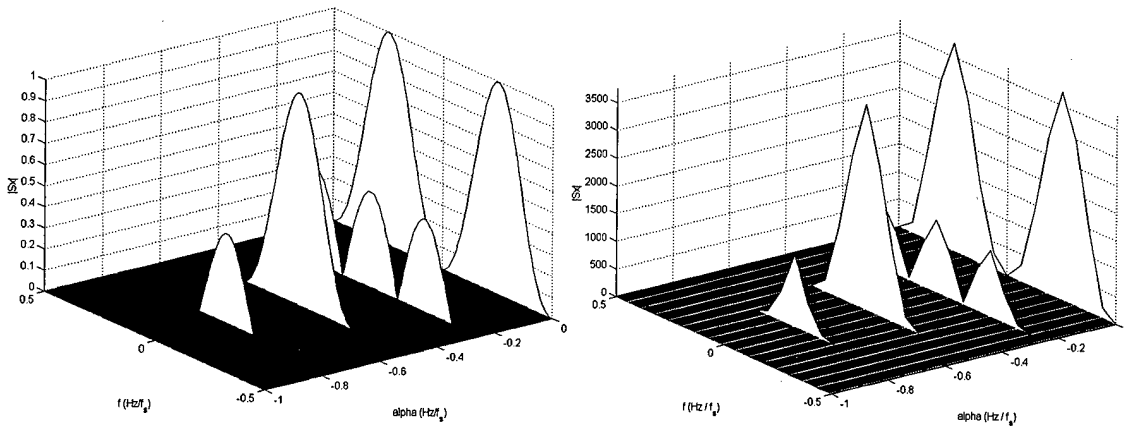


Figure 4-3. Summed Quadrature Receiver SCF: (a) Theoretical, and (b) Estimated

The test statistic for the summed quadrature receiver with a SNR of 0 dB is plotted in Figure 4-4. Comparing this to the complex input case shown in Figure 4-2, it is clear that the summed case has stronger cyclic features and provides more information, including the $\alpha = 2f_{IF}$ features. For these reasons, the following simulations use the summed input exclusively.
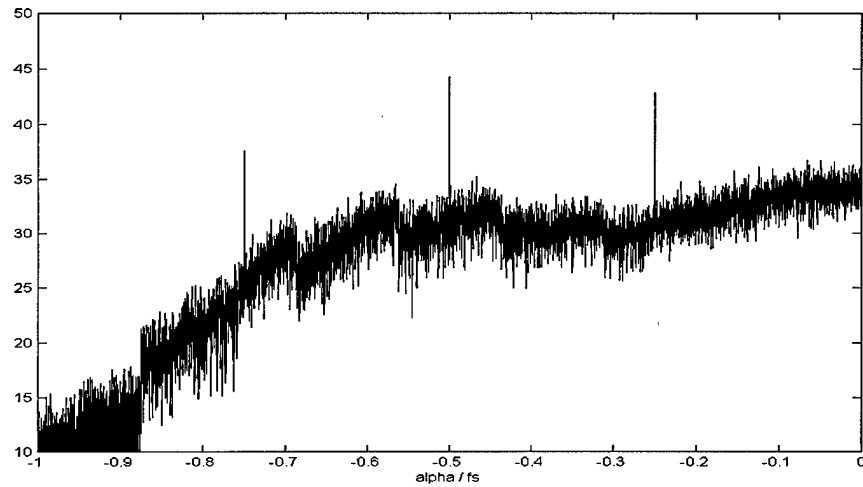


Figure 4-4. $\lambda_E(\alpha)$ for Summed Quadrature Receiver with $SNR_{IN} = 0$dB

As with Channel 1 of the Channelized CSA Receiver, signal attenuation varies as a function of the signal bandwidth because of the non-ideal filters. However, the important difference between the channelized and quadrature cases is that the quadrature RF passband is much wider than the IF passband. Therefore, when the IF passband is within the ideal region of the RF passband, there will be a more significant SNR improvement than the channelized case. This can be illustrated by plotting the SNR improvement against the BW Ratio as defined in (4-3). SNR improvement is defined as the difference between $SNR_{IN}$ defined in Section 3.4.3, and the SNR of the quadrature receiver output signal, $z(t)$. As shown in Figure 4-5, when the BW Ratio is unity, i.e. the null-to-null bandwidth of the signal equals the channel bandwidth, the Quadrature CSA Receiver exhibits a detection performance improvement of approximately 1 dB compared to the Ideal CSA Receiver. Again, this is specific to the filter realization used for this research, and as the signal bandwidth increases with respect to the receiver bandwidth, the SNR

91

improvement approaches zero. Given a BW Ratio of unity, this magnitude of performance improvement should be evident in the simulation results.
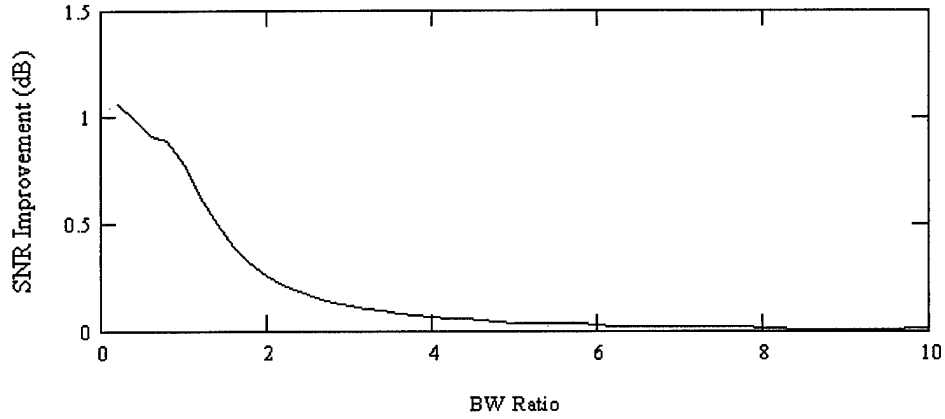


Figure 4-5. Quadrature CSA Receiver SNR Improvement

### 4.7.2 Stationary Noise

The detection performance of the Quadrature CSA Receiver with summed inputs is now examined. An identical scenario to that in Section 4.5.1 is simulated. The detector is presented with the following binary hypothesis

$$r(t) = \begin{cases} \sqrt{2P} \sum_{n=-\infty}^{\infty} a_n \, q(t - nT_c) \cos(2\pi f_0 t) + n(t) & (H_1) \\ n(t) & (H_0) \end{cases}$$ (4-1)

where the noise component, $n(t)$, is stationary additive white gaussian noise with a two-sided PSD, $S_n(f)$, of $N_0/2$. Using Eqns. (4-15) and (4-2), the $H_1$ hypothesis can be rewritten as in terms of the quadrature digital receiver output signal SCF,

92

$$S_z^\alpha(f) = \begin{cases} \frac{P}{2T_c}\left[Q\left(f+\frac{\alpha}{2}+f_{IF}\right)Q\left(f-\frac{\alpha}{2}+f_{IF}\right)+ \right. \\ \qquad\qquad \left. Q\left(f+\frac{\alpha}{2}-f_{IF}\right)Q\left(f-\frac{\alpha}{2}-f_{IF}\right)\right]+\frac{N_0}{2} & \alpha = 0 \\[6pt] \frac{P}{2T_c}\left[Q\left(f+\frac{\alpha}{2}+f_{IF}\right)Q\left(f-\frac{\alpha}{2}+f_{IF}\right)+Q\left(f+\frac{\alpha}{2}-f_{IF}\right)Q\left(f-\frac{\alpha}{2}-f_{IF}\right)\right] & \alpha = \frac{k}{T_c} \\[6pt] \frac{jP}{2T_c}Q\left(f+\frac{\alpha}{2}+f_{IF}\right)Q\left(f-\frac{\alpha}{2}-f_{IF}\right) & \alpha = \frac{k}{T_c}-2f_{IF} \\[6pt] \frac{-jP}{2T_c}Q\left(f+\frac{\alpha}{2}-f_{IF}\right)Q\left(f-\frac{\alpha}{2}+f_{IF}\right) & \alpha = \frac{k}{T_c}+2f_{IF} \\[6pt] 0 & e.w \end{cases}$$

(4-2)

assuming ideal filters and the noise component has been determined from Eqn. (4-7), by substituting $n(t)$ for $a(t)$. Simulation results are plotted in Figure 4-1. As predicted by Figure 4-5, the Quadrature CSA Receiver outperforms the Ideal CSA Receiver by approximately 1 dB. As discussed previously, it is important to note that an increase in chip rate, or signal bandwidth, such as the case presented in Figure 4-1 (b), results in the signal and noise powers being equally attenuated by the bandpass filters and the detection performance approaches that of the Ideal CSA Receiver.
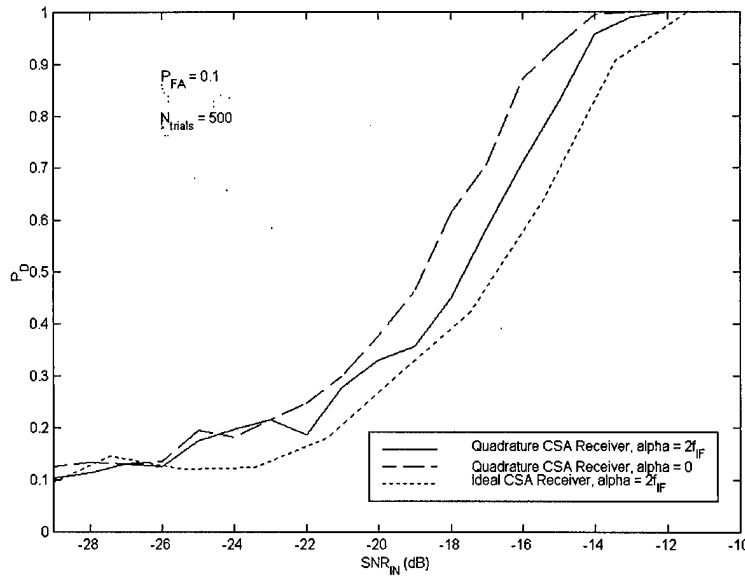


Figure 4-1. Quadrature CSA Receiver Performance

### 4.7.3 Nonstationary Noise

The noise component, $n(t)$ is now modeled as being nonstationary with $\rho_N$, the co-efficient of variation defined in Eqn.(4-2), equal to 0.1. With the null-to-null bandwidth of the signal equal to the receiver bandwidth, the Quadrature CSA Receiver is expected to outperform both the Ideal CSA Receiver and the Channelized CSA Receiver. Simulation results are presented in Figure 4-1.
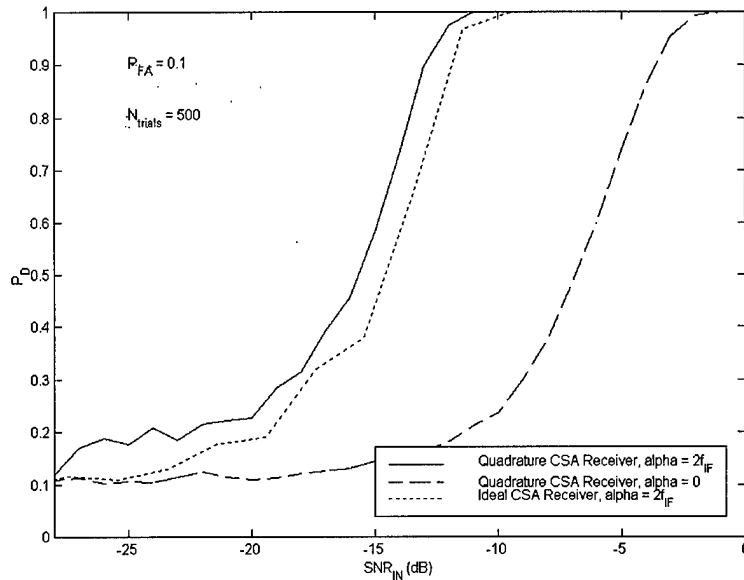


Figure 4-1. Quadrature CSA Receiver Performance for Nonstationary Noise with $\rho_N = 0.1$

Results in Figure 4-1 indicate that the Quadrature CSA Receiver at $\alpha = 0$, which is equivalent to a radiometer with identical bandpass filter characteristics as the quadrature receiver, outperforms the ideal radiometer shown in Figure 4-2. This is again because of SNR improvement due to the bandpass filters. As expected, the Quadrature CSA Receiver outperforms the Ideal CSA Receiver at $\alpha = 2f_{IF}$ by about 1 dB.

### 4.7.4 Narrowband Interference

The tone jammer and AM-SSB interferer introduced in Section 4.5.3 are now included in the Quadrature CSA Receiver simulation. Under the $H_1$ hypothesis for the AM-SSB case

$$
S_z^\alpha(f)=\begin{cases}
\frac{P}{2T_c}\left[Q^2(f+f_{IF})+Q^2(f-f_{IF})\right]+ & \\
\quad\frac{1}{2}\delta(f-f_i+f_m)+\frac{1}{2}\delta(f+f_j-f_m)+\frac{N_0}{2} & \alpha=0 \\
\frac{P}{2T_c}\left[Q(f+\frac{\alpha}{2}+f_{IF})Q(f-\frac{\alpha}{2}+f_{IF})+Q(f+\frac{\alpha}{2}-f_{IF})Q(f-\frac{\alpha}{2}-f_{IF})\right] & \alpha=\frac{k}{T_c},\,k\neq 0 \\
\frac{jP}{2T_c}Q(f+\frac{\alpha}{2}+f_{IF})Q(f-\frac{\alpha}{2}-f_{IF}) & \alpha=\frac{k}{T_c}-2f_{IF} \\
\frac{-jP}{2T_c}Q(f+\frac{\alpha}{2}-f_{IF})Q(f-\frac{\alpha}{2}+f_{IF}) & \alpha=\frac{k}{T_c}+2f_{IF} \\
\frac{jI}{2}\delta(f) & \alpha=-2(f_i-f_m) \\
\frac{-jI}{2}\delta(f) & \alpha=2(f_i-f_m) \\
0 & e.w
\end{cases}
\qquad (4\text{-}1)
$$

and for the tone jammer case

$$
S_z^\alpha(f)=\begin{cases}
\frac{P}{2T_c}\left[Q^2(f+f_{IF})+Q^2(f-f_{IF})\right]+\frac{1}{2}\delta(f-f_j)+\frac{1}{2}\delta(f+f_j)+\frac{N_0}{2} & \alpha=0 \\
\frac{P}{2T_c}\left[Q(f+\frac{\alpha}{2}+f_{IF})Q(f-\frac{\alpha}{2}+f_{IF})+Q(f+\frac{\alpha}{2}-f_{IF})Q(f-\frac{\alpha}{2}-f_{IF})\right] & \alpha=\frac{k}{T_c},\,k\neq 0 \\
\frac{jP}{2T_c}Q(f+\frac{\alpha}{2}+f_{IF})Q(f-\frac{\alpha}{2}-f_{IF}) & \alpha=\frac{k}{T_c}-2f_{IF} \\
\frac{-jP}{2T_c}Q(f+\frac{\alpha}{2}-f_{IF})Q(f-\frac{\alpha}{2}+f_{IF}) & \alpha=\frac{k}{T_c}+2f_{IF} \\
\frac{jI}{2}\delta(f) & \alpha=-2f_j \\
\frac{-jI}{2}\delta(f) & \alpha=2f_j \\
0 & e.w
\end{cases}
\qquad (4\text{-}2)
$$

The interferer and jammer contributions to the SCF of $z(t)$ are determined using Eqn. (4-7). Simulation results for the tone jammer and the AM-SSB interferer are presented in Figure 4-1 (a) and (b), respectively. For the tone jammer case, the Quadrature CSA Receiver detection performance is unaffected, as predicted by Eqn. (4-2), and shows an approximately 1 dB performance improvement over the Ideal CSA Receiver. In Figure 4-1 (b) it is evident that Quadrature CSA Receiver performance is effected by the AM-SSB interferer, even though Eqn. (4-1) shows that there are no overlapping cyclic features. As with the Ideal CSA Receiver, this is

95

due to the poor estimate of the cyclic spectrum of $i(t)$ by the SSCA. In both cases, the Quadrature CSA Receiver outperforms the Ideal CSA Receiver due to the effect of bandpass filtering and the fact that the signal's null-to-null bandwidth equals the receiver bandwidth.
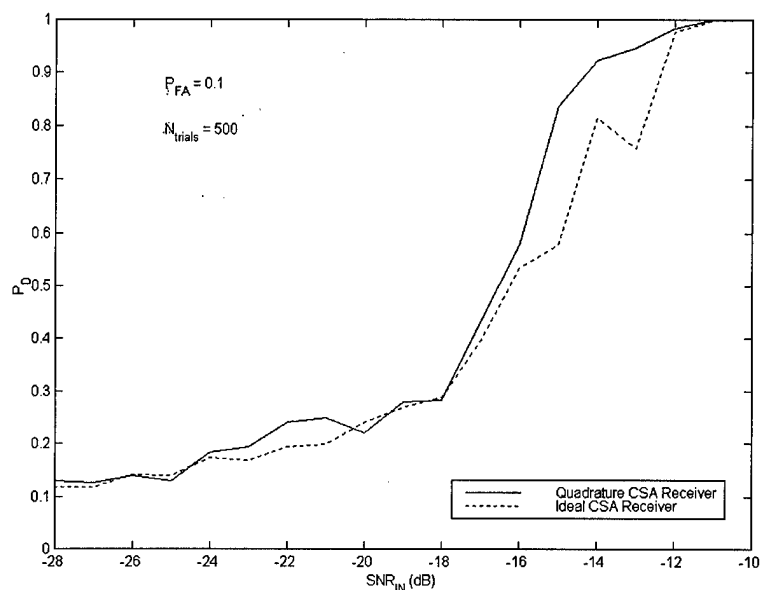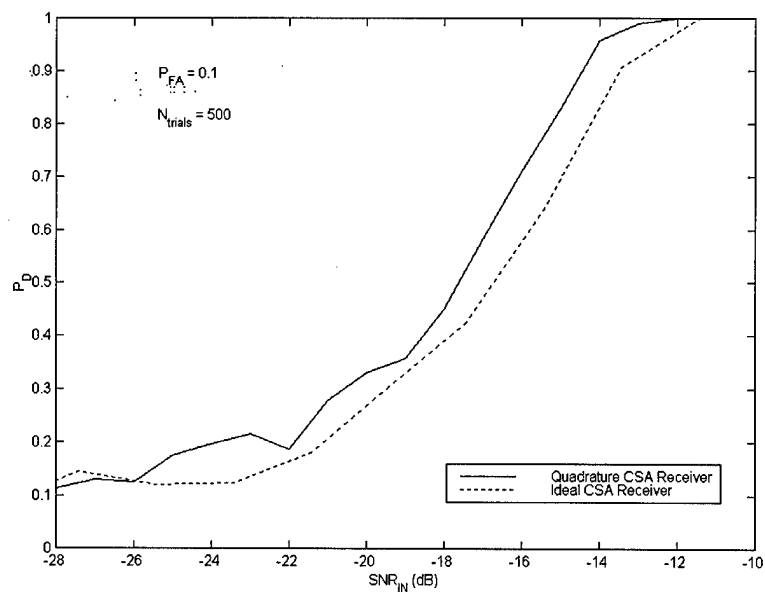


Figure 4-1. Quadrature CSA Receiver Performance at $\alpha = 2f_{IF}$ with:
(a) Tone Jamming, and (b) AM-SSB Interference

### 4.7.5 Summary

This section determined the Quadrature CSA Receiver performance by simulation and compared to the performance of the Ideal CSA Receiver. Analysis of the quadrature receiver cyclic spectrum reveals that when the I and Q channels are input as a complex ordered pair, then the double carrier feature is removed, making detection more difficult. When the I and Q channels are summed, the magnitude of the cyclic spectrum is identical to that of a single channel receiver. Therefore, the only difference in detection performance between the Quadrature CSA Receiver and the Ideal CSA Receiver is due to the non-ideal bandpass filters. This aids detection, as the noise power is attenuated more than the signal power because of the concentration of the signal power in the middle of the passband. Consequently, in all signal environments, the Quadrature CSA Receiver shows a detection improvement of 1 dB over the Ideal CSA Receiver. This improvement is a function of signal bandwidth, and the 1 dB improvement is only for the case where the signal bandwidth matches the receiver bandwidth. As with Channel 1 of the channelized receiver, if the signal bandwidth is greater than the receiver bandwidth the attenuation of the signal and noise is equal and the performance of the Quadrature CSA Receiver approaches the Ideal CSA Receiver.

### 4.8 Summary of Results and Analysis

The purpose of this chapter was to determine the detection performance of three receiver configurations: the *Ideal CSA Receiver*, the *Channelized CSA Receiver*, and the *Quadrature CSA Receiver*. Initially, the performance of the SCF estimation algorithm, the SSCA, was examined. Various sets of operating parameters were considered and optimal parameters chosen on the basis of estimate accuracy, resolution and processing speed. Receiver performance against differing signal bandwidths was examined. By evaluating the test statistic at $\alpha = 2f_{IF}$, the performance effect can be determined simply by taking into account the changing SNR. Three different data

97

reduction methods were examined. Based on detection performance, analytical advantages, and the simplicity in constructing a threshold for all cycle frequencies, the Energy test statistic proved most suitable.

The Ideal CSA performance was determined by simulation and compared to the performance of the radiometer. As cyclic feature detection theory suggests, the detection performance of the CSA receiver approaches that of the ideal radiometer in benign (stationary noise) environments. By applying radiometric detection principles to the test statistic, analysis shows that CSA receiver performance is directly related to noise quality. As the noise PSD becomes flatter, it is expected that the CSA receiver will outperform the radiometer. Simulation of a nonstationary noise environment shows that the CSA receiver outperforms the radiometer by approximately 10 dB, exhibiting only a slight decrease (less than 1 dB) in performance when compared to the stationary noise case. Analysis shows that the CSA detector is effected when the variance of the noise power exceeds the variance of the noise spectral correlation. When the signal environment includes tone jamming, the CSA receiver is unaffected, whereas the radiometer performs extremely poorly. In the presence of an AM-SSB interferer, the CSA receiver still outperforms the radiometer. However, performance is degraded by 1.5 dB due to the artificial cyclic features introduced by the SSCA when estimating the SCF of the AM-SSB signal.

The Channelized CSA Receiver performance was determined by simulation and compared to the Ideal CSA Receiver. First, SNR improvements due to filter effects were examined and Channel 1 was found to have a negligible (0.1 dB) SNR improvement when the null-to-null bandwidth of the signal equals the bandwidth of each channel. This is due to the concentration of the signal power in the middle of the channel bandwidth. However, as signal power is distributed more evenly from an increase in signal bandwidth, the attenuation of the signal and noise become identical and the SNR improvement approaches Under all conditions,

Channel 1 and Channel 2 performed identically as predicted. Therefore, the Channelized CSA Receiver performance is approximately equal to the Ideal CSA Receiver, independent of the channel selected.

Lastly, the Quadrature CSA Receiver performance was determined by simulation and compared to the performance of the Ideal CSA Receiver. Analysis of the quadrature receiver cyclic spectrum revealed that when the I and Q channels are input as a complex ordered pair, the double carrier feature is removed, making detection more difficult. When the I and Q channels are summed, the magnitude of the cyclic spectrum is identical to that of a single channel receiver. Therefore, the only difference in detection performance between the Quadrature CSA Receiver and the Ideal CSA Receiver is due to the non-ideal bandpass filters. This aids detection, as the noise power is attenuated more than the signal power due to the concentration of the signal power in the middle of the passband. Consequently, in all signal environments, the Quadrature CSA Receiver shows a detection improvement of 1 dB over the Ideal CSA Receiver. As with the channelized receiver, this is only for the case when the signal bandwidth matches the receiver bandwidth. If the signal bandwidth is greater than the receiver bandwidth, the attenuation of the signal and noise are equal and the Quadrature CSA Receiver performance approaches that of the Ideal CSA Receiver.

# 5. Conclusions and Recommendations

## 5.1 Restatement of Research Goal

The goal of this research is to:

1. Propose a method of detecting LPD/LPI communication signals using a non co-operative digital receiver.

2. Evaluate the performance of this detection technique through simulation in benign and adverse signal environments and compare these results to the radiometer.

3. Determine the effectiveness of this technique when combined with typical digital receiver architectures.

## 5.2 Conclusions

The Cyclic Spectrum Analysis (CSA) receiver is a robust detector which takes advantage of the spectral correlation properties of cyclostationary signals. Its performance closely matches the radiometer in benign signal environments and consistently outperforms the radiometer in adverse signal environments.

The detection method proposed consists of estimating the Spectral Correlation Function (SCF) using the Strip Spectral Correlation Algorithm (SSCA). The SSCA is the most suitable estimation algorithm due to its uniform resolution and fine cyclic resolution. The resulting estimate is then reduced to a test statistic that is a function of cycle frequency and time only. This test statistic is equivalent to sequentially running a single-cycle non co-operative cyclic feature detector over all possible cycle frequencies. The proposed method is more computationally efficient than this method and, by estimating the complete SCF, benefits post-detection tasks such as classification.

The operating parameters of the SSCA providing the best quality estimate in terms of resolution, variance, and minimizing processing time are $N'$ (the first FFT length) equal to 16, and

$N$ (the second FFT length) equal to 2048. It is expected that using state of the art FFT processing, each estimate would take approximately 0.6 ms to compute.

Out of three possible data reduction methods, the method producing the Energy test statistic is optimal based on cyclic feature strength, analytical traceability, and detection performance. By using an energy related test statistic, well established radiometric detection principles are applied to explain the detection performance of the CSA receiver at various cycle frequencies.

Under stationary noise conditions, the Ideal CSA Receiver performs within 1 dB of the ideal radiometer, the optimal non co-operative detector for stationary signals. By applying radiometric detection theory to the test statistic, analysis shows that the CSA receiver performance is directly related to the noise quality. As the power distribution of the noise becomes more uniform, the CSA receiver performance improves. When the noise distribution is perfectly uniform, the CSA receiver outperforms the radiometer. When the noise is modeled as being nonstationary, the radiometer exhibits a 10 dB decrease in performance whereas the CSA receiver is effected by less than 1 dB. In the presence of narrowband interference, the CSA receiver outperforms the radiometer. Specifically, in the presence of tone jamming with a Signal-to-Interference Ratio (SIR) of 0 dB, the CSA receiver performance is completely unchanged whereas the radiometer decreases by 7 dB. When the narrowband interferer is an AM-SSB signal, the CSA receiver performance is reduced by approximately 1.5 dB and the radiometer again decreases by 7 dB.

When the CSA receiver methodology is implemented in a channelized digital receiver, the detection performance is unchanged. Additionally, the detection performance of each channel is approximately equal, experiencing no degradation due to non-ideal IF bandpass filter characteristics.

When the CSA receiver methodology is implemented in a quadrature digital receiver, the in-phase and quadrature components of the signal must be summed and input to the SCF estimation algorithm. By inputting the signals as a complex ordered pair, the main cyclic feature is removed and the detection performance of the receiver effected accordingly. The quadrature receiver variant of the CSA receiver outperforms the ideal receiver in all cases by approximately 1 dB. This is due to the effects of the non-ideal IF bandpass filter and the fact that the majority of the signal power is distributed in the center of the bandwidth. This performance improvement is a function of ratio of the signal bandwidth to the receiver bandwidth. As the signal bandwidth increases, the signal and noise components are equally attenuated and the quadrature receiver performance approaches that of the ideal receiver.

## 5.3 Significant Results of Research

While the problem of detecting weak cyclostationary signals in the presence of noise has been previously examined from a theoretical viewpoint, only the performance of a single cycle co-operative detector has been evaluated and simulated [15,45]. Not only does this research look at the performance of a single cycle non co-operative detector, but it also proposes a method for efficiently formulating a sequence of single cycle feature detectors over a given input bandwidth by implementing an SCF estimation algorithm. The CSA receiver is found to outperform the radiometer in all adverse signal environments and performs within 1 dB of the radiometer in the presence of stationary noise.

Additionally, this research takes into account the effect of existing digital receiver architectures. Significantly, the performance of the Channelized CSA Receiver is independent of the channel selected and equals the performance of the ideal receiver. The quadrature receiver implementation improves upon the performance of the ideal and channelized receivers as a function of signal bandwidth.

## 5.4 Recommendations for Future Research

Recommendations for further research fall into four main categories: algorithm improvement, digital receiver modeling, detection performance evaluation and interception performance evaluation. The Strip Spectral Correlation Algorithm (SSCA) is well suited as an analytical tool. However, it suffers from a number of disadvantages when implemented in a real receiver. First, the SSCA requires a lowpass signal. In most cases, the IF signal in a digital receiver is a bandpass signal and requires additional processing to shift the signal in frequency. The SSCA should be modified to allow bandpass SCF estimation without sacrificing resolution or accuracy. Second, the SSCA could be optimized further through the use of wavelet signal processing. An improvement in efficiency means improved detection performance, either due to improved resolution or quicker computation.

Digital receiver modeling should be expanded to include scanning requirements, the use of energy detection for channelized receiver set on, and additional processing tasks the digital receiver is required to complete. This research assumed that the signal of interest is centered within the IF bandpass. This is not a particularly realistic assumption as a major factor in receiver performance is the time taken to scan the band of interest. In the case of the quadrature receiver, the modeling should include varying the local oscillator frequency to scan the receiver across the entire RF filter bandwidth. The channelized receiver model should include a method for determining which channel to set the SSCA onto, possibly through the use of a simple radiometric device. Additionally, the calculations performed to determine processing time assume the receiver can assign one hundred percent of its processing resources into this task. Again, this is not a realistic assumption, since the primary task of these receivers is typically radar signal detection. Therefore the task of detecting LPI/LPD communication signals is generally secondary.

An additional area for further research is detection performance evaluation. This research only determined detection performance of the CSA receiver when the signal of interest is a DS-SS BPSK signal. Clearly, there are many more LPI/LPD waveforms of interest and the receiver performance against these signals should be investigated. In addition to comparing the performance of this receiver against a radiometer, the performance of a chip rate detector and the co-operative single cycle detector should be compared.

The last area for possible research is the evaluation of the interception performance of the receiver. This research proposed a detection method that appears to have advantages in classifying the cyclic spectrum as well as in detection. The application of pattern recognition methods in this area should be explored further.

# Appendix: Notation and Terminology

The following notation and terminology is used throughout this thesis and is consistent with that found in the literature.

## Probabilistic Definitions

| | | |
|---|---|---|
| $R_x(\tau)$ | Autocorrelation of stochastic process x(t) | Eqn. (2-1) |
| $R_x^\alpha(\tau)$ | Cyclic Autocorrelation Function (CAF) | Eqn. (2-2) |
| $S_x^\alpha(f)$ | Spectral Correlation Function (SCF) | Eqn. (2-3) |
| $S_x(f)$ | Power Spectral Density (PSD) | Eqn. (2-1) |

## Deterministic Definitions

| | | |
|---|---|---|
| $\hat{R}_x^\alpha(\tau)$ | Limit cyclic autocorrelation function of infinite length time-series x(t) | Eqn. (2-1) |
| $\hat{S}_{uv}(f)$ | Limit cross spectral correlation | Eqn. (2-4) |
| $\hat{S}_x^\alpha(\tau)$ | Limit cyclic spectrum | Eqn. (2-5) |

## Spectral Estimators

| | | |
|---|---|---|
| $S_{x_T}(f)$ | Periodogram of finite length time-series $x_T(t)$ | Eqn. (2-1) |
| $S_{x_T}(t,f)$ | Time-variant periodogram | Eqn. (2-6) |
| $S_{uv_T}(t,f)$ | Time-variant cross periodogram | Eqn. (2-8) |
| $S_{x_{1/\Delta f}}(t,f)_{\Delta t}$ | Time-smoothed time-variant periodogram | Eqn. (2-3) |
| $S_{x_{\Delta t}}(t,f)_{\Delta f}$ | Frequency-smoothed time-variant periodogram | Eqn. (2-4) |

| $S_{x_T}^{\alpha}(t, f)$ | Time-variant cyclic periodogram | Eqn. (2-1) |
| $S_{x_{1/\Delta f}}^{\alpha}(t, f)_{\Delta t}$ | Time-smoothed time-variant cyclic periodogram | Eqn. (2-2) |
| $S_{x_{\Delta t}}^{\alpha}(t, f)_{\Delta f}$ | Frequency-smoothed time-variant cyclic periodogram | Eqn. (2-2) |
| $X_T(t, f)$ | Sliding finite-time Fourier transform or complex demodulate | Eqn. (2-7) |

**Test Statistics**

| $\lambda_{MC}$ | Multi-cycle Test Statistic | Eqn. (2-4) |
| $\lambda_{SC}^{\alpha}$ | Single Cycle Test Statistic | Eqn. (2-5) |
| $C_x^{\alpha}(f)$ | Coherence function | Eqn. (3-2) |
| $\lambda_{MAX}(t, \alpha)$ | Maximum Cut Test Statistic | Eqn. (3-1) |
| $\lambda_E(t, \alpha)$ | Energy Test Statistic | Eqn. (3-2) |
| DCS | Degree of Cyclostationarity | Eqn. (3-1) |
| $\text{DCS}^{\alpha}$ | Cycle Frequency Decomposed Degree of Cyclostationarity | Eqn. (3-2) |
| $\lambda_{DCS}(t, \alpha)$ | Degree of Cyclostationarity Test Statistic | Eqn. (3-3) |

**Digital Receivers**

| $x_T(t)$ | Ideal Digital Receiver Output | Section 3.4.1 |
| $y_{m_T}(t)$ | Channelized Digital Receiver *m*th Channel Output | Section 3.4.2 |
| $z_{I_T}(t), z_{Q_T}(t)$ | Quadrature Digital Receiver In-phase and Quadrature Outputs | Section 3.4.3 |

# Bibliography

[1]   April, E. *On the Implementation of the Strip Spectral Correlation Algorithm for Cyclic Spectrum Estimation.* Technical Note 94-2, Defence Research Establishment Ottawa, February 1994 (AD-A288721).

[2]   -----. *The Advantage of Cyclic Spectral Analysis.* Technical Note 92-4, Defence Research Establishment - Ottawa, October 1991.

[3]   Brown, W. A. and H. H. Loomis Jr. "Digital Implementation of Spectral Correlation Analyzers," in *IEEE Transactions on Signal Processing.* 41(2):703-720, February 1993.

[4]   Carter, G. C. "Receiver Operating Characteristics for a Linearly Thresholded Coherence Estimation Detector," in *IEEE Transactions on Acoustics, Speech, and Signal Processing.* 90-92, February 1977.

[5]   Carter, G. C. and E. H. Scannell Jr. "Confidence Bounds for Magnitude-Squared Coherence Estimates," in *Coherence Estimation,* Ed. G. C. Carter and A. H. Nuttall. Scientific and Engineering Studies, Newport RI: Naval Underwater Systems Center, 1979 (AD-A181684).

[6]   Carter, N.J., *Implementation of Cyclic Spectral Analysis Methods.* MS thesis, Monterey CA: Naval Postgraduate School, December 1992 (AD-A261715).

[7]   Da Costa, E. L. *Detection and Identification of Cyclostationary Signals.* MS thesis, Monterey CA: Naval Postgraduate School, March 1996 (AD-A311555).

[8]   Dillard, R. A. and G. M. Dillard. *Detectability of Spread Spectrum Signals.* Norwood MA: Artech House, 1989.

[9]   DSP Architectures. "DSP-24 Digital Signal Processor," Excerpt from performance data web page, http://www.dsparchitectures.com/dsp-24/dsp-24.htm, 16 January 99.

[10]  Gardner, W. A. "An Introduction to Cyclostationary Signals," in *Cyclostationarity in Communications and Signal Processing.* Ed. W. A. Gardner. New York: IEEE Press, 1994.

[11]  -----. "Exploitation of Spectral Redundancy in Cyclostationary Signals," in *IEEE Signal Processing Magazine,* 8-36, April 1991.

[12]  -----. "Signal Interception: A Unifying Theoretical Framework for Feature Detection," in *IEEE Transactions on Communications.* 36:897-906, August 1988.

[13]  -----. *Statistical Spectral Analysis: A Nonprobabilistic Theory.* New Jersey: Prentice Hall, 1988.

[14]  -----. *Introduction to Random Processes with Applications to Signals and Systems.* New York: Macmillan Publishing Company, 1986.

[15]  Gardner, W. A. and C. M. Spooner. "Robust Feature Detection for Signal Interception," in *IEEE Transactions on Communications,* 42:2165-2173, May 1994.

[16]  -----. "Detection and Source Location of Weak Cyclostationary Signals: Simplifications of the Maximum-Likelihood Receiver," in *IEEE Transactions on Communications.* 41:905-916, June 1993.

[17]  -----. "Signal Interception: Performance Advantages of Cyclic-Feature Detectors," in *IEEE Transactions on Communications.* 40:149-159, January 1992.

[18]  Giannakis, G. B. "Cyclostationary Signal Analysis," in *The Digital Signal Processing Handbook.* Ed. V. K. Madisetti and D. B. Williams. Boca Raton FL: CRC Press, 1988.

[19] Hero, A. "Signal Detection and Classification," in *The Digital Signal Processing Handbook.* Ed. V. K. Madisetti and D. B. Williams. Boca Raton FL: CRC Press, 1988.

[20] Hill, D. A. and B. E. Felstead. "Laboratory Performance of Spread Spectrum Detectors," in *MILCOM 1994 Proceedings.* 785-790, 1994.

[21] Imbeaux, J., "Performances of the Delay-Line Multiplier Circuit for Clock and Carrier Synchronization in Digital Satellite Communications", *IEEE Journal on Selected Areas in Communications,* Vol. SAC-1, pp. 82-95, January 1983.

[22] Kay, S. M. *Fundamentals of Statistical Signal Processing: Detection Theory.* New Jersey: Prentice Hall, 1998

[23] -----. *Fundamentals of Statistical Signal Processing: Estimation Theory.* New Jersey: Prentice Hall, 1993.

[24] -----. *Modern Spectral Estimation: Theory and Application.* New Jersey: Prentice Hall, 1988.

[25] Keuhls, J. F. and E. Geraniotis. "Presence Detection of Binary-Phase-Shift-Keyed and Direct-Sequence Spread-Spectrum Signals Using a Prefilter-Delay and Multiply Device," in *IEEE Journal on Selected Areas in Communications,* 8:915-933, June 1990.

[26] Krasner, N. F. "Optimal Detection of Digitally Modulated Signals," in *EEE Transactions on Communications.* COM-30:885-895, May 1982.

[27] Madden, C. B. *Effects of Jamming and Excision Filtering Upon Error Rates and Detectability of a Spread Spectrum Communication System.* MS thesis, AFIT/GE/ENG/95D-13, School of Engineering, Air Force Institute of Technology, Wright-Patterson AFB OH, December 1995.

[28] Mills, R. F. and G. E. Prescott. "A Comparison of Various Radiometer Detection Models," in *IEEE Transactions on Aerospace and Electronic Systems.* 32:467-473, January 1996.

[29] Naidu, P. S. *Modern Spectrum Analysis of Time Series.* Boca Raton FL: CRC Press, 1996.

[30] Nicholson, D. L. *Spread Spectrum Signal Design LPE and AJ Systems.* Maryland: Computer Science Press, 1988.

[31] Nikias, C. L. and A. P. Petropulu. *Higher-order Spectra Analysis: A Nonlinear Signal Processing Framework.* New Jersey: Prentice Hall, 1993.

[32] Pettit, R. H. *ECM and ECCM Techniques for Digital Communication Systems.* CA: Lifetime Learning Publications, 1982.

[33] Polydoros, A. and S. Hinedi. "DS/LPI Autocorrelation Detection in Noise Plus Random-Tone Interference," in *IEEE Transactions on Communications.* Vol. 38:805-817, June 1990.

[34] Polydoros, A., C. L. Nikias and K. T. Woo. *Advanced LPI Intercept Detector Research.* Prepared for the Office of Naval Research, Axiomatix Report No. R8511-3, November 1985 (AD-A164485).

[35] Polydoros, A. and C. L. Weber. "Detection Performance Considerations for Direct-Sequence and Time-Hopping LPI Waveforms," in *IEEE Journal on Selected Areas in Communications.* SAC-3:727-744, September 1985.

[36] -----. "Optimum Detection Considerations for Low Probability of Intercept," *MILCOM 1982 Proceedings.* 2.1.1-2.1.5, October 1982.

[37] Reed, D. E. and M. A. Wickert. "Minimization of Detection of Symbol-Rate Spectral Lines by Delay and Multiply Receivers," in *IEEE Transactions on Communications,* 36:118-120, January 1988.

[38] Roberts, R. A. and C. T. Mullis. *Digital Signal Processing*. Reading MA: Addison-Wesley, 1987.

[39] Roberts, R. S., W. A. Brown and H. H. Loomis Jr. "A Review of Digital Spectral Correlation Analysis: Theory and Implementation", in *Cyclostationarity in Communications and Signal Processing*. Ed. W. A. Gardner. New York: IEEE Press, 1994.

[40] Simon, M. K., J. K. Omura, R. A. Sholtz and B. K. Levitt. *Spread Spectrum Communications, Vol. III*. Maryland: Computer Science Press, 1985.

[41] Sklar, B. *Digital Communications, Fundamentals and Applications*. New Jersey: Prentice Hall, 1988.

[42] Slocumb, B. and P. West. *Tri-Service Digital Receiver Technology Engineering Integration*, Interim Report WL-TR-95-1140 under Contract F33615-92-C-1009, Wright Laboratory, April 1995.

[43] Snelling, W. E. and E. A. Geraniotis. "The Interception of Spread Spectrum Waveforms via the Amplitude Distribution Function," in *MILCOM 91 Conference Record*, 2:537-542, 1991.

[44] Sonnenschein, A. and P. M. Fishman. "Radiometric Detection of Spread-Spectrum Signals in Noise of Uncertain Power," in *IEEE Transactions on Aerospace and Electronic Systems*, 28:654-660, July 1992.

[45] Spooner, C. M. *Performance Evaluation of Detectors for Cyclostationary Signals*. MS thesis, Dept. of Electrical and Computer Engineering, University of California at Davis, June 1988.

[46] Statistical Signal Processing, Inc. *Spectral Correlation Analyzer: User's Guide*, Version 1.0. May 1997.

[47] Steil, J. S. and G. E. Prescott. "Analysis By Simulation of a Spread Spectrum Intercept Receiver," in *Proceedings of the IEEE 1989 National Aerospace and Electronics Conference*, 1: 248-54, 1989.

[48] Torrieri, D. J. *Principles of Secure Communications* (Second Edition). Norwood MA: Artech House, 1992.

[49] Tsui, J. *Digital Microwave Receivers: Theory and Concepts*. Norwood MA: Artech House, 1989.

[50] -----. *Digital Techniques for Wideband Receivers*. Norwood MA: Artech House, 1995.

[51] Van Trees, H. L. *Detection, Estimation, and Modulation Theory, Part I*. New York: Wiley, 1971.

[52] -----. *Detection, Estimation, and Modulation Theory, Part III*. New York: Wiley, 1971.

[53] Yeung, G. K. and W. A. Gardner. "Search-Efficient Methods of Detection of Cyclostationary Signals," in *IEEE Transactions on Signal Processing*, 44(5):1214-1223, May 1996..

[54] Zizanovic, G. D. and W. A. Gardner. "Degrees of Cyclostationarity and Their Applications to Signal Detection and Estimation," in *Signal Processing*, 22: 287-297, April 1991.

# VITA

Flight Lieutenant Andrew M. Gillman joined the Royal Australian Air Force in 1990 and commenced training at the Australian Defence Force Academy in Canberra. After graduating from the Academy in 1992 he completed the final year of his degree course and graduated from the University College with a Bachelor of Engineering in Electronic and Electrical Engineering with Honors in 1993. From January 1994 to April 1995 he served as Officer In Charge of Electronic Warfare Computer Support Systems, Engineering Squadron, Aircraft Research and Development Unit. Flight Lieutenant Gillman was then assigned to Electronic Warfare Squadron, ARDU where he served as the F/A-18 RWR Engineer, Tactical Support Flight. He entered the Air Force Institute of Technology in 1997 to pursue a Master's of Science degree in Electrical Engineering majoring in Communications and Electronic Combat. Following graduation Flight Lieutenant Gillman will serve in the Directorate of Electronic Warfare Projects - Air, Defence Acquisition Organization, Department of Defence.

Permanent Address:    DEWP-A
Department of Defence
Russell Offices, R2-6-A-099
Canberra, ACT, 2600
AUSTRALIA